Technische Universität Braunschweig

Michael Kazda

Advanced Microwave Control for Atomic Fountain Clocks

Dissertation
Braunschweig 2018

Berichte aus dem **Institut für Elektrische Messtechnik und Grundlagen der Elektrotechnik** Band 58

Hrsg. Prof. Dr. Meinhard Schilling

Advanced Microwave Control for Atomic Fountain Clocks

Von der Fakultät für Elektrotechnik, Informationstechnik, Physik
der Technischen Universität Carolo-Wilhelmina zu Braunschweig

zur Erlangung des Grades eines Doktors

der Ingenieurwissenschaften (Dr.-Ing.)

genehmigte Dissertation

von Michael Kazda

aus Hamburg

eingereicht am: 08.02.2018

mündliche Prüfung am: 10.07.2018

1. Referent: Prof. Dr. Meinhard Schilling

2. Referent: Prof. Dr. Fritz Riehle

Druckjahr 2018

Dissertation an der Technischen Universität Braunschweig,
Fakultät für Elektrotechnik, Informationstechnik, Physik

Zusammenfassung

Von allen physikalischen Größen können Frequenz und Zeitintervall mit den geringsten Unsicherheiten bestimmt werden. Für die Realisierung der SI-Sekunde werden Caesium-Fontänenuhren eingesetzt, dabei werden relative Unsicherheiten von wenigen 10^{-16} erreicht. In Fontänenuhren nutzt man Mikrowellenfelder, um die atomaren Zustände der Caesium-Atome zu manipulieren, die Felder werden mit eigens entwickelten Mikrowellen-Signalgeneratoren erzeugt. Im Rahmen dieser Arbeit wurde der Einfluss der Mikrowellenerzeugung auf die Gesamtunsicherheit der Fontäne untersucht und Methoden zu deren Reduzierung entwickelt und bewertet.

Der Fontänenbetrieb stellt hohe Anforderungen an die Zuverlässigkeit und Verfügbarkeit der verwendeten Elektronik. Im Rahmen dieser Arbeit wurde ein modularer Mikrowellensynthesizer aufgebaut. Als Referenzsignal wurde eine optisch stabilisierte Mikrowellenquelle verwendet. Damit konnte der Beitrag der Mikrowellensynthese zur statistischen Unsicherheit der Fontäne deutlich reduziert werden. Bei dem Synthesizer wurde die Rapid Adiabatic Passage Methode implementiert um die Unsicherheit in der Bestimmung der Stoßverschiebung zu reduzieren. Die Methode wird an der Fontänenuhr CSF2 eingesetzt und erlaubt den Fontänenbetrieb mit deutlich höheren Atomzahlen und damit einer geringeren statistischen Unsicherheit.

Wenn während der Manipulation der Atome Störungen in der Phase der Mikrowellenfelder auftreten, kann die Frequenzbestimmung beeinflusst werden. Sind diese Störungen synchron zum Abfragezyklus der Fontänenuhr, kann es zu einer Verschiebung der Fontänenfrequenz kommen. Im Rahmen dieser Arbeit wurde ein Phasentransienten-Analysator entwickelt mit dem die Auswirkungen von zyklus-synchronen Phasentransienten auf wenige 10^{-17} genau bestimmt werden können.

Eine weitere mögliche Quelle für Frequenzverschiebungen ist die Interaktion von Caesium-Atomen während der wechselwirkungsfreien Zeit. Eine Verstimmung des Mikrowellenfeldes während dieser Zeit kann diesen Effekt und die damit verbundenen systematischen Unsicherheiten deutlich reduzieren. Im Rahmen dieser Arbeit wurde ein System zur präzisen Steuerung der Frequenz des Mikrowellenfeldes entwickelt und charakterisiert. Damit konnte sichergestellt werden, daß Unsicherheitsbeiträge durch diesen Effekt bei CSF2 im niedrigen 10^{-17} Bereich liegen.

Schlagworte: Atomuhren, Mikrowellenspektroskopie, Phasenmessung, digital gesteuerter Oszillator, Frequenzsynthese, Frequenzstabilität

Abstract

Time interval and frequency can be measured with lower uncertainty and greater resolution than any other physical quantity. Using caesium fountain clocks, the SI-second can be realized with uncertainties of several parts in 10^{16}. In a fountain clock, microwave fields are used to manipulate the atomic states. These fields are driven by dedicated microwave signals. The generation of microwave signals is a key aspect for the operation of fountain clocks, as it can significantly contribute to the clocks statistical as well as the systematic uncertainty.

This thesis discusses the contributions of the microwave signal generation to the uncertainty of a caesium fountain. Several methods aimed at the reduction of the statistical as well as the systematic uncertainty were implemented and assessed.

A modular microwave synthesizer has been designed, ensuring high reliability and high availability. By utilizing a high stability local oscillator, the contribution of the microwave signal generation to the statistical uncertainty of the fountain clock could be reduced to an insignificant level. The synthesizer has been augmented with a modulation scheme to implement the method of Rapid Adiabatic Passage for collisional frequency shift measurements. Application of this method in the fountain clock CSF2 lead to a significant reduction of the collisional shift uncertainty and enabled fountain operation with high atom numbers.

Phase perturbations in the microwave fields during the state manipulation can lead to shifts of the fountain frequency if they are synchronous with the fountain cycle. To facilitate a detailed analysis of cyclic perturbations on the micro-radian level, a dedicated phase transient analyzer was developed. With this system, the effect of cyclic phase perturbations can be evaluated at the low 10^{-17} level.

Uncontrolled interactions between the caesium atoms and resonant microwave fields can also be a source of frequency shifts. A method for the suppression of such shifts has been developed, relying upon a precise control of the field's frequency detuning. By using this scheme, the uncertainty contributions due to such interactions at CSF2 could be limited to few parts in 10^{17}.

Keywords: Atomic clocks, Microwave spectroscopy, Phase measurement, Digital-controlled oscillators, Frequency synthesizers, Frequency stability

List of publications

V. Gerginov, N. Nemitz, D. Griebsch, M. Kazda, R. Li, K. Gibble, R. Wynands, and S. Weyers, "Recent improvements and current uncertainty budget of PTB fountain clock CSF2", in *EFTF-2010 24th European Frequency and Time Forum*, **2010**

M. Kazda, V. Gerginov, N. Nemitz, and S. Weyers, "Investigation of rapid adiabatic passage for controlling collisional frequency shifts in a caesium fountain clock", *IEEE Transactions on Instrumentation and Measurement*, vol. 62, pp. 2812-2819, **2013**

C. Tamm, N. Huntemann, B. Lipphardt, V. Gerginov, N. Nemitz, M. Kazda, S. Weyers, and E. Peik, "Cs-based optical frequency measurement using cross-linked optical and microwave oscillators", *Physical Review A*, vol. 89, p. 023820, **2014**

M. Kazda, V. Gerginov, N. Huntemann, B. Lipphardt, and S. Weyers, "Phase analysis for frequency standards in the microwave and optical domains", *IEEE Transactions on Ultrasonics, Ferroelectrics, and Frequency Control*, vol. 63, pp. 970-974, **2016**

M. Kazda and V. Gerginov, "Suppression of microwave leakage shifts in fountain clocks by frequency detuning", *IEEE Transactions on Instrumentation and Measurement*, vol. 65, pp. 2389-2393, **2016**

Contents

List of Figures

1 Introduction

In 1967, a hyperfine transition of the caesium atom in the microwave spectrum was chosen as the basis for the definition of the second [1]. At that time, this definition could be realized by a caesium beam clock with about 12 digits of precision [2]. Today, the second is realized with atomic fountain clocks, approaching uncertainties of 1 part in 10^{16} [3], an improvement by 4 orders of magnitude. Several secondary realizations of the second have been devised [1], some of them are based on optical transitions. Optical clocks in principle can realize the second with uncertainties of parts in 10^{18} [4]. This opens the door for a future redefinition of the second, which has to be based on a comparison between optical clocks and caesium fountain clocks [5], emphasizing the importance of low fountain uncertainties.

Even after a potential redefinition of the SI second in terms of an optical reference transition, atomic fountain clocks will play an important role in the generation of atomic time scales [6] for the foreseeable future. To pursue lower uncertainties, each contribution to the fountain clocks uncertainty is scrutinized, driven by technological advancement and fueled by a deeper insight into the atomic processes. This applies to the systematic uncertainty, as well as the statistical uncertainty, also referred to as the clock's frequency instability. A low instability is a prerequisite for the evaluation of a number of systematic uncertainty contributions.

In a fountain clock, the hyperfine transition is periodically excited by a resonant microwave field that is generated with a microwave synthesizer. The transition probability is probed with an optical detection system during each cycle, the detector signal is used to lock the field frequency to the atomic resonance [7]. The microwave signal generation can significantly deteriorate the performance of the atomic fountain clock [8–10]. In this work, the design and assessment of a microwave synthesizer for PTBs fountains CSF1 [11] and CSF2 [12] is presented. It has been fully characterized for its contribution to the systematic and statistical uncertainty of the fountains. It was shown, that the contribution of the signal-generating electronics to the fountain uncertainty is negligible.

A fountain clock operates in a periodic way, its frequency stability is limited by the so-called quantum projection noise [13]. This noise is proportional to the square root of the number of atoms detected during the individual fountain cycle [14]. This noise can be reduced down to an insignificant level by probing a fairly large number of caesium atoms within a single clock cycle [15]. Increasing the atom number, unfortunately, leads to higher frequency shifts due to inter-atomic collisions that have to be corrected for [16].

The correction of the collisional shift is associated with a relative uncertainty that depends on the correction method. Hence higher atom numbers will result in a higher systematic uncertainty [17]. At the required atom numbers, the contribution from the collisional shift would dominate the systematic uncertainty of the fountain. To reduce the systematic uncertainty contribution associated with the collisional shift, the method of rapid adiabatic passage can be applied [18]. Such a system has been implemented in the microwave synthesizer [19]. With this system, the fountain can be operated at the quantum projection noise limit [20] with a negligible uncertainty contribution due to the collisional shift.

Phase perturbations in the microwave signal synchronous to the fountain cycle can lead to significant frequency shifts [21]. Possible frequency shifts have to be accounted for in the systematic uncertainty budget of the fountain, thus these phase perturbations have to be evaluated and their effect on the fountain frequency has to be ascertained. To facilitate this evaluation, a phase transient analyzer is required [22]. In the scope of this work, such a system has been developed, capable of measuring cycle synchronous phase perturbations well below the inherent signal noise. It has been used to analyze the interrogation signals of atomic clocks in the microwave and optical domains [23].

Another source of frequency shifts are uncontrolled interactions between the caesium atoms and resonant microwave fields outside the designated interaction zones. Such a perturbing field can be a consequence of microwave leakage from the field-confining microwave cavities or the microwave generating electronics [24]. As these leakage fields cannot be modeled with sufficient accuracy, it is required to suppress interactions between the atoms and the field outside the cavities [25]. This can be achieved by altering the parameters of the field synchronous to the fountain cycle [26]. A well-known method based on a suppression of the field amplitude has been adapted for our microwave synthesis setup [21]. We also implemented a novel method to reduce the effect of microwave leakage [27]. It depends on

frequency detuning rather than amplitude suppression [28]. Both methods have been employed for atomic fountain use, the phase transient analyzer proving indispensable for their evaluation.

Design and operation of an atomic frequency standard and its individual components is of course an collaborative effort of numerous scientists and engineers. For this reason, I would like to briefly outline my particular contribution to the presented work.

The microwave synthesis described in Chapter 3 is based on an existing synthesizer design [29]. I have completely re-engineered the microwave synthesizer, following a modular approach. This includes the implementation of a new frequency control setup and reference selection scheme. Furthermore, I was strongly involved in the implementation of the method of rapid adiabatic passage [19]. I have designed and implemented the phase transient analyzer presented in Chapter 4, a system suitable for the analysis of phase transients occurring in microwave and optical clocks [23]. I was substantially engaged in the development of the frequency detuning method presented in Chapter 5 [27], and was solely responsible for the technical implementation and assessment.

2 Background

The International System of Units (SI) is the most widely used system of units of measurement. It was defined by the General Conference on Weights and Measures (CGPM) and is comprised of seven base units, the metre, kilogram, second, ampere, kelvin, candela and mole [1]. Of all base units, the second can be realized with the lowest uncertainty.

An atomic transition was chosen as the basis for the definition of the second, as it proved to be much better than any other type of periodic oscillator. The present definition for the second has been formulated in 1967 and is based on a hyperfine transition of the caesium atom [1]:

> The second is the duration of 9 192 631 770 periods of the radiation corresponding to the transition between the two hyperfine levels of the ground state of the Caesium 133 atom.

2.1 Hyperfine transition probing

In this section, a brief sketch of the hyperfine structure and the transition probing procedures used in fountain clocks will be given, an in-depth description is available in [26].

2.1.1 Hyperfine structure

The hyperfine structure is a result of the coupling of the magnetic moment of the nucleus with the magnetic field of the electrons. In the ground state of the ^{133}Cs atom, the electronic angular momentum is $1/2$ and the nuclear spin is $7/2$, resulting in the splitting of the ground state to two hyperfine levels characterized by quantum numbers $F = 3$ and $F = 4$.

The probabilities to find the atom in the states with $F = 3$ or $F = 4$ are given by P_3 and P_4 respectively, where $P_3(t) + P_4(t) = 1$. If a field with frequency f_0 is applied, corresponding to the transition energy of the two hyperfine

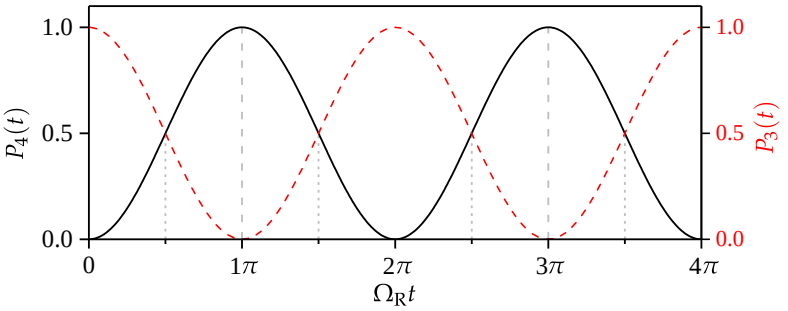

Figure 2.1: Rabi oscillations in a resonant field

levels, a periodical change of the probabilities in the two states will occur. These oscillations are known as Rabi oscillations, the oscillation period depends on the detuning from resonance ($\Delta\omega$) and on the Rabi frequency Ω_R. The Rabi frequency is dependent on the amplitude of the applied field.

Shown in Figure 2.1 are Rabi oscillations in a resonant field ($\Delta\omega = 0$). By controlling the duration t of the interaction, i.e. applying a microwave pulse with pulse area $\Omega_R t$, the probabilities can be manipulated. Two types of pulses are commonly used in this context, a π-pulse ($\Omega_R t = \pi$) and a $\pi/2$-pulse ($\Omega_R t = \pi/2$). If a π-pulse is applied to an atom in the state $F = 3$ (equivalent to $P_4 = 0$), it will be transferred to the state $F = 4$ ($P_4 = 1$) and vice versa. If a $\pi/2$-pulse is applied to an atom in the state $F = 3$, the result is a superposition of the two atomic states, equivalent to $P_3 = 0.5$ and $P_4 = 0.5$. Subjected to an external magnetic field, the hyperfine structure levels split up into $2F + 1$ magnetic sublevels m_F (Figure 2.2). The definition of the second refers to the transition between the $F = 3, m_F = 0$ and $F = 4, m_F = 0$ states (clock transition).

2.1.2 Probing schemes

The caesium hyperfine transition can be probed in a three step process: By using optical pumping, the caesium atoms are prepared in a single hyperfine level. They are then exposed to a resonant microwave field to excite the clock transition. This can be realized with a single atom-field interaction (Rabi scheme) or a temporal sequence of interactions (Ramsey scheme). In a last step, the final state of the atoms is probed with an optical detection system.

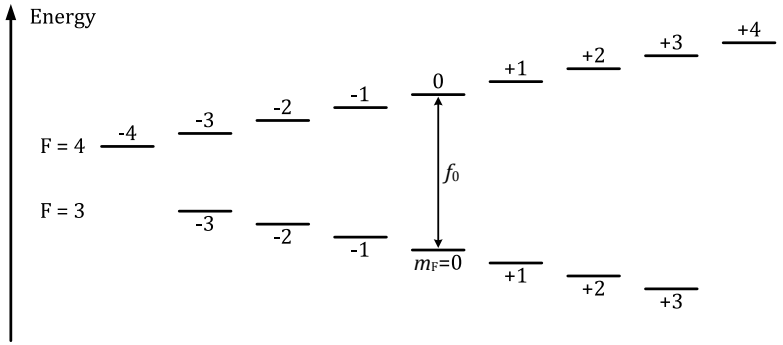

Figure 2.2: Simplified ^{133}Cs energy level diagram (not to scale) showing the Zeeman splitting of the electronic ground state and the $m_F = 0$ magnetic sublevels within an external magnetic field [30].

The transition probability of the atoms depends on the frequency of the microwave field. An excitation spectrum is obtained by changing the field frequency and recording the associated transition probability. Different transition probability functions are obtained when using the Rabi or Ramsey excitation schemes. In the following, the frequency of the clock transition will be denoted as f_0 while the frequency of the microwave field will be denoted as f_R.

2.1.3 Rabi Scheme

The first microwave spectroscopy setups used a method developed by I.I. Rabi, where the atoms are exposed to a single resonant field [31, 32]. During the interaction of duration ϑ (also denoted as Rabi time), the atomic transition is excited with a π-pulse and the resulting hyperfine state of the atoms is subsequently probed. The resulting transition probability function for the Rabi scheme is shown in Figure 2.3. The width of the function at a transition probability of 0.5 is denoted as the full width at half maximum (FWHM), it depends on the duration of the interaction between the caesium atoms and the resonant field. A longer interaction time ϑ leads to narrower line width and in turn to higher precision in determining f_0. Inhomogeneities in the external magnetic field during the interaction lead to broadening of the line shape, limiting the attainable line width.

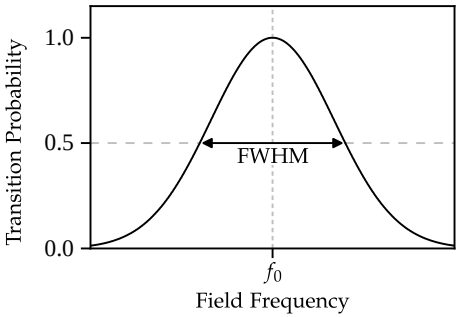

Figure 2.3: Excitation spectrum for the Rabi scheme

2.1.4 Ramsey Scheme

To overcome this limitation, the separated oscillatory fields method was developed by N.F. Ramsey [33, 34]. In the Ramsey scheme, the accumulated phase difference between the atomic superposition and the microwave field is evaluated. The scheme uses two short interactions of duration ϑ, separated by a much longer time T_R (Figure 2.4). During each interaction, a $\pi/2$-pulse is applied. The resulting transition probability function is different from the one obtained from the Rabi scheme. Instead of a single peak, it exhibits several fringes (Figure 2.5).

Before the first interaction (R_1 in Figure 2.4), the relation between the phase of the atomic superposition (φ_0) and the phase of the microwave field (φ_R) is undefined. After R_1, the atomic superposition is in phase with the resonant field ($\varphi_R - \varphi_0 = 0$). This interaction is followed by a period of free evolution (T_R), where no interaction with the microwave field occurs. During this time, a phase difference $\Delta\varphi$ is accumulated if $f_R \neq f_0$. After the atoms are exposed to a $\pi/2$-pulse a second time (R_2), their transition probability is probed. When the accumulated phase difference is zero, the application of the two $\pi/2$-pulses is equivalent to the application of a single π-pulse. The final transition probability is then 1, (marked A in Figure 2.5). When a π phase difference is accumulated during the Ramsey time, the probing of the atoms yields the initial hyperfine state and a transition probability of 0 (marked B in Figure 2.5). The line width of the central fringe δ depends on the Ramsey time T_R and is independent of the Rabi time.

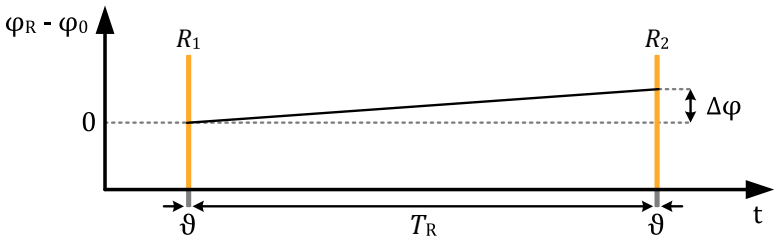

Figure 2.4: Ramsey interrogation scheme

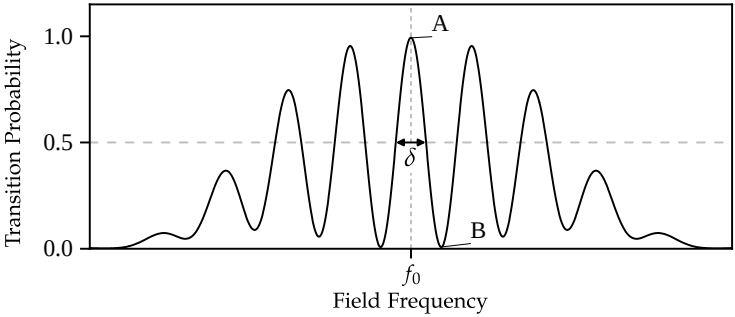

Figure 2.5: Excitation spectrum for the Ramsey scheme

The Ramsey scheme is executed repetitively, the results of the transition probability probing are used to lock the frequency of the interrogation field to the atomic resonance.

The transition probability is probed at both sides of the central fringe alternating. The field frequency is modulated by $\pm\delta/2$ and the difference between the two detected transition probabilities is evaluated. The difference is used as a process variable in a control loop, the set point is zero. In steady state, the two transition probabilities are equal and their respective field frequencies are $f_0 - \delta/2$ and $f_0 + \delta/2$.

2.2 Stability analysis

The operation of an atomic frequency standard is subject to statistical processes, leading to an instability of the locked frequency. The Allan variance $\sigma_y^2(\tau)$, and the Allan deviation $\sigma_y(\tau)$ are measures to describe the instability of oscillators and frequency standards in the time domain [35–37].

To determine the Allan variance, a time series of frequency measurements is taken with no dead-time between the samples. A frequency measurement is a comparison between a reference frequency f_{Ref} and an unknown frequency $f(t)$. The fractional frequency $y(t)$ is the normalized difference between f_{Ref} and $f(t)$:

$$y(t) = \frac{f(t) - f_{\mathrm{Ref}}}{f_{\mathrm{Ref}}}. \tag{2.1}$$

The fractional frequency is then averaged over an observation time τ to obtain the average fractional frequency:

$$\bar{y}(t,\tau) = \frac{1}{\tau}\int_0^{\tau} y(t+t_x)\,dt_x. \tag{2.2}$$

The Allan variance $\sigma_y^2(\tau)$ is computed from a consecutive series of average fractional frequencies with no dead time in between. It is defined as:

$$\sigma_y^2(\tau) = \frac{1}{2}\langle(\bar{y}_{n+1} - \bar{y}_n)^2\rangle, \tag{2.3}$$

where $\langle\rangle$ denotes the expectation value and $\bar{y}_n$ is the nth fractional frequency average. To specify the frequency instability of atomic fountain clocks, the Allan deviation $\sigma_y(\tau)$ is used.

As white frequency noise is the dominating source of noise in atomic fountain clocks, the usual double-logarithmic plot of the Allan deviation exhibits a characteristic slope of $\tau^{-1/2}$ [14]. This allows to compare the frequency instability of different frequency standards by stating a single value of the Allan deviation for $\tau = 1\,\mathrm{s}$. Instability of the fountain results in a measurement uncertainty, this statistical uncertainty is termed type A uncertainty, u_{a} in short [38]. In a fountain clock, the statistical uncertainty of a frequency measurement is usually given as 1σ.

2.3 Caesium fountain clocks

The quest for ever reduced uncertainties in the realization of the SI second has led to the development of the atomic fountain clock [39–42], to be described in Section 2.3.1. Fountain clocks use the Ramsey scheme consisting of two microwave interactions, separated in time, and laser cooled atoms [43–46] to determine the frequency of the caesium hyperfine transition. Fountain clocks are used for the steering of local atomic time scales [6, 47] and contribute to the steering of the international atomic time scale, TAI [48]. They have been utilized to perform fundamental physics tests [49, 50] and to search for variations of fundamental constants [51–53].

For a fountain to contribute to TAI, a complete evaluation of its statistical and systematic uncertainty is required. The first evaluation process can take several years and reevaluations are performed regularly. About a dozen caesium fountain clocks have been contributing to TAI in the last years [3, 11, 12, 15, 54–59]. Their actual designs differ in terms of physical setup as well as electronic and optical systems. We will give a very brief overview of the fountain principle, taking PTB's caesium fountain CSF2 [12] as an example. We will focus on the sections involved in the atom-microwave interaction. A more in-depth description of atomic fountain clocks is given in [7, 60–62].

2.3.1 Fountain principle

Atomic fountain clocks employ a cyclic process, consisting of multiple stages (Figure 2.6). As a first step, the caesium atoms are captured and subsequently cooled using an optical molasses (a). The optical molasses consists of three orthogonal pairs of counter propagating laser beams. The cooling process results in a cloud of caesium atoms with a temperature of about 1 µK and several millimeters in diameter. At this temperature, the average velocity of the caesium atoms is in the order of 1 cm/s, during the fountain cycle the cloud of atoms is only slightly expanding. After the cooling process is completed, the cloud is launched upwards using the moving molasses technique (b). The frequency of the three upward-directed laser beams is increased (blue-detuned) while the frequency of the three downward-directed laser is decreased (red-detuned). The generated moving interference pattern accelerates the atomic cloud to a velocity of several meters per second. The laser beams are then switched off and the cloud follows a ballistic trajectory.

After the cooling phase, the atoms are in the $F = 4$ state, distributed among the m_F substates. In a subsequent state selection process, the atoms are prepared in the $F = 3, m_F = 0$ state. At first, atoms in the $F = 4, m_F = 0$ state are transferred to the $F = 3, m_F = 0$ state. This is done in a microwave state selection cavity (c). Here a magnetic field is applied and the clock transition is excited by a microwave π pulse. All atoms remaining in the $F = 4$ state are then removed by a clearing laser tuned to their specific resonance (d). The resulting cloud passes the Ramsey cavity where the atoms interact with the microwave field for the first time (e). After reaching the apogee (f), the cloud begins to descend and several hundred milliseconds after the first interaction it passes the Ramsey cavity on the way down (g). In a last step, detection lasers probe the atom state population by induced fluorescence (h). The atoms in the $F = 3$ and $F = 4$ states are detected separately. The detector signal is used by a computer to control the frequency of the interrogation field.

2.3.2 Fountain design

A schematic diagram of PTB's caesium fountain clock CSF2 is shown in Figure 2.7 [12]. The cooling zone is located in the lower part of the vacuum enclosure and has several windows used to feed the laser beams. Slightly above the cooling zone is the state selection cavity, surrounded by field coils, used to manipulate the Zeeman splitting of the hyperfine levels. The adjacent detection zone contains several windows for lasers and photo detectors. The Ramsey cavity and the upper part of the ballistic trajectory are screened by magnetic shields, field coils are used to apply a homogenous magnetic field. Two vacuum pumps are located at the top and bottom. Not shown is the caesium reservoir, located close to the cooling zone. It is temperature controlled in order to obtain a caesium partial pressure of about 10^{-6} Pa in the cooling zone. Due to the ballistic flight, the Ramsey time depends on the launch height h_{max} of the atoms with respect to the Ramsey cavity:

$$T_R = 2\sqrt{\frac{2h_{max}}{g}}, \tag{2.4}$$

where g is the standard acceleration due to gravity. In CSF2, the apogee is located 36.5 cm above the Ramsey cavity, resulting in a Ramsey time of about 0.54 s and a line width $\delta \approx 0.9$ Hz. The duration of a complete fountain cycle is about 1.2 s. Most caesium fountains use similar flight parameters.

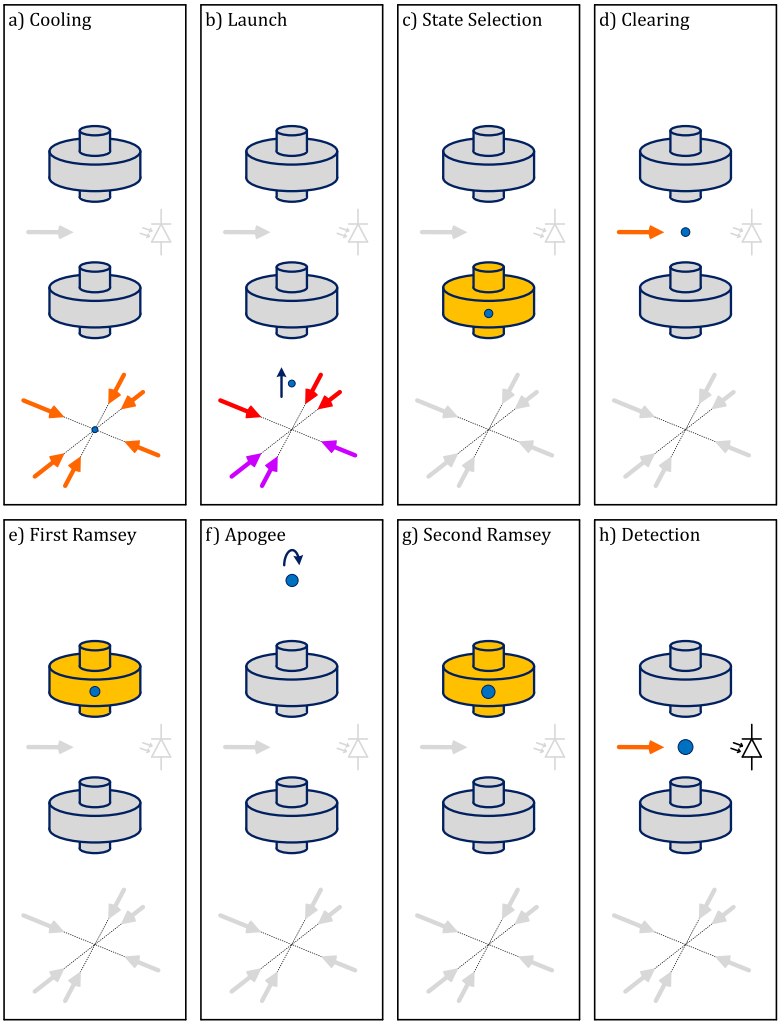

Figure 2.6: Operation sequence of an atomic fountain clock. Shown are the cooling zone, the state selection resonator, the clearing and detection zone and the Ramsey resonator (from bottom to top).

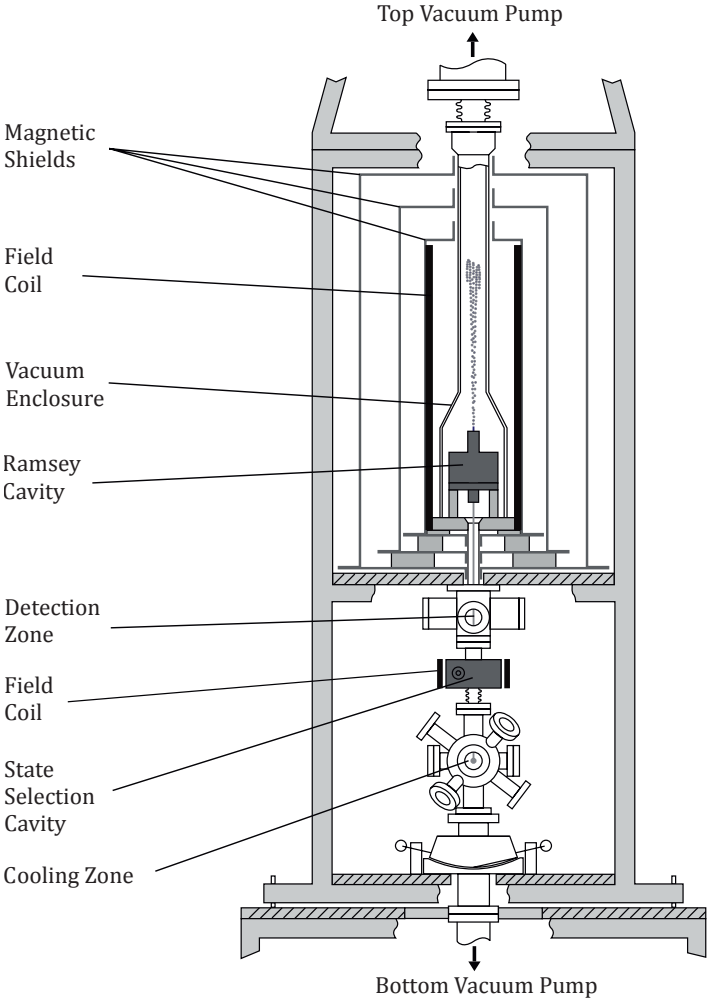

Figure 2.7: Schematic diagram of the caesium fountain clock CSF2 [12]

2.3.3 Statistical uncertainty

In atomic fountain clocks, several noise effects contribute to the statistical uncertainty of a measurement. In this work, two major contributions to the statistical uncertainty need to be considered, namely the quantum projection noise [13, 14] and the Dick effect [9].

Quantum projection noise

A fountain clock is alternately probing the left and right sides of the central Ramsey fringe. The outcome of this quantum measurement cannot be predicted with certainty as the obtained transition probability is neither 1 nor 0. The associated fluctuations are known as quantum projection noise (QPN) [13]. For long measurement durations with respect to the fountain cycle time T_C ($\tau \gg T_C$), the fountain instability resulting from QPN can be expressed as [14]:

$$\sigma_y(\tau) = \frac{\delta}{\pi f_0}\sqrt{\frac{T_C}{\tau \cdot N_{at}}}, \tag{2.5}$$

where δ is the line width and N_{at} the total detected number of atoms in the $F = 3$ and $F = 4$ hyperfine components of the caesium ground state. Increasing the number of probed atoms will lead to a reduction of the relative quantum projection noise. The atom number can be increased by prolonging the cooling process at the beginning of the fountain cycle.

However, longer loading times will reduce the duty cycle of the fountain and increase the dead time between consecutive interrogations of the atoms. On the other hand, it is possible to use optical pumping [63] or a low-velocity intense source of atoms [64–66] to increase the number of atoms independent of the loading time.

Dick effect

The resonant field in the Ramsey cavity is driven by a microwave signal, the Ramsey interrogation signal. Phase noise contained in this signal will perturb the phase of the microwave field experienced by the atoms during the two Ramsey interactions. This will result in the addition of a random phase offset to the phase difference accumulated during the Ramsey time,

and thus to a random change of the detected transition probability. The detector signal is used in a control loop to steer the frequency of the field-driving signal, effectively converting the phase noise into frequency noise.

Due to the pulsed operation of the clock, even harmonics of the pulse rate are subject to aliasing and the phase noise around these harmonics is down-converted into the base band. This effect is known as the Dick effect [9], and the resulting frequency noise contribution may limit the stability of a fountain clock. The Dick effect depends upon the fountain timing and the phase noise of the Ramsey interrogation signal [67, 68]. The Ramsey interrogation signal phase noise depends on the synthesizer and the local oscillator. Low-noise 5 MHz quartz oscillators have been widely used as local oscillators in atomic fountains. In this case, the Dick effect limits the frequency stability of an atomic fountain to about $1 \times 10^{-13}(\tau/s)^{-1/2}$ [69].

An expedient way to reduce the Dick effect is the utilization of a local oscillator with superior phase noise close to the carrier. A possible choice of oscillator would be a cryogenic sapphire oscillator [70–72] or a microwave source locked to an optical resonator [73–76]. When an optically stabilized microwave is used, the Dick effect can be reduced to less then $5 \times 10^{-15}(\tau/s)^{-1/2}$ [20], well below the contribution of the QPN. At this level, the Dick effect would thus be insignificant for the statistical uncertainty of the fountain.

2.3.4 Systematic uncertainty

Systematic effects can lead to a shift between the detected resonance frequency and the unperturbed resonance frequency f_0 [26]. These frequency shifts are individually evaluated for a specific fountain and can depend on operation parameters. The evaluation of each shift is associated with an uncertainty. These systematic uncertainties are designated as type B uncertainties (u_b) [77]. Each shifting effect, the applied correction, and the corresponding uncertainty at 1σ are listed in a dedicated fountain uncertainty budget.

Three contributions to the systematic uncertainty of a fountain clock are closely related to the microwave signal generation: perturbations of the resonant microwave field inside the Ramsey cavity, the collisional shift and uncontrolled interactions of the atoms with resonant fields during the Ramsey time.

Ramsey interrogation signal

During the fountain cycle, the caesium atoms are interacting two times with a resonant microwave field in the Ramsey cavity, driven by the Ramsey interrogation signal. Undesired spectral components in the Ramsey interrogation signal can lead to a shift of the detected frequency [8, 26]. The extent of the shift depends on the symmetry of the spectral components as well as their amplitude and frequency offset with respect to the carrier (the desired signal at f_0). These effects will be discussed and evaluated in Section 3.4.1.

Phase transients in the Ramsey interrogation signal can perturb the phase of the microwave field experienced by the atoms during the two Ramsey interactions. If these transients are synchronous to the fountain cycle, a fixed phase offset will be added to the phase difference accumulated during the Ramsey time, leading to a shift of the fountain frequency. A phase offset of 1 µrad between the two Ramsey interactions would result in a relative shift of 3×10^{-17}. To detect such cycle-synchronous phase differences, a phase transient analyzer is required. The development is described in Chapter 4, along with an evaluation of possible frequency shifts.

Collisional shift

During the fountain cycle, the atoms are subject to inter-atomic collisions that can lead to a shift of the detected frequency. The collisional cross-section for caesium is unusually large at the low cloud temperatures used in a fountain [16]. The collisional shift depends on the cloud density [16, 78] and is a significant factor in fountain uncertainty budgets [17, 79]. To determine the collisional frequency shift and to apply a correction, the fountain is operated with two different cloud densities. The cloud density can be varied by changing the loading time of the optical molasses or by modifying the parameters of the state selection process. From the frequency difference for the two atom densities, a collisional shift slope factor is estimated and used to calculate the frequency shift for the actual atom density.

However, it is not possible to directly detect the cloud density. Instead, the fluorescence signal measured during the detection is used to determine the atom number and calculate the cloud density. The proportionality between the number of atoms and the cloud density can be imperfect, resulting in an uncertainty in the estimation of the cloud density. This leads to an uncertainty in the estimation of the collisional shift.

The state selection can be performed by using a microwave field of constant amplitude and zero frequency detuning from the clock transition in the state selection cavity (resonant field method). The atom density is varied by applying different microwave amplitudes during the state selection process. For high atom densities, a π-pulse is applied, for low atom densities a $\pi/2$-pulse is used. The local transition probability depends on the pulse area experienced by the atoms which in turn depends on the local field amplitude and atom velocity. Due to the non-uniform distribution of the field amplitude across the cavity aperture and the velocity distribution of the atoms, the pulses experienced by the atoms deviate from ideal π or $\pi/2$-pulses. This leads to a non-uniform distribution of the transition probability. When the clearing laser is applied, the local probability distribution is converted into a local atom density variation. The corresponding systematic uncertainty of this method can be conservatively estimated to around 10% of the applied collisional shift correction [11, 80]. For atom numbers of 3×10^4, the systematic uncertainty associated with the collisional shift is on the order of 1×10^{-16} [12] when this method is used. With this atom number, fountain instabilities would be limited by quantum projection noise to the 10^{-13} level [14].

A much more robust method for controlling the cloud density in a fountain is rapid adiabatic passage (RAP) [18, 81]. In this scheme, a static magnetic field is applied and the frequency and amplitude of the microwave field are modulated during the state selection process. The field's frequency is chirped while its amplitude is modulated by a pulse. The detuning of the field frequency from resonance is given by $\Delta\omega(t)$. The amplitude change results in a time-dependence of the Rabi frequency (we neglect the effect of the frequency detuning), the instantaneous Rabi frequency is denoted as $\Omega_R(t)$. The adiabatic condition is given by [18]:

$$\frac{d}{dt}\Delta\omega(t) < \Omega_R^2(t). \tag{2.6}$$

In most applications of RAP, the detuning is varied from $-\Delta$ to $+\Delta$, leading to complete inversion. For the variation of the atomic density in fountain clocks, the RAP pulse is constructed such that its amplitude is maximum when the atom cloud is in the cavity center. At this point, the frequency detuning is zero. For sufficiently high microwave amplitudes and appropriate pulse parameters, the local transition probability is very close to 1. If the pulse is interrupted at zero frequency detuning, the transition probability is very close to 0.5, independent of the atom positions and velocities

in the state selection cavity [18]. It has been shown that the systematic uncertainty can be below 1% of the applied collisional shift correction when using the RAP method [19]. This will result in a collisional shift uncertainty of 4×10^{-17} [82] for atom numbers on the order of 10^6. At this atom number, a frequency instability of $2.6 \times 10^{-14}(\tau/s)^{-1/2}$ can be attained [66]. This method has been implemented in CSF2, the implementation and the parameters of the RAP pulses are discussed in Section 3.3.4.

Microwave leakage

Interactions between the atoms and a resonant field during the period of free evolution or before the probing of the atom state population can lead to frequency shifts [24, 25, 83]. Such a disturbing field can be a consequence of microwave leakage from the Ramsey or state selection cavity or the microwave synthesizer. The phase and amplitude of possible leakage fields can not be modeled with sufficient accuracy to apply a shift correction [25]. It is thus necessary to reduce their frequency shifting effects. Methods for the reduction can be passive - better shielding of the atom environment against such fields - or active, by changing the parameters of a possible leakage field, thus suppressing the interactions between the field and the atom cloud [26].

Passive methods include the screening of microwave components located outside the vacuum enclosure and the application of filters and isolators in the synthesizer. By adding a waveguide inside the vacuum enclosure on top of the Ramsey resonator, leakage fields above the Ramsey cavity can be significantly attenuated [84]. Due to the mechanical design of the waveguide, access to the atomic trajectory is limited, prohibiting the application of a vertical laser or the utilization of a top vacuum pump. Also, leakage fields below the Ramsey cavity are not affected and their frequency shifting effect has to be reduced with an active method [84].

Active methods can be based on a reduction of the amplitude of the leakage field [21] or a detuning of the field frequency [28]. These methods require a modulation of the Ramsey interrogation signal synchronous to the fountain cycle. This modulation can introduce cycle synchronous phase transients that have to be evaluated with a dedicated phase transient analyzer. Both methods have been employed in PTB's fountains, their implementation and evaluation are discussed in Chapter 5.

3 Microwave synthesis

Two microwave signals are required for the operation of a caesium fountain clock, driving the fields inside the Ramsey cavity and the state selection cavity. They are generated by a microwave synthesizer that is referenced to a low phase noise local oscillator. A possible choice of local oscillator is a microwave oscillator that is disciplined by a low phase noise quartz oscillator [85]. This combination is a robust system, albeit at a limited phase noise performance. A superior phase noise performance is achieved by using a cryogenic sapphire oscillator [70–72, 86–88]. It is also possible to transfer the superior phase noise performance of an optical resonator to the microwave regime [89, 90].

The early caesium fountains [17, 40, 42] employed microwave synthesis setups that were originally developed for caesium beam clocks [91]. A low noise quartz oscillator was used as a local oscillator, the caesium interrogation frequency was generated by means of frequency multiplication. While this was sufficient for the first implementations of laser-cooled atomic fountain clocks, the synthesizers were soon identified as a limiting factor for fountain uncertainties. This led to the development of several new microwave synthesizers, tailored to the specific fountain design and choice of local oscillator [54, 88, 92–98]. Our synthesizer is based on a design originally devised at the National Institute of Standards and Technology (NIST) [99]. It has been developed in a collaboration between PTB and the National Physical Laboratory of India (NPLI) [29]. Unlike prior synthesizers, it features a modular architecture: the synthesizer is partitioned into functional blocks. Each block combines associated functions and is implemented within a single module. The modular system ensures high reliability in tandem with high availability. The complexity of individual modules is kept low, module parameters can be specified and tested during manufacturing. Shielding of the modules ensures low electromagnetic interference and crosstalk. The modules are “hot-pluggable”, modules can be exchanged without disassembly, easing maintenance and upgrades.

Altogether, six synthesizers were fabricated at PTB, four are designated for local use, two were modified for usage at NPL India [100]. Two of the four

synthesizers used at PTB are allotted to the fountain clocks CSF1 and CSF2 whereas one pair of synthesizers was combined in a test rig to facilitate system evaluation and research.

In the following Section 3.1, the technical requirements for the microwave synthesizer are described, based on the permissible uncertainty contributions. An appropriate local oscillator for the synthesis is determined in Section 3.2. In Section 3.3, the general design of the synthesizer is described and an in-depth explanation of the different modules is given. The synthesizer performance is evaluated in Section 3.4, measurement data are presented and assessed to determine the contribution of the microwave synthesizer to the statistical and systematic uncertainty of the fountain clocks.

Several quantities can be used to describe phase noise. In this thesis, the phase noise will be reported according to IEEE Standard 1139 [101]. Phase noise will be represented by $\mathcal{L}(f)$ and given in dBc/Hz.

3.1 Technical requirements

During the fountain cycle, controlled interactions between the atoms and resonant fields take place in two confined spaces, the state selection cavity and the Ramsey cavity. The state selection process is relatively robust. On the contrary, interactions between the atoms and the resonant field throughout the Ramsey scheme are highly sensitive to external disturbances. Both cavities are driven by individual signals of the microwave synthesizer. These microwave signals are fundamental for the operation of the fountain, requiring a high level of operational performance.

3.1.1 State selection signal

Depending on the preparation method (resonant field or RAP), a microwave signal in the range of 9.19 GHz to 9.20 GHz is required to drive the resonant field inside the state selection cavity. The output level of the state selection signal has to be modulated within the range of -50 dBm to $+30$ dBm.

3.1.2 Ramsey interrogation signal

During the two Ramsey interactions, microwave pulses are applied to manipulate the caesium hyperfine state. The pulse area and thus the transition

probability depend on the amplitude and frequency of the resonant field in the Ramsey cavity, driven by the Ramsey interrogation signal. During regular fountain operation, the signal level is kept fixed and the frequency is controlled by the fountain control computer. A signal level in the range of $-45\,\mathrm{dBm}$ to $-20\,\mathrm{dBm}$ and a frequency tuning range of several kHz is required to accommodate different operating scenarios. In order not to limit the attainable short-term stability of the fountain clock, the frequency resolution has to be $100\,\mu\mathrm{Hz}$ at least. Also, the long-term frequency stability of the fountain should not be limited by instabilities or drifts of the signal-generating electronics.

The phase noise of the Ramsey interrogation signal can adversely affect the stability of the fountain (Dick effect). This effect is negligible for a phase noise $\mathcal{L}(f)$ of less than $-90\,\mathrm{dBc/Hz}$ from $1\,\mathrm{Hz}$ to $10\,\mathrm{Hz}$ offset from the carrier [69]. The phase noise of the Ramsey interrogation signal is limited by the phase noise of the local oscillator.

3.2 Local oscillator

3.2.1 Quartz oscillator

Quartz oscillators at $5\,\mathrm{MHz}$ can provide the best phase noise performance close to the carrier [102]. Their phase noise properties can be transferred to a microwave oscillator using a phase locked loop (PLL) [103] and a method of frequency conversion (frequency multiplication or frequency division). In the first scheme, the phase detection in the PLL is implemented in the microwave band. The output signal of the quartz oscillator is frequency multiplied using nonlinear elements and the microwave oscillator is phase locked to the resulting signal. In the latter scheme, the output signal of the microwave oscillator is divided down to match the frequency of the quartz oscillator and the output of the phase detector is used to lock the microwave oscillator. Both methods have their distinctive drawbacks, while frequency multipliers are very sensitive to thermal effects, frequency dividers are prone to additive phase noise [104].

Frequency multiplication or division affects the relative phase noise level of the converted signal [104]. When the output signal of a microwave oscillator at frequency f_{in} is converted to f_{out}, the phase noise of the output signal $\mathcal{L}_{\mathrm{out}}(f)$ at carrier frequency offset f can be calculated as:

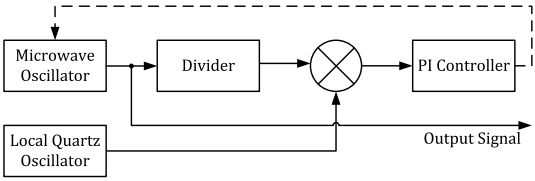

Figure 3.1: Combination of two oscillators with different frequencies

$$\mathcal{L}_{\text{out}}(f) = \mathcal{L}_{\text{in}}(f) - \log \frac{f_{\text{in}}}{f_{\text{out}}} \cdot 20\,\text{dB}. \tag{3.1}$$

We use a scheme based on frequency division, displayed in Figure 3.1. A quartz oscillator OSC8607 from Oscilloquartz [85] is the local oscillator. It is a very low noise 5 MHz oscillator with superior phase stability, this type of quartz oscillator is denoted as BVA (Boîtier à Vieillissement Amélioré - enclosure with improved aging). The disciplined microwave oscillator is a dielectric resonator oscillator (DRO) type from PSI, the DRO-9.600 [105]. It provides an output signal in the microwave frequency band at 9.6 GHz and has excellent phase noise properties far from the carrier. The phase noise properties of the two oscillators at their native frequencies are given in Table 3.1. The phase noise level of the OSC8607 at 9.6 GHz as derived from equation 3.1 is listed for comparison. To preserve the superior phase noise close to the carrier of the local quartz oscillator, the frequency division is performed with integrated circuits that feature a specified phase noise below this level [106, 107].

With the applied PLL bandwidth of 1 kHz, the phase noise at 9.6 GHz at carrier offsets of 1 Hz and 10 Hz can be expected to be -64 dBc/Hz and -79 dBc/Hz respectively. Due to the Dick effect, this would limit the fountain frequency stability to about $1 \times 10^{-13}(\tau/s)^{-1/2}$ [69].

3.2.2 Optically stabilized microwave

It has been shown that the superior phase noise of a laser locked to an optical resonator can be transferred to the microwave regime [89, 90]. The laser frequency is divided down to the microwave regime by means of a frequency comb. This microwave signal is used in a PLL to lock a DRO

Carrier offset f (Hz)	Phase noise $\mathcal{L}(f)$ (dBc/Hz)		
	OSC8607 at 5 MHz	OSC8607 at 9.6 GHz	DRO-9.600 at 9.6 GHz
1	-130	-64	
10	-145	-79	(-32)
100	-153	-87	-62
1000	-156	-90	-90
10000	-156	-90	-119

Table 3.1: Phase noise performance of the employed oscillators [85, 105]. The number in brackets indicates estimation based on [102].

at 9.6 GHz. The disciplined oscillator is used as a local oscillator for the caesium fountain clock [73–76]. The phase noise $\mathcal{L}(f)$ close to the carrier is below -95 dBc/Hz, at this level the fountain stability will not be limited by the Dick effect [20].

The optically stabilized microwave (OSM) comprises a fibre laser that is locked to a temperature controlled optical resonator as well as a frequency comb, requiring careful tuning and regular maintenance. This is a rather complex system in comparison to the robust approach with the BVA. To achieve a high availability, the microwave synthesizer was designed for the use of two different local oscillators, the OSM and the BVA disciplined DRO. The local oscillator selection is implemented in the microwave band at 9.6 GHz. The OSM is used as default and the fountain control has an automatic fall-back system to the BVA disciplined DRO.

3.3 Microwave synthesizer

3.3.1 Synthesizer principle

A signal with a frequency of 9.192 631 770 GHz is required to drive the resonant field inside a cavity, in the following abbreviated as 9.193 GHz. The signal has to be phase locked to the local oscillator (LO) at 9.6 GHz. To generate the required signals, we use a two-stage mixing approach with digital frequency synthesis [29]. This scheme requires the use of several filters to suppress undesired mixing components and maintain a high signal-to-noise ratio. The principle is shown in Figure 3.2, filters are omitted for clarity.

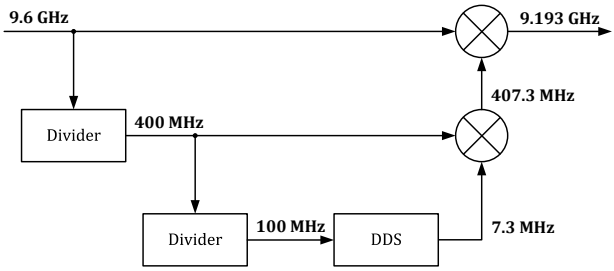

Figure 3.2: Synthesizer principle, filters are omitted

The output signal at 9.193 GHz is obtained by mixing the 9.6 GHz reference signal with a locally generated 407.3 MHz signal. This signal is generated in an additional mixing stage, using several dividers and a digital direct synthesizer (DDS) [108].

The digital frequency control is implemented at a frequency of 7.3 MHz, three orders of magnitude below the frequency of the output signal. This results in a minimal impact of phase noise from the frequency control path to the phase noise of the output signal, maintaining the low phase noise close to carrier of the LO. The output signal has a tuning range of ± 4 MHz featuring a frequency resolution of less than 1 µHz.

3.3.2 Synthesizer implementation

The synthesizer principle is realized in a modular system. Two independent frequency control sections are implemented for the Ramsey interrogation signal and the state selection signal to achieve a high crosstalk immunity. This includes dedicated mixers and a separate control of frequency and signal level for each signal path as well as the intensive use of filters. In the following figures, the modules are represented by gray boxes, they will be shown in condensed form, e.g. filters and computer connections are omitted.

The 9.6 GHz signal for the synthesizer can be sourced from two local oscillators (OSM and BVA) (Fig. 3.3). The OSM is the primary local oscillator, it directly supplies the required frequency. When referencing to the secondary local oscillator at 5 MHz, a DRO is disciplined to generate the required 9.6 GHz signal, using the scheme described in Section 3.2.1. A

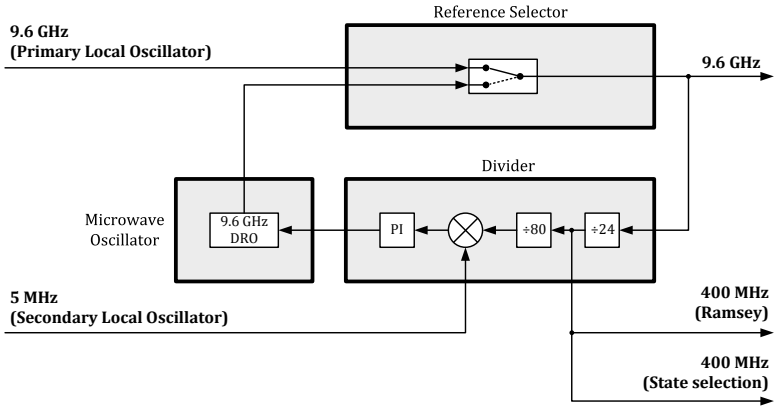

Figure 3.3: Synthesizer - reference selector and divider

400 MHz signal is sourced to the frequency control sections for the Ramsey interrogation signal and the state selection signal. A picture of the divider module is shown in Figure 3.6.

The setup for frequency control of the Ramsey interrogation signal is depicted in Figure 3.4, the setup for the state selection signal is similar. The 400 MHz signal from the reference section is divided down to 100 MHz to serve as a reference for the DDS module. The DDS output frequency is controlled by the fountain control computer by sending a tuning word to the DDS chip. The employed chip ISL5314 from Intersil [109] has a 48-bit frequency tuning word, resulting in a frequency resolution of $50\,\mathrm{MHz}/2^{48} \approx 0.2\,\mu\mathrm{Hz}$. Using an active single sideband (SSB) mixer [110, 111] to achieve a high suppression of undesired mixing components, the 7.3 MHz output from the DDS is mixed with the 400 MHz signal. A picture of the single sideband mixer module is shown in Figure 3.7.

Due to the modular design and the choice of reference frequency common to a range of commercial RF synthesizers, the frequency control section can easily be modified. Modifications for special experiments are described in Sections 3.3.4 and 5.2.

The two 407.3 MHz signals are supplied to a single microwave mixer module, where they are mixed with the 9.6 GHz signal from the microwave selector (Figure 3.5). The microwave mixer module outputs two signals at 9.193 GHz, used to drive the Ramsey cavity and the state selection cavity.

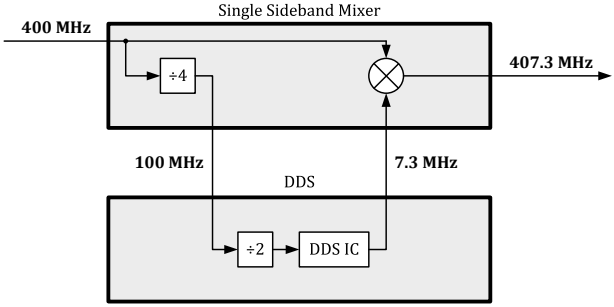

Figure 3.4: Synthesizer - frequency control and RF mixing for the Ramsey interrogation signal

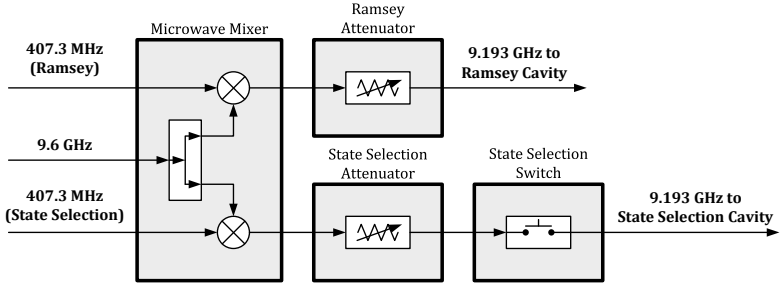

Figure 3.5: Synthesizer - microwave mixing and amplitude control

The crosstalk between these channels was verified by a measurement to be below $-80\,\mathrm{dB}$. The level of the signal fed to the Ramsey cavity is set with a continuously variable attenuator with negligible impact on the phase stability.

To facilitate control of the atom cloud density, the signal for the state selection is routed through a voltage controlled attenuator which provides a damping of the signal of up to 80 dB. In addition, to further reduce potential microwave leakage from the state selection cavity, the connection can be disconnected using a switch, resulting in an additional damping of at least 120 dB. The connection to the fountain control interface is realized via an external control module.

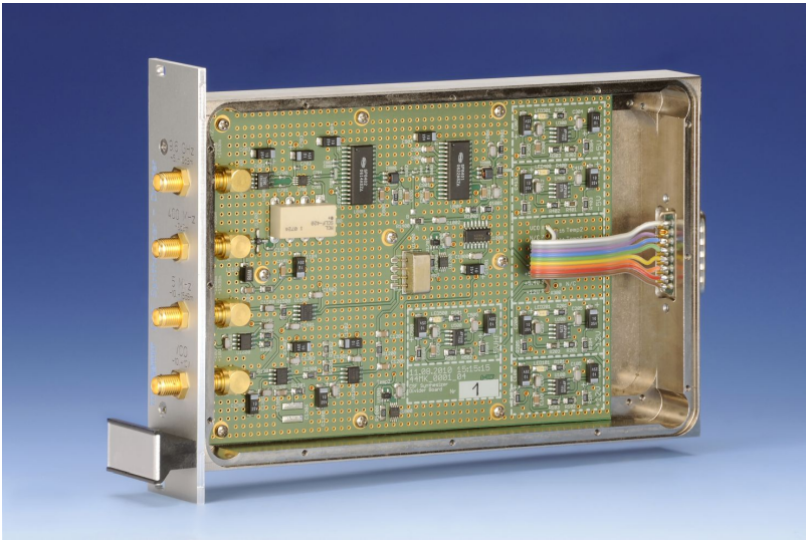

Figure 3.6: Synthesizer - divider module

Figure 3.7: Synthesizer - single sideband mixer

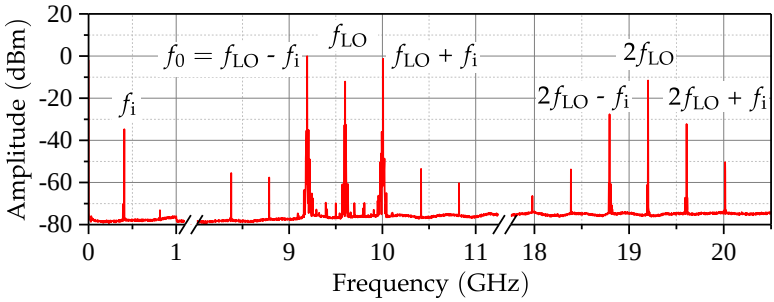

Figure 3.8: Spectrum of the Ramsey interrogation signal

3.3.3 Output spectrum

The spectrum of the Ramsey interrogation signal was measured in the frequency range from 1 MHz to 26 GHz. As is shown in Figure 3.8, the frequency axis is split into three ranges of interest. The output spectrum contains the intermediate frequency f_i at 407.3 MHz, as well as several frequencies centered around f_{LO} (9.6 GHz) and $2f_{LO}$. These are products from the nonlinear mixing process, at frequencies of $m \cdot f_{LO} \pm n \cdot f_i$ (for integer m and n). The two main spectral components are the desired frequency $f_0 = f_{LO} - f_i$ at 9.193 GHz and the mirror frequency $f_{LO} + f_i = 10.007$ GHz.

The synthesizer was designed to drive the resonant microwave fields the caesium atoms are exposed to. The interaction between the atoms and the microwave fields is limited to a tiny portion of the spectrum, defined by the atomic resonance. Physical filters at the synthesizer output were consequently omitted, as they are prone to temperature induced phase drifts.

3.3.4 Implementation of rapid adiabatic passage

To estimate a correction for the frequency shift due to inter-atomic collisions, the fountain is operated with two different cloud densities alternatingly [112]. Depending on the method of density control, this correction can be subject to a relevant relative uncertainty, resulting in a significant contribution to the systematic uncertainty of the fountain. Building upon the modular synthesizer, the method of rapid adiabatic passage (RAP) [18]

was implemented in CSF2, resulting in a significant reduction of the collisional shift uncertainty [19]. Details on the RAP method and the parameter space were given in Section 2.3.4.

The RAP method can not be implemented in CSF1 [11]. In this fountain, the state selection cavity is situated next to the Ramsey cavity and the magnetic field strength required for the RAP method can disturb the subsequent Ramsey interaction.

The RAP method requires a modulation of the state selection signal frequency and amplitude. During the state selection process, a magnetic field is applied to manipulate the transition frequencies of the $m_F \neq 0$ substates. The interaction between the atom cloud and the microwave field in the state selection takes about 10 ms in CSF2 [12]. During this time, the signal frequency f is chirped over resonance while its amplitude A is modulated by a pulse. The detuning from resonance given by $\Delta f(t)$ has to fulfill the condition [18]:

$$\frac{d}{dt}\Delta f(t) \propto A^2(t). \tag{3.2}$$

A pulsed signal contains harmonics that could result in the preparation of undesired $m_F \neq 0$ substates. The pulse shape has to be selected such that harmonics are kept to a minimum [113]. It has been shown that a Blackman pulse can be used to minimize off-resonant excitation [114]. When a Blackman pulse with a duration of 10 ms is used, the excitation of $m_F = \pm 1$ substates can be suppressed (Figure 3.9).

The progression of amplitude and frequency during the state selection process for a Blackman pulse is shown in Figure 3.10. When this pulse and the corresponding frequency chirp are applied during the state selection process, 100 % of the atoms are prepared in the desired state. When the adiabatic passage is stopped when the state selection frequency is on resonance, a preparation efficiency of (50.0 ± 0.4) % can be realized [19]. The shape of the resulting amplitude pulse and the corresponding frequency chirp are shown in Figure 3.11.

To generate the required signals, a two-channel arbitrary waveform generator was utilized. One channel was used to generate a chirped signal at a frequency of 7.3 MHz, replacing the DDS-based frequency synthesizer for the state selection. A second channel was used to generate the Blackman and half-Blackman pulses, fed to the control module of the state selection

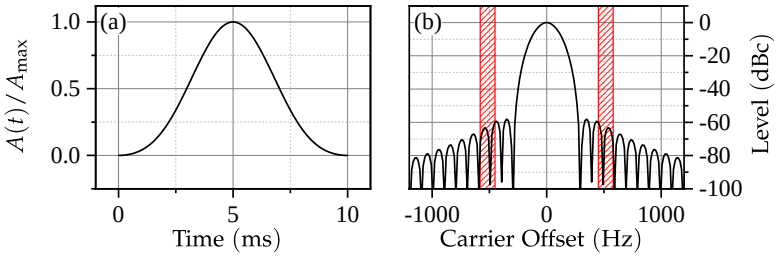

Figure 3.9: Blackman pulse with a duration of 10 ms. Time domain (a) and frequency domain (b). Red boxes indicate the excitation frequencies of the $m_F = \pm 1$ substates at normal operating conditions of CSF2 [115].

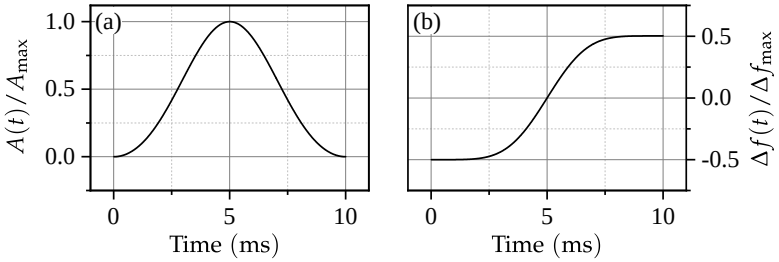

Figure 3.10: RAP modulation scheme for 100 % preparation efficiency (simulated values). Blackman pulse (a) and corresponding frequency chirp (b).

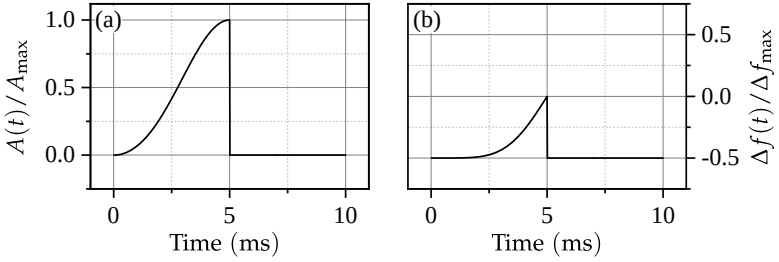

Figure 3.11: RAP modulation scheme for 50 % preparation efficiency (simulated values). (a) Half-Blackman pulse (a) and corresponding frequency chirp (b).

attenuator. The magnetic field inside the cavity was driven by a programmable current source. The entire sequence was controlled by the fountain control computer.

3.4 Characterization

Several properties of the field-driving microwave signals can have a direct influence on the statistical and systematic uncertainty of the caesium fountain. The systematic uncertainty contribution of the microwave synthesizer should be on the low 10^{-17} level, its statistical uncertainty contribution should be negligible. In the following, the relevant properties of the Ramsey interrogation signal will be evaluated and the implications on the fountain uncertainty will be determined. This includes the spectral purity and the phase noise close to the carrier as well as the long-term stability of the synthesized signal.

3.4.1 Spectral purity

It is well known that spectral impurities in the excitation signal can lead to frequency shifts [8, 116, 117]. Such impurities can be introduced by components used for the microwave synthesizer (e.g. dividers, amplifiers, digital synthesis chips) [104, 118–121] or can be a result of mains interference. We have assessed the extent of frequency shifts, based on an analysis of carrier sidebands. Sidebands are distinguished into spectral components at frequencies below the carrier - lower sidebands (LSB) and spectral components at frequencies above the carrier - upper sidebands (USB). When both LSB and USB contain the same power, the corresponding sidebands are symmetric. If the power levels of LSB and USB differ, the sidebands are referred to as asymmetric.

Asymmetric sidebands will lead to a second-order shift of the fountain frequency [8, 122]. The shift depends on the carrier offset, the sideband power and the sideband asymmetry, i.e. the difference between LSB and USB. The shift is maximum if only a single sideband is present (either LSB or USB). The Ramsey interrogation signal was examined for sidebands and, in a subsequent step, the worst case second-order frequency shift was calculated.

Due to the pulsed operation of the fountain, symmetric sidebands can cause first-order frequency shifts when the sideband offset frequency is coherent

with the measurement cycle [123, 124]. The frequency shifting mechanism is different for sidebands resulting from phase modulation (PM) or amplitude modulation (AM). If the sideband is the result of PM, the phase of the microwave field experienced by the atoms during the two Ramsey interactions is affected. This will result in the addition of a phase offset to the phase difference accumulated during the Ramsey time. In the case of AM, the pulse areas of the two $\pi/2$-pulses applied during the Ramsey interactions are disturbed and the detected transition probability is affected. The duration of the Ramsey interaction is on the order of 10 ms, during this time the atoms are exposed to the modulation. If the modulation period is less than 4 ms (equal to a carrier offset frequency of 250 Hz), the atoms sample a large variation of the sideband phase. This leads to an elimination of the frequency shift [123].

The extent of the first-order shift depends on the sideband modulation (AM or PM), the sideband power and the relation between offset frequency and fountain cycle time. The sideband offset frequencies and power levels are known from frequency-domain measurements. For sidebands at carrier offsets below 250 Hz, the modulation type was determined and the first-order frequency shift was evaluated. The calculations were performed for CSF1 and CSF2, taking into account their individual cycle times.

Carrier sidebands

Spectral components in the Ramsey interrogation signal can be evaluated with a spectrum analyzer [125]. Using the model FSWP26 with option B1 from Rohde & Schwarz [126], we determined the carrier sidebands at f_0 individually for the two available reference options, BVA and OSM. The spectra of the Ramsey interrogation signal were measured with a resolution bandwidth (RBW) of 1 Hz at spans of 1 kHz and 100 kHz.

Shown in Figure 3.12 is the spectrum of the synthesizer output signal when referenced to the 5 MHz BVA quartz, centered at the 9.193 GHz carrier frequency. The measurement presented on top of the figure shows the spectrum close to the carrier with a span of 1 kHz while the data displayed on the bottom graph shows the spectrum at a larger span of 100 kHz.

Clearly visible are several spectral components close to the carrier at multiples of the mains frequency (50 Hz) and a small number of peaks further off. The noise level at 500 Hz carrier offset frequency is -90 dBc. Spectral components with a signal level above -90 dBc are summarized in Table 3.2.

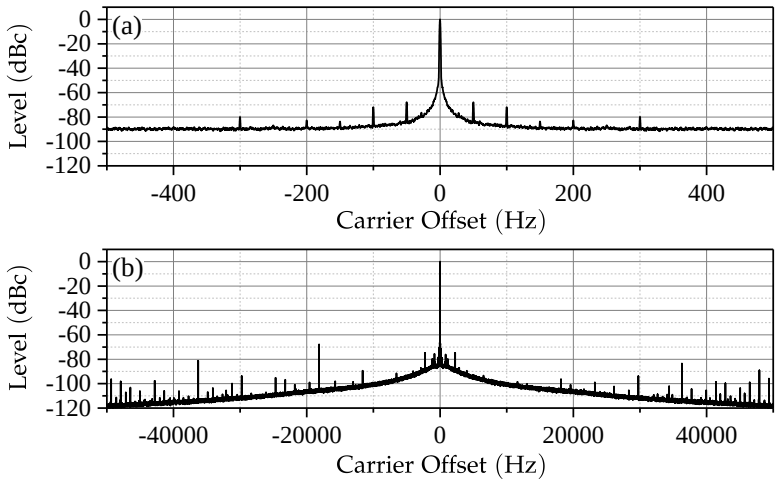

Figure 3.12: Spectrum of the Ramsey interrogation signal, centered at the 9.193 GHz carrier frequency when referenced to the 5 MHz BVA quartz. (a) close to carrier. (b) far from carrier.

Carrier Offset (Hz)	LSB Level (dBc)	USB Level (dBc)	Difference (dB)
50	-68	-68	0
100	-72	-72	0
150	-84	-84	0
200	-83	-83	0
300	-80	-80	0
840	-76	-76	0
1156	-80	-80	0
2262	-75	-75	0
11621	-89	-98	9
18151	-68	-92	24
36301	-81	-75	6
47920	-98	-89	9

Table 3.2: Sideband characteristics of the Ramsey interrogation signal when referenced to the 5 MHz BVA quartz. Broken down into signals below the carrier (lower sidebands - LSB) and above the carrier (upper sidebands - USB).

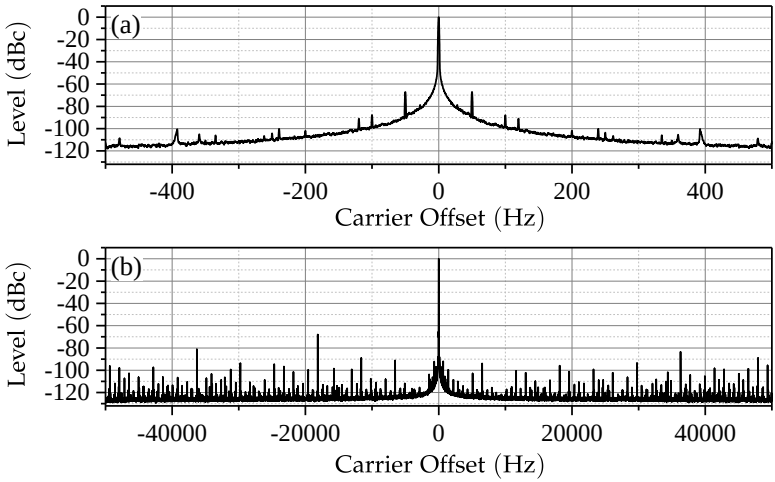

Figure 3.13: Spectrum of the Ramsey interrogation signal for different frequency ranges, centered at the 9.193 GHz carrier frequency when referenced to the OSM.

A similar examination was carried out for the output signal of the microwave synthesizer when referenced to the OSM. Again, the spectra of the Ramsey interrogation signal were measured with a RBW of 1 Hz at spans of 1 kHz and 100 kHz. The results are presented in Fig. 3.13, with the top graph and bottom graph showing the spectrum close to the carrier and further off, respectively. The noise floor close to the carrier is much lower, ascribed to the superior phase noise properties of the OSM. Further off from the carrier, the spectrum contains many spectral components that originate from the optical stabilization system. Due to their low level, they will not have detrimental effects. Spectral components at levels above -90 dBc are summarized in Table 3.3.

Second-order frequency shifts

We estimated the worst-case second-order frequency shift caused by sidebands. The shift is maximum if the sideband power is contained within a single sideband, either LSB or USB. Taking the maximum level for each sideband from Tables 3.2 and 3.3, the worst-case shift was calculated. The sidebands and their associated shifts were treated as independent, the amounts

Carrier Offset (Hz)	LSB Level (dBc)	USB Level (dBc)	Difference (dB)
50	-67	-67	0
100	-88	-88	0
120	-91	-91	0
6531	-91	-94	3
11621	-89	-101	12
18151	-68	-92	24
36301	-81	-75	6
47920	-98	-89	9

Table 3.3: Sideband characteristics of the Ramsey interrogation signal when referenced to the OSM. Broken down into signals below the carrier (lower sidebands - LSB) and above the carrier (upper sidebands - USB).

of the shift were calculated and then linearly summed. For the calculations, the procedure described in [8] was used. The results are given in Tables 3.4 and 3.5. The maximal expected frequency shift is 3.8×10^{-18} when referenced to the BVA and 4×10^{-18} when referenced to the OSM.

Modulation analysis

Using only data obtained from the frequency spectrum it is not possible to determine the modulation type. The FSWP26 also offers a dedicated noise analysis mode. In this mode, the single sideband noise (SSB noise) of a carrier is measured, differentiated into AM noise and PM noise. The SSB noise resulting from PM corresponds to the phase noise $\mathcal{L}(f)$. Sidebands resulting from modulation are shown as spurious signals. This permits to differentiate the carrier sidebands from Tables 3.2 and 3.3 into AM and PM. Only symmetric sidebands at carrier offsets below 250 Hz were considered.

The Ramsey interrogation signal at 9.193 GHz was investigated, using the 5 MHz BVA quartz as a reference (Figure 3.14). Shown in red is the noise resulting from phase modulation (PM noise) whereas the noise due to amplitude modulation (AM noise) is depicted in blue. Sidebands at 50 Hz, 100 Hz, 150 Hz and 200 Hz are clearly visible in the PM plot with no apparent contribution of AM.

We measured the SSB noise of the Ramsey interrogation signal at 9.193 GHz when referenced to the OSM. Shown in red in Figure 3.15 is the PM noise of the signal, the AM noise is depicted in blue. The sidebands at 50 Hz, 100 Hz

Carrier Offset (Hz)	Max. Sideband Level (dBc)	Rel. Frequency Shift
50	-68	3.2×10^{-18}
100	-72	5.0×10^{-19}
150	-84	3.0×10^{-20}
200	-83	2.0×10^{-20}
300	-80	3.0×10^{-20}
840	-76	3.0×10^{-20}
1156	-80	7.0×10^{-21}
2262	-75	4.0×10^{-21}
11621	-89	8.0×10^{-23}
18151	-68	7.0×10^{-21}
36301	-75	7.0×10^{-22}
47920	-89	2.0×10^{-23}
	Sum:	3.8×10^{-18}

Table 3.4: Worst-case estimate of the second order fountain frequency shift when the synthesizer is referenced to the BVA

Carrier Offset (Hz)	Max. Sideband Level (dBc)	Rel. Frequency Shift
50	-67	4.0×10^{-18}
100	-88	2.0×10^{-20}
120	-91	5.0×10^{-21}
6531	-91	9.0×10^{-23}
11621	-89	8.0×10^{-23}
18151	-68	7.0×10^{-21}
36301	-75	7.0×10^{-22}
47920	-89	2.0×10^{-23}
	Sum:	4.0×10^{-18}

Table 3.5: Worst-case estimate of the second order fountain frequency shift when the synthesizer is referenced to the OSM

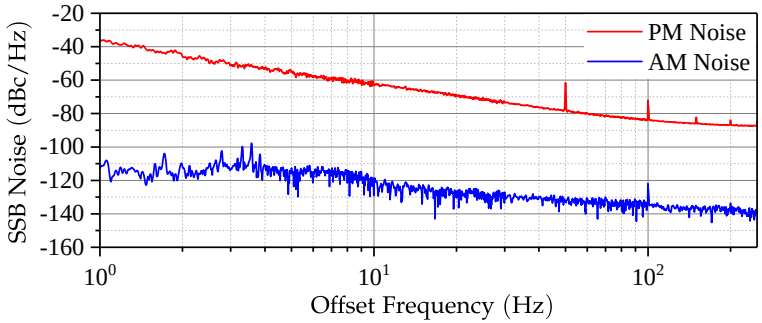

Figure 3.14: Single sideband noise measured at 9.193 GHz carrier frequency when the synthesizer is referenced to the BVA

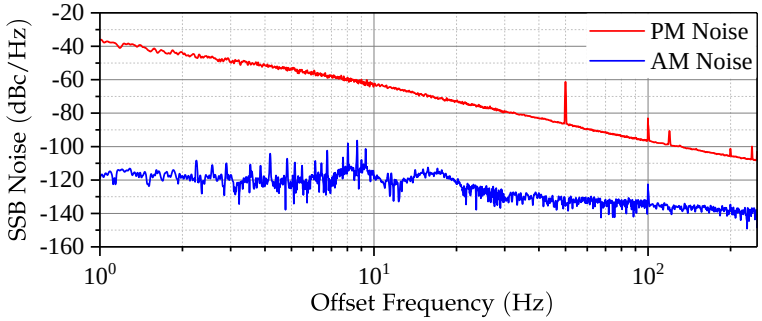

Figure 3.15: Single sideband noise measured at 9.193 GHz carrier frequency when the synthesizer is referenced to the OSM

and 120 Hz are clearly visible in the PM curve and do not show a significant signature in the AM plot. Two additional sidebands at 200 Hz and 240 Hz can be identified, no frequency shifting effect is to be expected due to their low levels.

First-order frequency shifts

The sidebands at carrier offsets below 250 Hz result from PM. Their carrier offset frequencies will be denoted as f_{i}. The first-order frequency shift resulting from sideband i depends on the relation between its modulation

period T_i and the fountain cycle time T_cycle [124]. If T_cycle is an integer multiple of T_i, a fixed phase offset will be added to the phase difference accumulated during the Ramsey time, leading to a constant shift of the fountain frequency.

This phase offset can be distributed over several cycles such that the integral of the resulting frequency shift is zero. By choosing the cycle time to be an odd multiple of $T_\mathrm{i}/2m_\mathrm{i}$, the phase offset would be alternating, distributed over $2m_\mathrm{i}$ cycles:

$$T_\mathrm{cycle} = (2n_\mathrm{i} + 1) \cdot \frac{T_\mathrm{i}}{2m_\mathrm{i}} \tag{3.3}$$

with integer $n_\mathrm{i}, m_\mathrm{i}$ and $n_\mathrm{i} \gg m_\mathrm{i}$. The frequency shift caused by the sideband with index i at carrier offset frequency f_i is zero after $2m_\mathrm{i}$ cycles. In the simplest case, for $m_\mathrm{i} = 1$, each cycle has an additional π phase difference with respect to the previous cycle. The frequency shift caused by the modulation would be alternating, resulting in a cancellation after 2 cycles.

We calculated the number of averaging cycles required for a cancellation of the first-order frequency shifts. For the calculation to be valid for BVA as well as OSM operation, the sidebands at carrier offsets below 250 Hz given in Tables 3.2 and 3.3 were combined. The calculations are based on the the cycle times of CSF1 (1114.5 ms) and CSF2 (1234.5 ms). The number of averaging cycles for both fountains are identical, as their cycle times differs by 120 ms, the least common multiple of the modulation periods. The result of the calculation is given in Table 3.6. For both fountains the condition $n_\mathrm{i} \gg m_\mathrm{i}$ is fulfilled.

The least common multiple of the different values of m_i given in Table 3.6 is 100. Thus every 200 cycles, the first-order frequency shift resulting from symmetric sidebands in the Ramsey interrogation signal will be zero.

3.4.2 Phase noise

The phase noise measurements shown in Figures 3.14 and 3.15 were performed with the FSWP26 at f_0. For small carrier frequency offsets, the phase noise specifications for the FSWP26 exceed the phase noise of the local oscillators the synthesizer is referenced to [126]. The acquired data thus can not be used to determine the phase noise of the synthesizer. Instead, two synthesizers and a heterodyne mixing technique are used to evaluate

f_i (Hz)	T_i (ms)	m_i	n_i	
			CSF1	CSF2
50	20	20	1114	1234
100	10	10	1114	1234
120	8,33	25	3343	3703
150	6,66	20	3343	3703
200	5	5	1114	1234

Table 3.6: Ramsey interrogation signal sidebands, modulation periods and corresponding values for m_i and n_i required for cancellation of the first-order frequency shift.

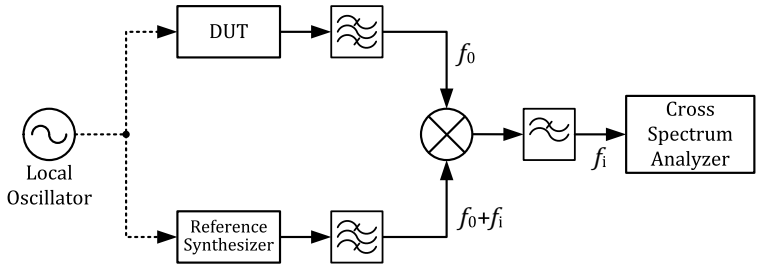

Figure 3.16: Measurement setup for phase noise and Allan deviation

the phase noise of a single synthesizer (Fig. 3.16). Two synthesizers, the device under test (DUT) and a reference synthesizer, are locked to the same local oscillator. Both synthesizers are tuned to different output frequencies, f_0 and $f_0 + f_i$. Their output signals are fed to a mixer, resulting in an intermediate frequency f_i that can be analyzed. As only the phase noise of the signal at f_0 is of interest, narrow bandpass filters are inserted between the synthesizer outputs and the mixer. Under the realistic assumption that both synthesizers equally contribute to the phase noise of f_i, their individual phase noise can be calculated by subtracting 3 dB from the measured phase noise. To avoid signal deterioration from the internal oscillator of the measurement device, a cross spectrum analyzer is used. It utilizes a direct sampling technique and applies digital cross correlation to remove noise contributions from its local oscillator and the sampling process [127]. The used cross spectrum analyzer TimePod 5330A from miles.io [128] is now available as model 3120A from Microsemi [129].

The phase noise of the synthesizer was determined for the two available reference options, BVA and OSM. For BVA operation, the local oscillator frequency is 5 MHz. In each synthesizer, a 9.6 GHz DRO is phase locked to the 5 MHz signal, as shown in Figure 3.3. The locking bandwidth is 1 kHz. The measurement data are displayed in Figure 3.17, in which the black curve shows the phase noise of a single synthesizer. The phase noise specifications of the local 5 MHz BVA oscillator OSC8607 [85] are shown in red with square symbols. The Dick effect is dominated by noise close to the carrier, at offset frequencies between 1 Hz and 10 Hz [69]. Here the phase noise of the synthesizer is at least 6 dB better than the employed local oscillator. This phase noise is the result of additive noise from the frequency dividers in the PLL. For offset frequencies above the locking bandwidth of 1 kHz, the phase noise of the two synthesizers is uncorrelated. The measured phase noise can be attributed to the two DROs. The specified phase noise of the DRO [105] is displayed in green with triangle symbols. The instrument noise is well below the measured values.

We now determined the residual phase noise of the synthesizer when referenced to the 9.6 GHz OSM. In this operational mode, the local oscillator frequency is 9.6 GHz and the PLL is not utilized. The phase noise $\mathcal{L}(f)$ of a single synthesizer is displayed as black curve in Figure 3.18. At 1 Hz offset, the phase noise is about $-100\,\mathrm{dBc/Hz}$ and drops well below $-100\,\mathrm{dBc/Hz}$ for higher offset frequencies. The overall phase noise performance is limited by amplifier phase noise [119]. Shown for reference is the phase noise of the OSM (red with square symbols) [20]. The instrument noise is at least 20 dB below the measured values.

The fountain instability caused by the Dick effect is related to the fountain cycle time and the phase noise properties of the Ramsey interrogation signal. It would be limited to about $1 \times 10^{-13}(\tau/s)^{-1/2}$ when the BVA is used as a reference [69]. When the OSM is used, the instability attributed to the Dick effect can be reduced to a level well below the instability resulting from QPN. For fountain cycle times of 1114.5 ms and 1234.5 ms for CSF1 and CSF2, respectively, the instability contribution of the Dick effect in this case was estimated to be $4.8 \times 10^{-15}(\tau/s)^{-1/2}$ and $5.7 \times 10^{-15}(\tau/s)^{-1/2}$ [20]. The QPN depends on the number of detected atoms, the atom number for each fountain is selected in consideration of the systematic uncertainty contribution from the collisional shift. It has been shown that CSF1 can be operated at $9.1 \times 10^{-14}(\tau/s)^{-1/2}$, while CSF2 can reach a level of $2.5 \times 10^{-14}(\tau/s)^{-1/2}$ [20].

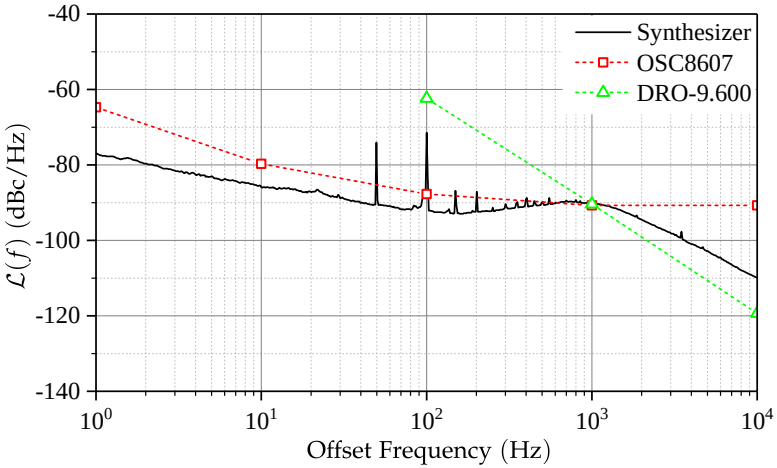

Figure 3.17: Phase noise $\mathcal{L}(f)$ of a single synthesizer chain for BVA operation at 9.193 GHz

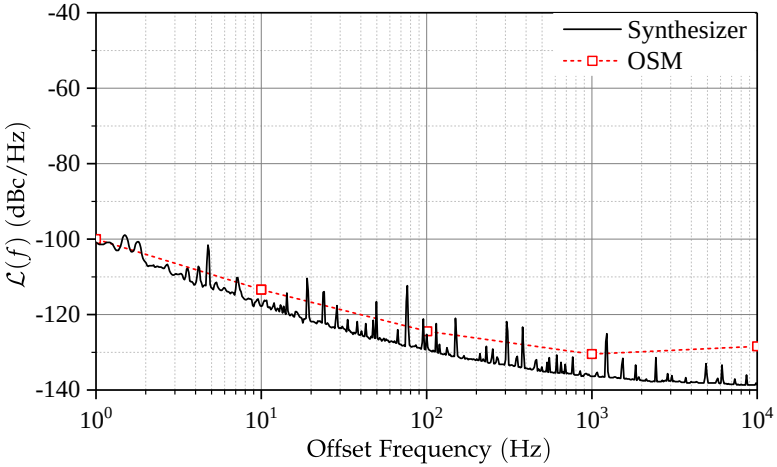

Figure 3.18: Phase noise $\mathcal{L}(f)$ of a single synthesizer chain for OSM operation at 9.193 GHz

3.4.3 Long-term phase stability

Using the heterodyne measurement scheme, the long-term phase stability of the synthesizer was evaluated. The measurement was set up in a temperature stabilized room and the Allan deviation $\sigma_y(\tau)$ for the combination of two synthesizers was determined. The values are compared with the fountain frequency instability. Due to the lower systematic uncertainty of the collisional shift correction, CSF2 can utilize higher atom numbers in regular operation and thus reaches lower instabilities than CSF1. In the following, the instabilities for CSF2 are given for reference.

It has to be considered that phase deviations resulting from external influences are strongly suppressed in this measurement setup, as both synthesizers are exposed to the same environment. We assume that the temperature has by far the largest impact on the individual synthesizer, compared to other environmental factors, e.g. ambient pressure and humidity. The synthesizer was examined for temperature induced phase shifts, individually determining the effect of each module. The overall temperature sensitivity of the microwave synthesizer was determined to be 16 ps/K, primarily resulting from the frequency dividers used in the PLL. These dividers are only used when the Ramsey interrogation signal is referenced to the local 5 MHz BVA oscillator. When referenced to the OSM, the temperature sensitivity of the synthesizer is less than 1 ps/K.

The synthesizer will be used in a temperature stabilized environment. The expected temperature changes are reasonably small and we assume the fluctuations of the synthesizer temperature to be equal to the fluctuations of the ambient temperature. The temperature at the prospective synthesizer location was measured for several weeks and the temperature differences were converted into a relative phase. These values indicate the expected phase differences of the output signal relative to a synthesizer at constant temperature. Using these differential phase values, the corresponding Allan deviation can be estimated. The worst-case estimations for temperature-induced phase effects of a single synthesizer were computed for the two referencing schemes (BVA and OSM). The temperature measurements were dominated by white noise. As the temperature values were converted into phase values, this noise was converted into white phase noise. The corresponding Allan deviation is expected to exhibit a slope of τ^{-1} [37].

At first, we determined the long-term phase stability for operation with the BVA oscillator. For this measurement, both synthesizers were referenced to the same 5 MHz BVA via a distribution amplifier. A measurement duration

of 60 days was chosen, allowing to evaluate the Allan deviation for values of τ up to 10^6 s. The resulting values of $\sigma_y(\tau)$ for a pair of synthesizers are shown in green with circles in Figure 3.19. The calculated worst-case estimate for temperature-induced phase effects is displayed in blue with star symbols. This curve shows an increase around 4000 s, originating from the air conditioning system. No temperature values were acquired for $\tau < 60$ s, here the large thermal mass of the modules acts as a low-pass filter, effectively suppressing temperature effects. Shown for comparison are the values of the Allan deviation established for CSF2 (red curve). When referenced to the BVA oscillator, the Dick effect limits the stability of the fountain to $1 \times 10^{-13}(\tau/s)^{-1/2}$. It can be deduced that neither temperature-induced phase deviations nor the instability of the synthesizer will impair the long-term phase stability of the fountain.

The measurement was repeated, this time both synthesizers were referenced to the OSM via a power splitter. In this operational mode, the local oscillator frequency is 9.6 GHz and the PLL is not utilized. A shorter measurement duration was selected, enabling the determination of the Allan deviation for up to 6000 s. The resulting Allan deviation $\sigma_y(\tau)$ is given in Figure 3.20, displayed in green with circles. The curve exhibits a slope of nearly $\tau^{-1/2}$. Due to the noise characteristics it can be expected to have the same slope for $\tau > 6000$ s. Shown in blue with star symbols is the Allan deviation computed from the temperature sensitivity (1 ps/K). Shown for comparison is the frequency instability of CSF2 when referenced to the OSM (red curve). With this reference, deteriorations caused by the Dick effect are minimized, resulting in a stability improvement over BVA operation. The frequency stability of CSF2 is dominated by quantum projection noise, resulting in an instability of $2.5 \times 10^{-14}(\tau/s)^{-1/2}$ [20]. It can be concluded that the stability of the primary fountain clocks will not be limited by the long-term phase stability of the microwave synthesizer when the optically stabilized microwave is used as a reference.

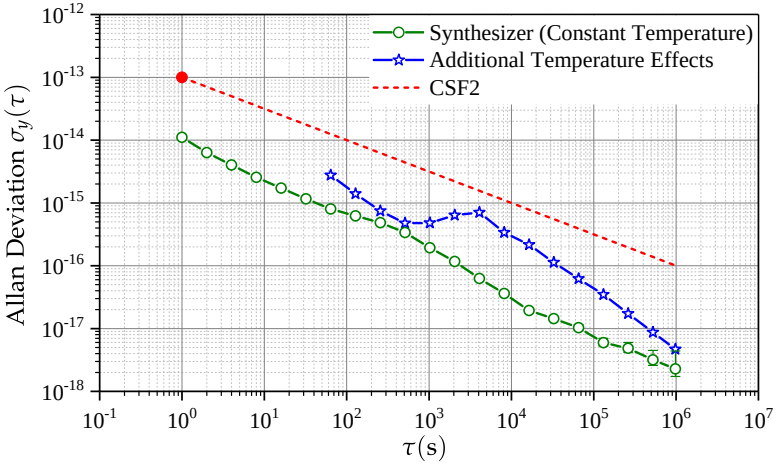

Figure 3.19: Allan Deviation of the Ramsey interrogation signal, estimated for a pair of microwave synthesizers when referenced to the 5 MHz BVA oscillator. The effect of temperature induced phase drifts in a single synthesizer is calculated from the fountain temperature.

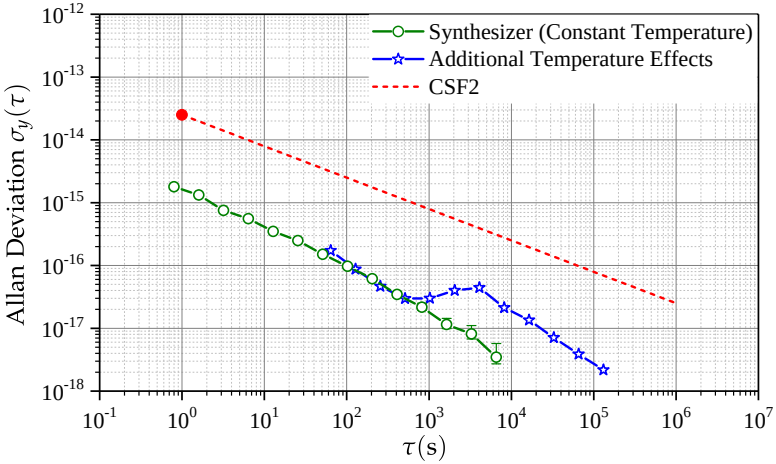

Figure 3.20: Allan Deviation of the Ramsey interrogation signal, estimated for a pair of microwave synthesizers when referenced to the optically stabilized microwave at 9.6 GHz. The effect of temperature induced phase drifts in a single synthesizer is calculated from the fountain temperature.

3.5 Assessment

3.5.1 Statistical uncertainty and long-term stability

The synthesizer has been investigated for contributions to the statistical uncertainty of a fountain clock and its impact on the clock's long-term frequency stability. In Section 3.4.2, we investigated the implications of the Dick effect as it can be a dominant source of instability in fountain clocks. This effect is linked to the phase noise of the Ramsey interrogation signal. We were able to reduce it to a level below the quantum projection noise limit by referencing the microwave signal to an optical resonator. In this case, the contribution of the microwave signal generation to the statistical uncertainty of the fountain clock becomes insignificant.

The clock's long-term stability can be constrained by the phase stability of the Ramsey interrogation signal. The stability of the microwave synthesizer has been examined for the two available reference options in Section 3.4.3. For both cases, a negligible contribution to the fountain's long-term stability could be demonstrated.

3.5.2 Systematic uncertainty

As mentioned in Section 2.3.4, three contributions to the systematic uncertainty of a fountain clock have to be considered: perturbations of the Ramsey interrogation signal, the collisional shift, and microwave leakage.

In Section 3.4.1, we examined the effect of spectral impurities in the Ramsey interrogation signal. It could be demonstrated that first-order frequency shifts resulting from symmetric sidebands can be canceled by selecting appropriate fountain timing parameters. The second-order frequency shifts resulting from asymmetric sidebands were verified to be below 4×10^{-18}. Taking into account the rectangular distribution [38], this corresponds to a systematic uncertainty contribution of 2.3×10^{-18}. The effect of cycle-synchronous phase transients will be assessed in the following chapter. A measurement setup to investigate this kind of phase disturbances will be presented, along with an evaluation of possible frequency shifts.

To reduce the systematic uncertainty contribution of the collisional shift in CSF2 and enable operation of CSF2 with high atom numbers, the method of rapid adiabatic passage was implemented. The synthesizer was modified

and a modulation scheme was prepared (Section 3.3.4). Before the application of the RAP method, the resonant field method was used to determine the collisional shift correction. When using the resonant field method, the collisional shift uncertainty is estimated to be around 10% of the applied collisional shift correction [11, 80]. Application of the RAP method led to a significant reduction of the collisional shift uncertainty to less than 0.5% of the applied correction. The systematic uncertainty attributed to the collisional shift was reduced to 4×10^{-17} [82].

Interactions between the atoms and microwave leakage fields can lead to uncontrolled frequency shifts. In previous publications, an uncertainty contribution of 1×10^{-16} had been attributed to microwave leakage for both CSF1 and CSF2 [82, 130]. Two techniques to suppress this effect were implemented in the caesium fountains, they will be described in Chapter 5, along with a reevaluation of the systematic uncertainty.

4 Phase transient analysis

In a caesium fountain clock, the frequency of a microwave interrogation signal is locked to the atomic resonance. The frequency steering is derived from a phase difference measurement. This measurement is performed in a cyclic fashion, during each cycle the accumulated phase difference between the atomic superposition and a resonant field is evaluated. If the phase of the field-driving signal is disturbed, an error in the phase difference measurement can occur. For the case of cycle-synchronous disturbances, the error will be identical for every cycle. This will affect the frequency steering and thus cause a shift of the fountain frequency

The fountain clock cycle involves the actuation of e.g. field coils, lasers, and shutters. All these switching processes can result in a disturbance of the field-driving signal. It is possible to detect such cycle-synchronous phase disturbances in the Ramsey interrogation signal and estimate their effect on the fountain frequency [21, 22]. We designed a system that facilitates a detailed analysis of cyclic disturbances in pulsed clocks; it allows the detection of cyclic errors in the phase of the relevant fountain signals as well as the detailed investigation of possible sources. In the following, a compendious description on frequency shifting factors along with the required specifications of a phase transient analyzer will be given. The principle of the phase transient detection system will be discussed, accompanied by a delineation of the technical implementation. Measurements of the Ramsey interrogation signal phase for the two fountains will be presented and evaluated.

4.1 Design considerations

4.1.1 Phase transients and frequency shifts

In the Ramsey scheme, the accumulated phase difference between the atomic superposition and a microwave field is evaluated. The scheme involves a modulation of the Ramsey interrogation signal. In the following we will neglect this modulation and assume a single Ramsey interrogation frequency

f_R. The phase of f_R is denoted as φ_R. The central Ramsey fringe is located at f_0, the phase of the atomic superposition is denoted as φ_0. The phase difference $\Delta\varphi$ evolving between φ_R and φ_0 during the Ramsey time T_R is evaluated during the two Ramsey interactions. $\Delta\varphi$ is used to control the Ramsey interrogation frequency. The two Ramsey interactions are denoted in the following as R_1 and R_2.

Shown in Figure 4.1 is the temporal evolution of the phase difference $\Delta\varphi$ in the course of the Ramsey interaction. In both cases, the fountain control loop is in steady state, $\Delta\varphi$ is thus zero during both Ramsey interactions. Part (a) shows the case of a transient-free Ramsey interrogation signal. In this case, the average frequency difference between f_R and f_0 is zero: $\overline{\Delta f} = \overline{f_R - f_0} = 0$. Shown in Fig. 4.1(b) is the case of a reversible phase perturbation that occurs during the Ramsey time, but outside of the two Ramsey interactions. As the phase difference $\Delta\varphi$ is only determined during the interactions R_1 and R_2, the phase relation is not disturbed. Thus, the average frequency difference $\overline{\Delta f}$ is zero.

Figure 4.2(a) shows the occurrence of a non-reversible phase perturbation. A phase transient occurs during the Ramsey time, resulting in a cyclic phase offset in φ_R. The phase evaluation during the second Ramsey interaction R_2 is thus perturbed. The control loop tunes the Ramsey interrogation frequency f_R so that $\Delta\varphi = 0$ during R_2 (Figure 4.2(b)). This detuning from resonance results in a fountain frequency shift $\overline{\Delta f}$. The frequency shift corresponds to a relative fountain frequency error δ_f:

$$\delta_f = \frac{\overline{f_R - f_0}}{f_0} = \frac{\overline{\Delta f}}{f_0}. \tag{4.1}$$

The relative fountain frequency error can be calculated from the phase difference $\Delta\varphi$, the resonance frequency f_0 and the Ramsey time T_R [62]:

$$\delta_f = \frac{1}{2\pi \cdot f_0 \cdot T_R} \cdot \Delta\varphi. \tag{4.2}$$

4.1.2 Phase noise requirements

We demand that the phase analyzer should be able to detect phase transients that would lead to a relative fountain frequency error δ_f of more than $5 \cdot 10^{-17}$. Given the caesium resonance frequency f_0 of 9.193 GHz and assuming a Ramsey time of 500 ms, a relative frequency error of $5 \cdot 10^{-17}$

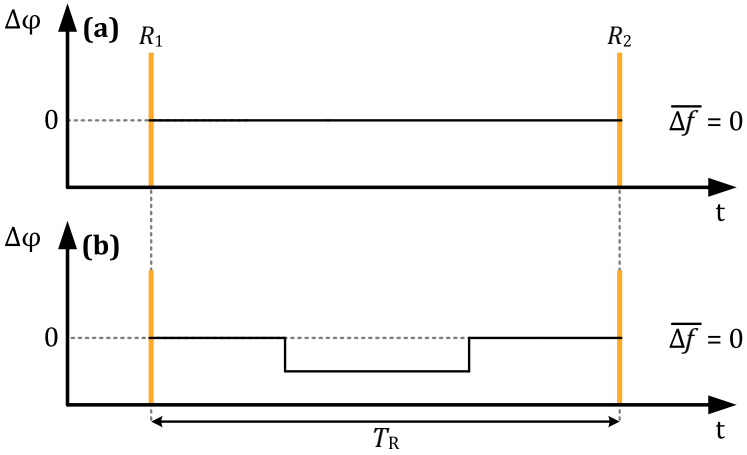

Figure 4.1: Temporal evolution of the accumulated phase difference $\Delta\varphi$ during the Ramsey interaction. The fountain control loop is in steady state. (a) Undisturbed Ramsey interrogation signal. (b) Cycle-synchronous phase disturbance in the Ramsey interrogation signal, effective only during the Ramsey time T_R.

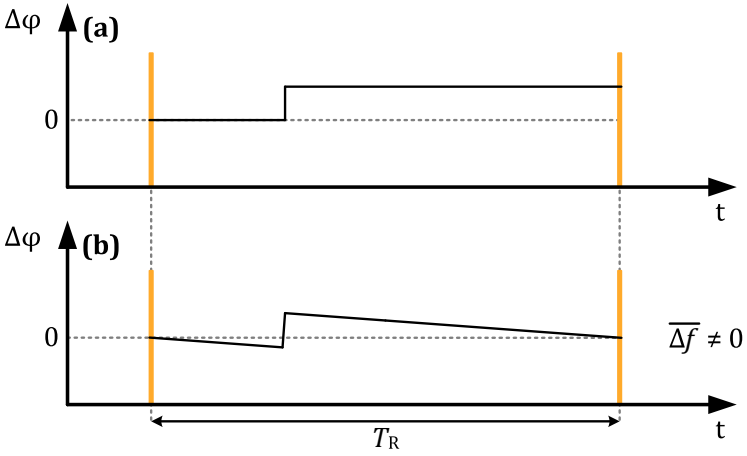

Figure 4.2: Temporal evolution of the accumulated phase difference $\Delta\varphi$ during the Ramsey interaction. Shown is the effect of a cycle-synchronous phase transient in the Ramsey interrogation signal, effective during R_2. (a) The fountain control loop is not in steady state. (b) The fountain control loop is in steady state.

corresponds to a phase difference $\Delta\varphi$ = 1.5 µrad. We furthermore assume that such phase difference can be detected at a statistical significance of 2σ, e.g. in a data set with a standard deviation of less than 0.75 µrad.

The standard deviation of the signal in the time domain is estimated from its phase noise, using the root-mean-square (RMS) phase noise ϕ_{rms} of the signal as an estimator for the standard deviation σ. Taking into account the system passband, e.g. an rectangular filter with a bandwidth of f_{min} to f_{max}, the RMS phase noise can be calculated from $\mathcal{L}(f)$ [131]:

$$\phi_{\text{rms}} = \sqrt{2 \cdot \int_{f_{\text{min}}}^{f_{\text{max}}} 10^{\frac{\mathcal{L}(f)}{10}} \mathrm{d}f}. \tag{4.3}$$

As mentioned earlier in Section 3.3.2, the synthesizer can be referenced to a local quartz oscillator (BVA) or an optically stabilized microwave signal (OSM). In Section 3.4.2, the phase noise of the Ramsey interrogation signal was measured for the two different references. Solving equation 4.3 for the two cases (BVA and OSM) with a bandwidth of f_{min} = 1 Hz to f_{max} = 10 kHz, we get the RMS phase noise for both cases. When the synthesizer is referenced to the BVA, the synthesizer output signal has an RMS phase noise level of 4250 µrad, for the case of OSM referenced operation, the RMS phase noise is 65 µrad. In both cases, the RMS phase noise is substantially higher than the required 0.75 µrad. At this noise level, it is not possible to make a prediction of relative fountain frequency errors on the 10^{-16} level.

To achieve the desired phase noise level, we can take advantage of the cyclic nature of the fountain interaction scheme, utilizing a special averaging technique. This so called coherent averaging [132] (also referred to as time-synchronous averaging) can be regarded as a type of lock-in-technique with a low frequency carrier wave. The signal is averaged over multiple fountain cycles, reducing the contribution of asynchronous noise. The standard deviation of the averaged signal can be calculated as:

$$\sigma_{\text{avg}} = \frac{\sigma_{\text{signal}}}{\sqrt{N}}. \tag{4.4}$$

To reduce the measurement time, the RMS phase noise can be reduced by decreasing the bandwidth. As this low pass filtering will also conceal shorter phase transients, a compromise must be found between filter bandwidth and measurement time. To assess the relation between bandwidth and measurement time, the phase noise as well as the measurement time

Bandwidth	BVA Reference		OSM Reference	
	Phase noise (µrad)	Averaging time (h)	Phase noise (µrad)	Averaging time (h)
1 Hz - 10 Hz	660	350	28	0,7
1 Hz - 100 Hz	1600	2100	34	1,0
1 Hz - 500 Hz	2800	6500	38	1,2
1 Hz - 1 kHz	3400	9500	40	1,3
1 Hz - 10 kHz	4250	15000	65	3,5

Table 4.1: Phase noise and estimated averaging time

required to reach a standard deviation σ_{avg} of less than 0.75 µrad have been calculated for different bandwidths. A fountain cycle time of 1.2 s is used for the calculations. The results are given in Table 4.1 for the two reference options.

For the signal in the example above with ϕ_{rms} = 4250 µrad, more than 3×10^7 averaging cycles are required for σ_{avg} to reach 0.75 µrad. This would require more than 1 year of measurement time. Due to the superior phase noise of the OSM, the averaging time is on the order of 4 h for a bandwidth of 1 Hz to 10 kHz.

For BVA referenced operation, a bandwidth of 1 Hz to 500 Hz was chosen. With these settings, a relative fountain frequency error δ_f of more than $3 \cdot 10^{-16}$ would be detectable after a week of averaging. A smaller bandwidth can also be beneficial for OSM-referenced operation, as it would facilitate the early identification of trends and phase aberrations. We therefore implemented two analysis bandwidths in parallel, 1 Hz to 10 kHz and 1 Hz to 500 Hz. These are in the following abbreviated as 10 kHz bandwidth and 500 Hz bandwidth.

4.1.3 Signal preprocessing

The output signal from the microwave synthesizer has to be digitized to enable post-processing and filtering and facilitate coherent averaging. The conversion is affected by clock jitter, leading to a deterioration of the signal. The requirements for the sampling clock jitter can be estimated from the timing jitter of the sampled signal. The absolute timing jitter Δt_{rms} for a signal with frequency f can be calculated from the RMS phase noise ϕ_{rms}:

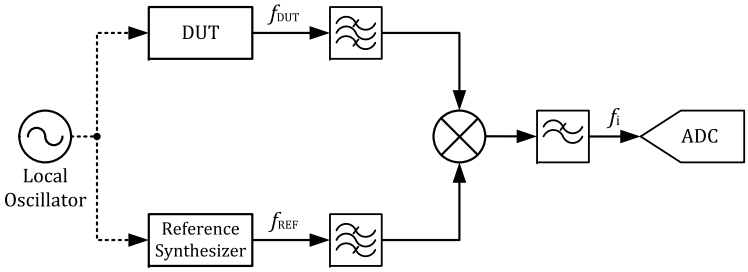

Figure 4.3: Heterodyne mixing front-end

$$\Delta t_{\mathrm{rms}} = \frac{1}{2\pi \cdot f} \cdot \phi_{\mathrm{rms}}. \tag{4.5}$$

The Ramsey interrogation signal frequency f is 9.193 GHz, using the values for the OSM at a bandwidth of 10 kHz from Table 4.1, we get a timing jitter of about 1 fs. It is not feasible to directly digitize this signal without significant deterioration, therefore, it is required to reduce the frequency of the signal while preserving its phase information. This can be achieved with a heterodyne mixing scheme (Fig. 4.3), similar to the setup described in Section 3.4.2.

The device under test (DUT) and a reference synthesizer are locked to the same local oscillator. The frequency of the reference synthesizer f_{Ref} is offset from f_{DUT} by f_{i}. This scheme allows to transfer the phase information contained in f_{DUT} to f_{i}, reducing the absolute timing jitter equal to the ratio of the two frequencies. It is therefore beneficial to select a low intermediate frequency f_{i} that meets the Nyquist criterion for the applied analysis bandwidth [133]. The intermediate frequency must not be a multiple (or possible mixing product) of present system frequencies to avoid crosstalk. Based on the bandwidth requirement of 10 kHz for OSM reference operation, f_{i} was selected to be 32 323 Hz. At this intermediate frequency, the RMS phase noise of 65 µrad is equivalent to a timing jitter Δt_{rms} of 320 ps.

4.2 Phase transient analyzer

After the AD-conversion, the digitized data are processed to extract the phase values, involving the extensive use of digital filters. These filters can be efficiently implemented in a field-programmable gate array (FPGA), allowing high data throughput and thereby a high sampling rate.

For the phase transient analyzer, a modular FPGA-based system was built, based on a Virtex-5 SX95T FPGA from Xilinx [134]. The analog to digital conversion was performed with an AD converter from Analog Devices, the AD9268BCPZ-125 [135]. The ADC has to be complemented with signal conditioning circuitry and a sampling clock converter, implemented in the 5734R ADC module from National Instruments [136]. National Instruments Labview FPGA was used to program the FPGA as well as the host software.

4.2.1 Analyzer principle

The design principle of the phase analyzer is shown in Figure 4.4. The device under test and the reference synthesizer are referenced to a common clock to ensure a fixed phase relation. Cycle-synchronous phase disturbances of the reference synthesizer could lead to measurement errors. Several measures were taken to isolate the DUT from the reference synthesizer, e.g. signal transformers and separate power supplies. Disturbances in the phase of the local oscillator will affect both synthesizers in the same way (common mode) and are therefore not detectable.

The frequency of the Ramsey interrogation signal is changed by the fountain control computer with every cycle, this control signal is sent to the DUT as well as the reference synthesizer. The frequency sent to the reference synthesizer is offset by 32 323 Hz, the intermediate frequency thus stays constant. After passing an antialiasing low pass filter, the signal is fed to the ADC, with its internal sample clock being phase locked to the common clock. The data stream from the ADC is fed to the FGPA for data processing. The internal FGPA clocks also are referenced to the common clock. The FPGA is programmed with specifically engineered code, filter procedures are applied to the data stream and phase and amplitude values are computed. The phase and amplitude values are coherently averaged, using a cycle synchronous trigger signal from the fountain control computer.

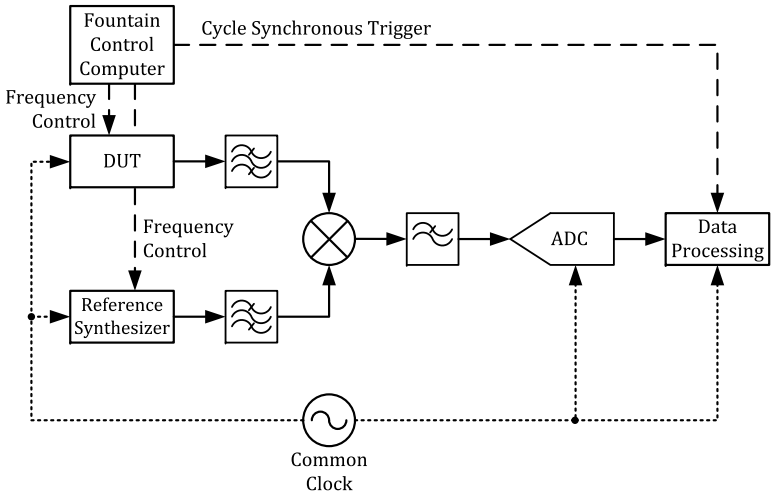

Figure 4.4: Phase transient analyzer principle

4.2.2 Implementation

The implementation of the phase transient analyzer is shown in Figure 4.5. The FPGA part is symbolized by the red border, the code running on the host computer is marked with a green border. The AD-conversion of the input signal results in a digital data stream. This data stream is processed by the FPGA with two different analysis bandwidths in parallel, 10 kHz (upper part) and 500 Hz (lower part).

In the following the process is described for a bandwidth of 10 kHz, the processing at lower bandwidth is analogous. As a first step, the data rate is reduced, using an array of filters and decimators [137]. The decimation process results in an averaging of the signal. During each decimation, the sample rate is reduced and the number of significant data bits is increased. To avoid aliasing effects, each decimation is preceded by a low-pass filter. Finite impulse response (FIR) filters are used as they can be efficiently implemented on an FPGA [138]. The data stream with the reduced sample rate can now be demodulated. The demodulation is done with a digital implementation of the IQ-demodulator [138]. Here a DDS is implemented in software to generate two signals of frequency f_i with a phase difference of

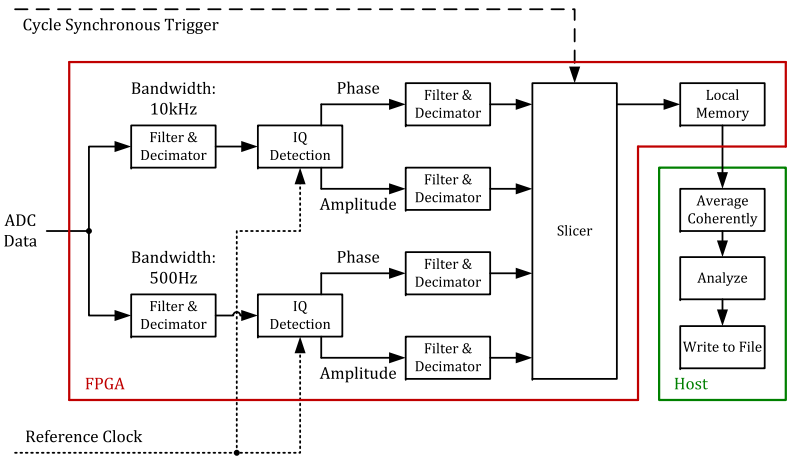

Figure 4.5: Phase transient analyzer data processing

90 degrees. These two signals are multiplied (mixed) with the original data stream, the output signals are referred to as in-phase (I) and quadrature (Q) components. Using the Coordinate Rotation Digital Computer (CORDIC) algorithm [139], the phase φ and amplitude A are calculated:

$$\varphi = \arctan \frac{Q}{I} \tag{4.6}$$

$$A = \sqrt{I^2 + Q^2}. \tag{4.7}$$

The carrier frequency f_i is then removed by a filter stage and the data stream is subsequently decimated to a sample rate adequate for the processing bandwidth. The phase as well as the amplitude stream are divided in packages to facilitate coherent averaging. A trigger signal synchronous to the fountain cycle is connected to a digital input of the FPGA. This trigger is used in the slicer to divide the data stream into equally sized packages. The data points are provided with time stamps relative to the cycle synchronous trigger. Further post-processing will not introduce any delays or lead to synchronization issues. The data packages are written to local memory directly addressable for the FPGA.

The host computer monitors the acquisition and moves completed slices into host memory. Here the data are post-processed, coherently averaged and analyzed, e.g. statistical calculations and consistency checks are performed. The averaged data sets and the statistics are then each written to separate files.

4.2.3 System performance

During the sampling process, a digital representation of the analog input signal is generated, the timing of each sample is controlled by an external clock. The timing of the sampling clock as well as the effective amplitude resolution of the ADC need to be addressed, as both can be the source of additive noise when measuring the phase of sinusoidal signals.

A timing jitter in the sampling system will affect the sample timing and thus the phase values computed from the digitized signal [131]. The timing jitter is attributable to the jitter of the external clock supplied to the module as well as the clock processing performed within the module. An external clock of 10 MHz is supplied from the synthesizer chain with a jitter of less than 0.06 ps [106]. The timing jitter of the ADC modules sampling clock is specified to be 0.5 ps when locked to an external clock [136]. The overall timing jitter of the sampling system can be expected to be less than 1 ps. As described in Section 4.1.2, the timing jitter of the sampled signal is about 320 ps, so no degradation is expected due to the ADC sample clock performance.

The AD9268 is an analog to digital converter with a nominal resolution of 16 bits. Not all of these bits contain information about the digitized signal as the signal preprocessing and sampling is affected by noise. For AD converters, the term effective number of bits (ENOB) is used to indicate the number of bits with valid information. The ENOB is equivalent to a signal to noise ratio (SNR). To translate ENOB into SNR, we convert from dB to bits with a conversion factor of $20 \log_{10} 2$ and take into account the quantization error of the ADC, which is equal to 1.76 dB in the ideal case [140]:

$$\mathrm{SNR(dB)} = (20 \log_{10} 2) \cdot \mathrm{ENOB} + 1.76. \tag{4.8}$$

In order to avoid signal deterioration due to the conversion process, the SNR of the ADC should be at least 10 dB better than the SNR of the analog input signal. The SNR of the input signal can be calculated from its RMS phase noise:

$$\mathrm{SNR(dB)} = -20\log(\phi_{\mathrm{rms}}). \tag{4.9}$$

When using the OSM as a reference, the RMS phase noise of the Ramsey interrogation signal within an analysis bandwidth of 10 kHz is 65 µrad (Table 4.1). This corresponds to a SNR of 84 dB. In this case an ADC with a SNR of 94 dB is required, equal to 15.3 effective bits.

At the present operating conditions, the ADC is specified with a SNR of 78 dB for a full scale input of +10 dBm [135]. The noise contributions of the sampling process are independent of the input level, as a consequence the SNR is deteriorated for lower input levels. The ADC module provides an internal amplifier with a selectable gain of 6 dB or 12 dB [136]. For an input signal level of −9 dBm and an amplifier gain setting of 12 dB, the SNR is 71 dB, resulting in 11.5 effective bits at a data rate of 120 MSamples/s. To achieve the required signal to noise ratio, the ADC data is decimated by the FPGA. The data rate is reduced and the effective number of bits is increased. Due to the binary representation of the data, it is most effective to reduce the sample rate in steps of 2. A sample rate reduction by a factor of 2^9 will increase the effective number of bits by 4.5, resulting in 16 effective bits. Using equation 4.8, we get an SNR of 98 dB, 14 dB below the SNR of the input signal. After the different decimation stages, the data rate is 52 kSamples/s, fulfilling the Nyquist criterion for the 10 kHz analysis bandwidth.

4.2.4 Characterization

The transient phase analyzer was characterized in several steps. At first, the step response of the data processing system was evaluated and the system delays were determined. We then examined the IQ detection scheme and verified the phase processing. As a final step, the noise properties of the data conversion and data processing system were determined.

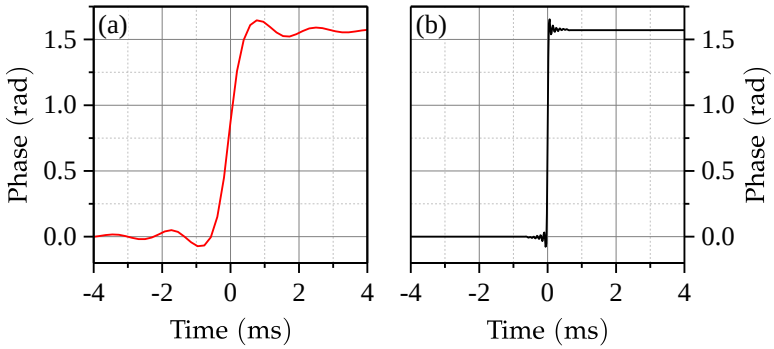

Figure 4.6: Filter settling time for (a) 500 Hz bandwidth and (b) 10 kHz bandwidth.

Step response

The step response of the data processing system is essential for the detection of short transients. Two signal paths with different analysis bandwidths were used, depicted in the processing scheme in Figure 4.5. Each path features a different set of filters and decimators. Both signal paths were evaluated individually for their step response and signal processing delay.

The ADC input signal was modulated synchronously with the measurement cycle, applying a phase step of $\pi/2$. The phase values were coherently averaged, using filter bandwidths of 500 Hz and 10 kHz (Figure 4.6). At a bandwidth of 500 Hz, the filter settling time is several milliseconds (Fig. 4.6(a)), the analyzer path with 10 kHz bandwidth (Fig. 4.6(b)) has a much faster response time of less than one millisecond.

IQ detection

To verify the IQ detection scheme and the processing of the phase values, we detuned the frequency of the reference synthesizer and measured the phase values for 1 s, using an analyzer bandwidth of 500 Hz. The frequency of the reference synthesizer f_{Ref} was detuned by $+1$ µHz and -1 µHz. The phase values were coherently averaged for 9000 measurement cycles. Over the sampling duration of 1 s, consistent linear phase ramps of $\pm 2\pi$ µrad can be observed (Fig. 4.7). The measurement was repeated for an analyzer bandwidth of 10 kHz, showing comparable results.

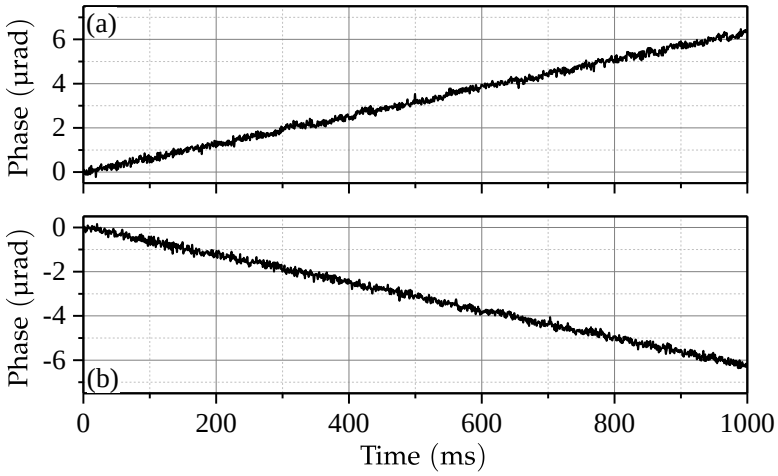

Figure 4.7: Phase progression for different frequency offsets. a) $+1\,\mu Hz$ b) $-1\,\mu Hz$

Data conversion and processing

To evaluate the noise properties of the phase detection system, measurements of the synthesizer signal were compared with measurements of a test signal. For these measurements, an analyzer bandwidth of 10 kHz was used. A sampling duration of 1114.5 ms was selected, analogous to the CSF1 cycle time.

The two synthesizers were connected to the analyzer, utilizing the heterodyne mixing front-end from Figure 4.3. The frequency of the reference synthesizer f_{Ref} was set to $f_{DUT} + 32.323\,kHz$, resulting in a difference frequency of 32.323 kHz that was fed to the ADC input stage. The standard deviation $\sigma_{avg}(n)$ of the coherently averaged trace after n averaging cycles was calculated. The plot for $\sigma_{avg}(n)$ for the microwave synthesizer signal is shown in black in Figure 4.8. It exhibits a slope of $n^{-1/2}$, as expected from equation 4.4 for a dominant contribution of white noise. A test signal of 32.323 kHz was generated with a commercial waveform generator, phase locked to the common clock. This signal was connected directly to the ADC input and the measurement was repeated. The resulting plot for $\sigma_{avg}(n)$ for the test signal is shown in orange in Figure 4.8. It is well below the standard deviation obtained from measurements of the synthesizer signal.

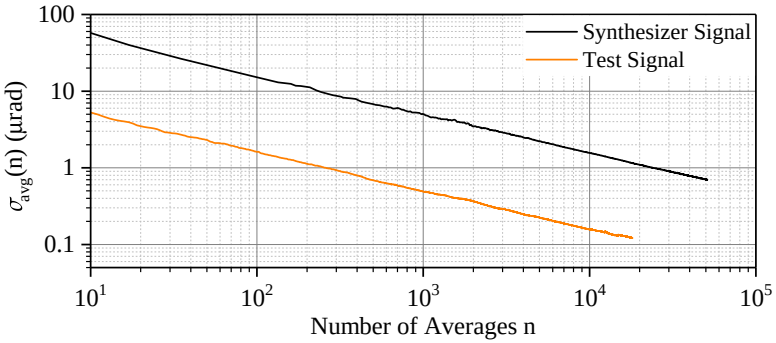

Figure 4.8: Standard deviation of coherently averaged phase sample sets

The measurements were repeated with an analyzer bandwidth of 500 Hz, showing comparable results. It can be concluded that the analysis of phase transients is not limited by the detection and processing system.

4.3 Fountain evaluation

Using the phase transient analyzer, the microwave synthesizer described in Chapter 3 was evaluated. This investigation was conducted for the Ramsey interrogation signals used for the fountain clocks CSF1 [11, 80] and CSF2 [12]. The synthesizers were referenced to the OSM. Both fountain clocks were configured in operational mode: all signals and switching processes were applied in the same way as during regular frequency measurements.

The Ramsey interrogation signal was disconnected from the Ramsey cavity and fed to the phase analyzer. The frequency of the Ramsey interrogation signal was slightly varied by the control computer with random frequency offsets of several millihertz at every cycle, similar to the behavior of the control loop used to lock the frequency of the Ramsey interrogation signal to the atomic resonance. The phase of the Ramsey interrogation signal was recorded for a duration of 1000 ms, starting with the launching of the atoms, shown as phase (b) in Figure 2.6.

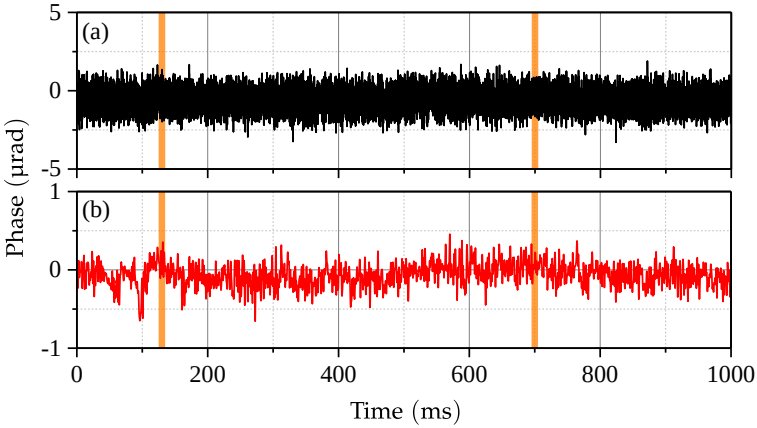

Figure 4.9: Phase progression of the Ramsey interrogation signal during the CSF1 fountain cycle when referenced to the optically stabilized microwave. (a) 10 kHz analysis bandwidth. (b) 500 Hz analysis bandwidth. The two Ramsey interactions are symbolized by orange boxes.

4.3.1 CSF1

The analysis was conducted with bandwidths of 10 kHz and 500 Hz simultaneously. The results are given in Figure 4.9(a) and Figure 4.9(b) respectively. The data were averaged for 21 hours, equaling 68000 fountain cycles in CSF1. The fountain cycle time is 1114.5 ms. The two Ramsey interactions have a duration of 10 ms, they are symbolized by orange boxes in Figure 4.9. The first Ramsey interaction takes place at 125 ms, the second interaction is occurring at 695 ms.

The coherent averaging over 68 000 fountain cycles results in a single phase sequence. The data were also stored in 13 phase sequences, each resulting from 5000 coherently averaged traces. For each sequence, the average value of the phase during the Ramsey interactions was calculated and the phase difference between the two Ramsey interactions was determined. From this series of phase difference values, we calculated the mean difference and the standard deviation.

Fast phase transients could lead to inaccurate data at low bandwidth. No such transients are visible in the 10 kHz bandwidth plot in Figure 4.9(a). We can thus assume the measurement data acquired with a bandwidth of

500 Hz to be valid. Based on the data acquired with a bandwidth of 500 Hz, the phase difference between the two Ramsey interactions was evaluated to be (0.00 ± 0.52) µrad. Using equation 4.2, the resulting systematic uncertainty was calculated to be 1.6×10^{-17}.

4.3.2 CSF2

The fountain cycle time for CSF2 is 1234.5 ms, the two Ramsey interactions of duration 10 ms are centered at 195 ms and 745 ms. The phase measurement of the Ramsey interrogation is shown in Fig. 4.10, the phase values were synchronously averaged for 45 000 fountain cycles, requiring a measurement time of 15 h. A large phase transient is visible at 45 ms, before the first Ramsey interaction. This is provoked by the switching of the magnetic field in the state selection cavity for the RAP method as explained in Section 3.3.4.

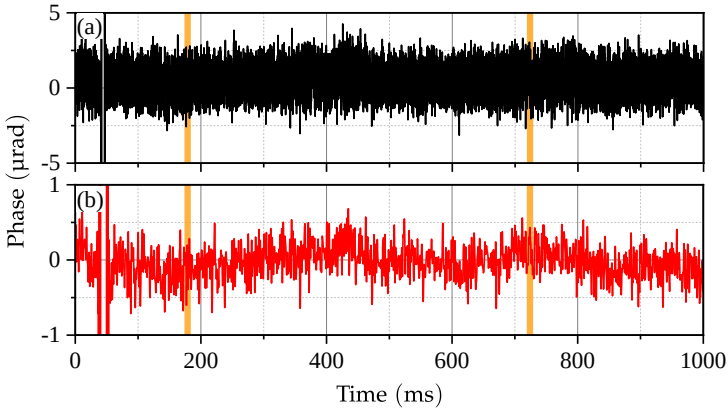

Figure 4.10: Phase progression of the Ramsey interrogation signal during the CSF2 fountain cycle when referenced to the optically stabilized microwave. (a) 10 kHz analysis bandwidth. (b) 500 Hz analysis bandwidth. The two Ramsey interactions are symbolized by orange boxes.

The phase sequences were also stored in sets, each resulting from of 2000 coherent averages. From the resulting phase sequences, the individual phase differences between the two Ramsey interactions were calculated and used to compute the mean value and standard deviation. Based on the measurement data acquired with a bandwidth of 10 kHz, the phase difference

between the two Ramsey interactions was evaluated to be (0.23 ± 1.14) µrad. Using the measurement data acquired with a bandwidth of 500 Hz, the phase difference was calculated to be (0.14 ± 1.04) µrad. We assume a maximum phase difference of 1.18 µrad, as obtained from the measurement data acquired with a bandwidth of 500 Hz. This phase difference corresponds to a systematic uncertainty contribution of 3.7×10^{-17}.

Even though this value is higher than the results obtained for CSF1, this does not necessarily imply a lower phase stability of the microwave synthesis used in CSF2. The difference can be attributed among other things to the longer measurement time and slightly different data processing and statistical analysis.

In summary, it can be stated that the phase transient analyzer performs as expected and can be readily used to investigate the Ramsey interrogation signals in fountain clocks. Furthermore, it could be demonstrated that the effect of cycle-synchronous disturbances is on the low 10^{-17} level during normal fountain operation.

5 Transient-free switching

Interactions between the caesium atoms and microwave fields during the free evolution or before the population probing can lead to a shift of the fountain frequency [24]. Such a disturbing field can be a consequence of microwave leakage from the Ramsey or state selection cavity or the microwave synthesizer. The interaction is dependent on the parameters of the resonant field, e.g. field strength, field frequency and phase [26]. It can be reduced by changing leakage field parameters synchronously with the fountain cycle, right before and after the two Ramsey interactions. Field parameters available to external modification are the field strength as well as the field frequency.

Modifying the Ramsey interrogation signal synchronous with the fountain cycle is very likely to result in phase disturbances, in turn causing frequency shifts. The effect of such phase shifts can be orders of magnitude larger than the effect of microwave leakage itself. Therefore, the development and application of an active method has to be accompanied by an evaluation of the phase shifts. This can be achieved with a dedicated phase transient analyzer, the development of such an analyzer has been presented in Chapter 4.

A method to manipulate the field strength has been described previously [21]. Here the microwave signal is attenuated using an interferometric switch. This method has been implemented for the use at one of the fountains at PTB. A brief explanation of the general idea and the setup used at CSF1 is given in Section 5.1. This is accompanied by measurement data recorded with the phase transient analyzer and an assessment of the method.

For CSF2, we devised a different method to reduce the effect of microwave leakage. It depends on frequency detuning rather than amplitude reduction [28]. The field frequency is detuned with negligible effects on the field phase during the Ramsey interactions. Possible errors during operation can be detected by the fountain itself and do not require the assignment of a phase transient analyzer. In Section 5.2, we will outline the principle of the

method and give a detailed description of its implementation with a digital frequency synthesizer. This includes a description of the setup used for coherently detuning the interrogation frequency of CSF2 and an analysis of the parameter space. We will present measurement data and evaluate the contribution of microwave leakage to the systematic uncertainty of the fountain.

Finally, the advantages and disadvantages of the interferometric switching and the phase-coherent frequency detuning scheme are discussed in Section 5.3.

5.1 Interferometric switching

5.1.1 Principle

A leakage field can be originating from the Ramsey cavity or the microwave synthesizer as well as from signal connections, its strength is dependent on the amplitude of the Ramsey interrogation signal. To reduce the effect of field leakage, the signal can be set to nominal amplitude at the beginning of each Ramsey interaction and attenuated right after. The amplitude could be controlled directly at the output of the synthesizer, at a frequency of about 9.193 GHz. Implementing a switching scheme for the Ramsey interrogation signal at this frequency can cause a high insertion loss and cannot guarantee that leakage from the synthesizer will not arrive at the fountain by free-space propagation [21, 141]. The modular design of the synthesizer allows for an implementation of the amplitude control at a frequency of 407.3 MHz, between the Ramsey frequency control section and the microwave mixer (for details refer to Section 3.3.2).

Conventional radio frequency (RF) switches exhibit large phase transients with time constants in the hundreds of milliseconds when they are actuated. These phase transients are most noticeable when closing the switch, rendering them unsuitable for direct control of the signal amplitude. By implementing the RF switch in one arm of a balanced interferometer (Figure 5.1), the amplitude of the Ramsey interrogation signal can be switched with negligible phase transients. Two directional couplers are used to split and combine the RF signal, their attenuation is compensated using an amplifier. The interferometer is tuned to a dark fringe with a phase shifter and

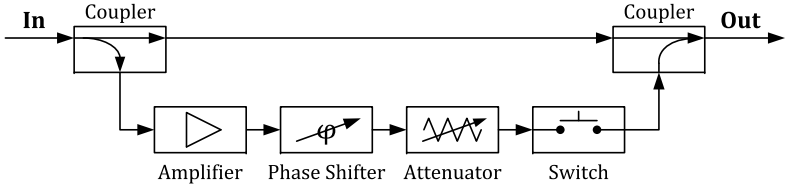

Figure 5.1: Principle of the interferometric switch [21]

an attenuator. When the switch is actuated, the output of the interferometer is strongly attenuated by destructive interference. When the switch is opened, the signal at the output is virtually unperturbed [21].

5.1.2 Implementation

Using a mechanical phase shifter and attenuator, an interferometric switch (IFS) was implemented in CSF1. The amplitude tuning proved to be demanding, several mechanical attenuators had to be investigated. Most of them were either unstable or suffered from backlash during amplitude setting. In contrast, the phase control was rather uncomplicated, eased by the long wavelength of 0.73 m at 407.3 MHz. The coarse phase was set by cable length and the fine tuning was performed with a mechanical precision phase shifter. Switches with different technologies (e.g. bipolar, electromechanical relays and micro electromechanical systems (MEMS)) were evaluated. The attenuation of the interferometric switch at 407.3 MHz was monitored over the course of several months and proved to be at least 35 dB.

The spectrum of the Ramsey interrogation signal was measured for the two switch states (Figure 5.2). The attenuated signal is represented in black color, the spectrum of the signal applied during the two Ramsey interactions is shown in green. Figure 5.2(a) shows the spectrum close to the carrier, the Ramsey interrogation signal is attenuated by more than 35 dB. Such an attenuation would imply a reduction of possible leakage effects by at least a factor of 50 [24, 25].

The switch can only be tuned to attenuate a single frequency, sidebands and spurious emissions are largely unaffected as shown in Fig. 5.2(b). Due to the single-sideband mixing of the Ramsey interrogation signal (for details see Section 3.3.2), the sidebands are more than 30 dB lower than the frequency

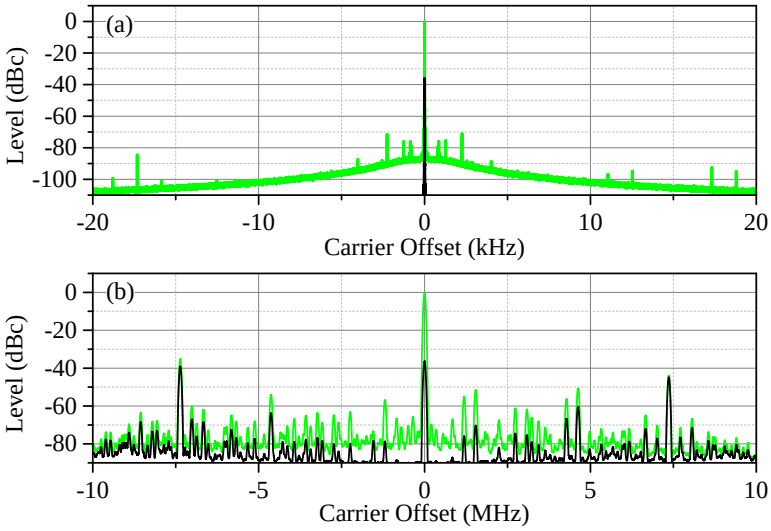

Figure 5.2: Interferometric switch attenuation. (a) Close to carrier and (b) far from carrier. The attenuated signal is represented in black color, the signal used during the two Ramsey interactions is shown in green.

of interest. Owing to this low level and their large frequency detuning, their frequency shifting effect will be negligible.

It is not possible to monitor the interferometric switch online during fountain operation, as a measurement of the attenuation requires the switch to be disconnected from the synthesizer. Therefore, the interferometric switch has to be checked regularly before and after longer fountain measurement campaigns.

5.1.3 Amplitude transients

The measurement data presented in Figure 5.2 only provide information about the steady state attenuation. Additional time-resolved measurements of the output amplitude were carried out to obtain confidence on the attenuation during the Ramsey time T_R and to rule out disturbing effects due to amplitude transients during the interactions. The two Ramsey interactions will be symbolized by orange boxes in the following figures, light orange boxes indicate the time interval the atoms spend in the cut-off tubes of

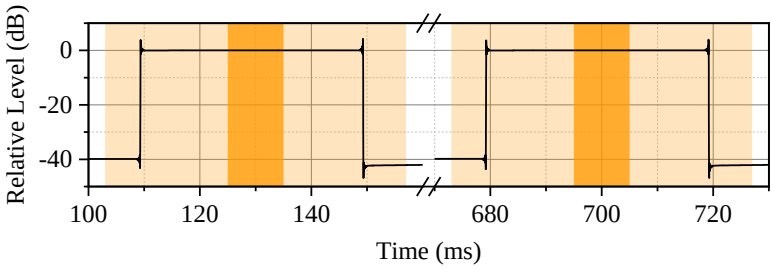

Figure 5.3: Temporal evolution of the signal level during interferometric switching. The two Ramsey interactions are symbolized by orange boxes. The time interval the atoms spend in the cut-off tubes is indicated by light orange boxes.

the Ramsey cavity [142]. The interferometric switch is actuated for 530 ms, symmetrical with respect to the atom-microwave interactions. During this time the microwave field is attenuated and the effect of leakage fields is reduced.

Time-resolved amplitude values are a by-product of the phase analysis system discussed in Chapter 4, however with a limited measurement range. To overcome this limitation, the amplitude at 407.3 MHz was detected with a spectrum analyzer set to zero span [143]. The analyzer converts the displayed signal level to an analog voltage. This signal was recorded with a modified transient analyzer firmware, the amplitude values were then averaged synchronously to the fountain cycle. The measurement data are given in Fig. 5.3, the IFS attenuates the signal by more then 35 dB in less than a millisecond.

5.1.4 Phase transients

Phase perturbations in the Ramsey interrogation signal caused by the interferometric switch were examined using the phase transient analyzer described in Chapter 4. Bandwidths of 10 kHz and 500 Hz were used for the analysis. The data were averaged for 40 hours, equal to 125000 fountain cycles in CSF1. The measurement data are shown in Figures 5.4(a) (10 kHz) and 5.4(b) (500 Hz). The measurement data at high bandwidth (a) reveal small phase drifts, overlaid by rather large levels of noise with no apparent outliers. Such outliers would be masked at lower bandwidth. At 500 Hz bandwidth (b), the phase noise is considerably lower, revealing a small

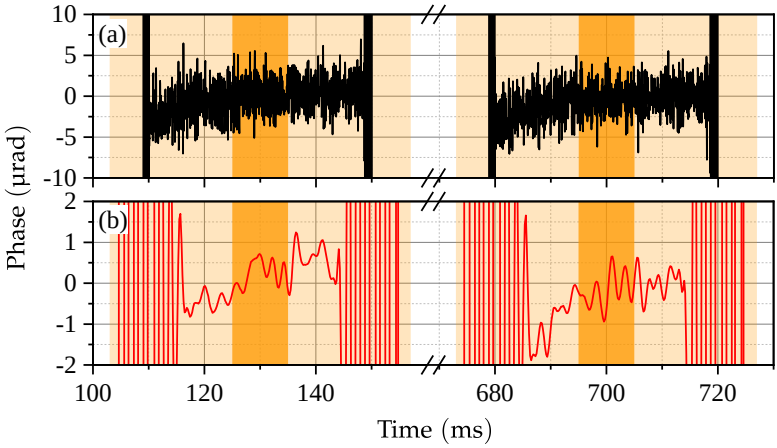

Figure 5.4: Phase transients during interferometric switching. (a) 10 kHz analysis bandwidth and (b) 500 Hz analysis bandwidth. The two Ramsey interactions are symbolized by orange boxes. The time interval the atoms spend in the cut-off tubes is indicated by light orange boxes.

phase difference between the two Ramsey interactions. At low bandwidth, a significant filter settling time (discussed earlier in Section 4.2.4) can be observed.

The data were also recorded in 25 sets of 5000 coherent averages. Based on this data, the phase difference between the two Ramsey interactions was evaluated to be (0.42 ± 0.85) µrad. Using the calculations explained in Section 4.1.1, the resulting fountain frequency shift was determined. A phase difference of 1.27 µrad corresponds to a relative shift of 3.9×10^{-17}.

5.1.5 Assessment

The IFS was installed in the fountain CSF1. Two modes of operation were used, normal mode and IFS mode. In normal mode, the switch is not actuated and the output signal is not attenuated. In IFS mode, the interferometric switch is triggered synchronously to the cycle. The fountain frequency was recorded independently for both operation modes. We have to take into account, that the frequency shift resulting from microwave leakage could be correlated with the shifts caused by the cycle synchronous field alterations.

Assuming a correlation coefficient of -1, the resulting shift is obtained by adding linearly the frequency shifts induced by the switching process to the leakage shift estimate obtained from the frequency difference [38].

Fountain operation alternating between normal mode and IFS mode showed a frequency difference of $(1.5 \pm 1.4) \times 10^{-16}$. The maximal expected leakage shift can be calculated to be $2.9 \times 10^{-16} + 3.9 \times 10^{-17} \approx 3.3 \times 10^{-16}$. Use of the interferometric switch will reduce the amplitude of the resonant field by at least 35 dB during the Ramsey time, resulting in a reduction of possible frequency shifts by at least a factor of 50. Therefore, the maximal expected leakage shift during IFS operation can be estimated to be 6.6×10^{-18}.

The total uncertainty of microwave leakage related effects can be calculated by the quadratic addition of the maximum expected leakage shift and possible frequency shifts induced by the switching process (3.9×10^{-17}). The systematic uncertainty contribution associated with microwave leakage in CSF1 is 4.0×10^{-17} when using the interferometric switch.

5.2 Phase-coherent frequency detuning

5.2.1 Principle

Undesired interactions of the caesium atoms with an external leakage field can also be reduced by detuning the field frequency from resonance [28].

We assume f_0 to be the frequency of the Ramsey interrogation signal, tuned to the atomic resonance, f_{Det} the frequency detuning, and $f_1 = f_0 + f_{\mathrm{Det}}$ to be the detuned frequency. Due to the sinusoidal nature of the signals involved, the two frequencies f_0 and f_1 repeatedly have the same phase after time t given by $t = 1/f_{\mathrm{Det}}$. Therefore, the phase before and after the frequency detuning will be the same if the detuning time t_{d} is an integer multiple n of the period of the detuning frequency:

$$t_{\mathrm{d}} = n \cdot \frac{1}{f_{\mathrm{Det}}}. \tag{5.1}$$

In Figure 5.5, the two Ramsey interactions R_1 and R_2 are shown, separated by the Ramsey time T_{R}. Shortly after the end of the first Ramsey interaction, when the atoms have passed the microwave resonator, the frequency of the microwave field is detuned by f_{Det}. The relative phase between the microwave field and the atomic superposition starts to progress, wrapping

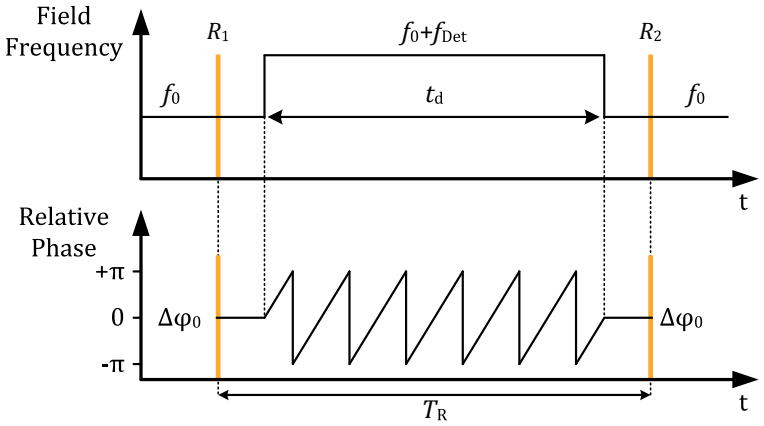

Figure 5.5: Phase-coherent frequency detuning - principle

over several times. After time t_d, before the caesium atoms enter the Ramsey cavity for the second time, the microwave frequency is switched back to f_0. If equation 5.1 is fulfilled, the phase difference resulting from the frequency detuning is zero. The frequency detuning is thus imperceptible when only looking at the phase relation before and after the detuning, as done in the Ramsey scheme.

5.2.2 Direct digital synthesis

Direct digital synthesis (DDS) is a well established signal generation method, a detailed description is available in [144], for a concise introduction refer to [145, 146]. The main parts of a direct digital synthesizer are a phase accumulator, a phase-to-amplitude look-up table and a digital-to-analog converter (DAC) (Fig. 5.6).

The phase accumulator is a N-bit register that is incremented by the value of a N-bit tuning word with every cycle of the DDS reference clock. The maximum value of the phase accumulator register is 2^N, further incrementation will lead to overflow. The digital phase value at the output of the accumulator therefore has a repetitive range of 0 to 2^N. This corresponds to the repetitive angular phase range of 0 to 2π of continuous-time sinusoidal signals. The output of the phase accumulator is converted to an amplitude

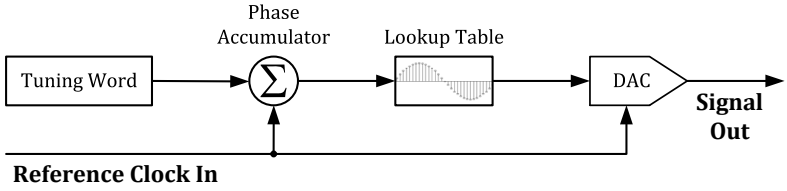

Figure 5.6: Direct digital synthesis - principle

value by using a sine wave look-up table, the minimum (0) and maximum (2^N) values of the phase accumulator are mapped to 0 and 2π respectively. The amplitude value is then fed to a DAC, clocked with the DDS reference clock. The output frequency depends on the value of the tuning word and the reference clock. For a DDS with a resolution of N bits and a reference clock frequency f_{clk}, the frequency tuning word M_0 can be calculated for the desired output frequency f_0:

$$M_0 = \frac{f_0}{f_{clk}} \cdot 2^N. \tag{5.2}$$

Direct digital synthesizers are available as integrated circuits with different feature sets. In the phase-coherent frequency detuning setup, the chip AD9956 from Analog Devices is utilized [147]. Characteristic features of this DDS chip are depicted in Figure 5.7. Eight 48-bit tuning words are available from which two are shown, the tuning words M_0 and M_1. The active tuning word is selected by the internal state machine based on the logic level of an input pin of the DDS chip. The state machine is clocked with an internal system clock (f_{sysclk}), phase locked to the reference clock (f_{clk}). The tuning word selection input is evaluated by the state machine at rising edges of the system clock only.

By changing the tuning word for a certain time t_d, the DDS frequency can be increased so that the additional phase increment due to this detuning equals $n \cdot 2\pi$ (for integer n). If the phase accumulator is incremented by an additional M_{Det} (with $M_1 = M_0 + M_{Det}$) with every clock cycle, the frequency is increased correspondingly and becomes $f_1 = f_0 + f_{Det}$. By selecting appropriate parameters, equation 5.1 can be satisfied and the additional phase increment becomes zero ($n \cdot 2\pi$), when switching back to the original frequency f_0 after the detuning time t_d:

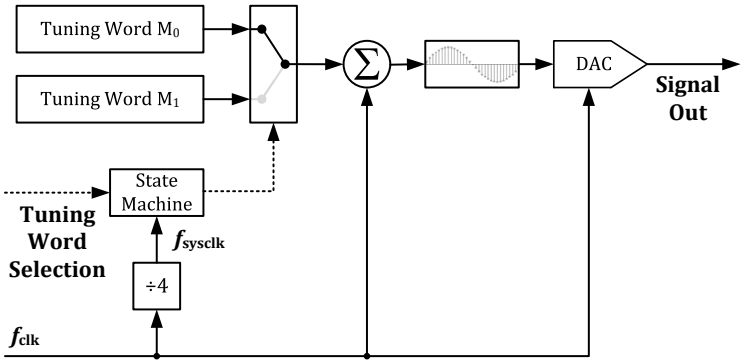

Figure 5.7: Direct digital synthesis - implementation in the AD9956

$$t_{\mathrm{d}} = \frac{n \cdot 2^{\mathrm{N}}}{M_{\mathrm{Det}} \cdot f_{\mathrm{clk}}}. \tag{5.3}$$

In reality, due to the finite frequency resolution of the DDS there will be a slight phase error accumulated as a result of the detuning. For a DDS reference clock f_{clk} of 50 MHz and a DDS resolution of 48 bits, the least significant bit of the tuning word corresponds to $50\,\mathrm{MHz}/2^{48} = 0.18\,\mu\mathrm{Hz}$, resulting in a maximum quantization error $\Delta f_{\mathrm{quant}}$ of 0.09 µHz [148]. This quantization error will give rise to the phase error $\Delta\varphi_{\mathrm{quant}}$, linearly increasing over the detuning time:

$$\Delta\varphi_{\mathrm{quant}} = \Delta f_{\mathrm{quant}} \cdot t_{\mathrm{d}} \cdot 2\pi. \tag{5.4}$$

Using equation 4.2, the effect of the quantization on the fountain frequency error δ_{f} can be calculated:

$$\delta_{\mathrm{f}} = \frac{\Delta\varphi_{\mathrm{quant}}}{f_0 \cdot T_{\mathrm{R}} \cdot 2\pi} = \frac{\Delta f_{\mathrm{quant}} \cdot t_{\mathrm{d}}}{f_0 \cdot T_{\mathrm{R}}}. \tag{5.5}$$

For a quantization error $\Delta f_{\mathrm{quant}} = 0.09\,\mu\mathrm{Hz}$ and a detuning duration $t_{\mathrm{d}} = 500\,\mathrm{ms}$, the accumulated phase error due to the detuning would be 0.3 µrad. Such a phase offset between the two Ramsey interactions would lead to a relative frequency error of 1×10^{-17} for a Ramsey time T_{R} of 550 ms. Taking into account the rectangular distribution, this corresponds to a systematic uncertainty contribution u_{quant} of 0.6×10^{-17}.

5.2.3 Implementation

The aforementioned DDS chip AD9956 is used to control the frequency of the Ramsey interrogation signal, a detailed explanation of the synthesizer was given in Section 3.3.2. The experimental control computer programs the DDS with two tuning words: M_0 (corresponding to the original frequency of the Ramsey interrogation signal) and M_1 (corresponding to the detuned frequency). Each tuning word is written to a different register and the registers can be selected from an input pin of the DDS chip (offset enable). The detuning time t_d has to match the detuning $M_{Det} = M_1 - M_0$ according to equation 5.3.

As shown in Figure 5.7, the offset tuning word is processed inside the DDS chip, the state machine is clocked with the DDS system clock: $f_{sysclk} = f_{clk}/4$. In our case, a DDS reference clock of 50 MHz is used. The system clock is 12.5 MHz, equivalent to a clock period of 80 ns. The tuning word selection input is evaluated at the rising edges of the system clock only, the DDS can not resolve changes of the tuning word within a clock period. The tuning word selection signal is expected to have a timing jitter of a few nanoseconds. If the edges of the tuning word selection signal coincide with a rising edge of f_{sysclk}, t_d could jitter by one clock cycle as a result. This would result in a wrong phase value after the detuning. Taking advantage of the 50% duty cycle of the system clock, we align the falling and rising edges of the tuning word selection signal with the falling edges of f_{sysclk}, thus achieving maximum jitter tolerance.

This alignment is performed by a dedicated trigger synchronization setup, complementing the DDS module (Fig. 5.8). The 100 MHz signal required for the DDS module is also supplied to the trigger synchronization module, enabling a fixed phase relation to the DDS clock. Magnetical isolators and optocouplers are used to avoid ground loops and minimize phase disturbances of the 7.3 MHz output signal. The trigger for the frequency detuning sent from the fountain control computer is asynchronous with respect to the DDS clock. Its length is adjusted to match equation 5.1 for the applied detuning frequency f_{Det}. The rising and falling edges of the resulting pulse are aligned with the falling edges of f_{sysclk}. The synchronized tuning word selection signal is fed to the DDS chip.

The trigger synchronization has been implemented with a delay generator and a simple synchronization logic for the trigger input. The detuning time

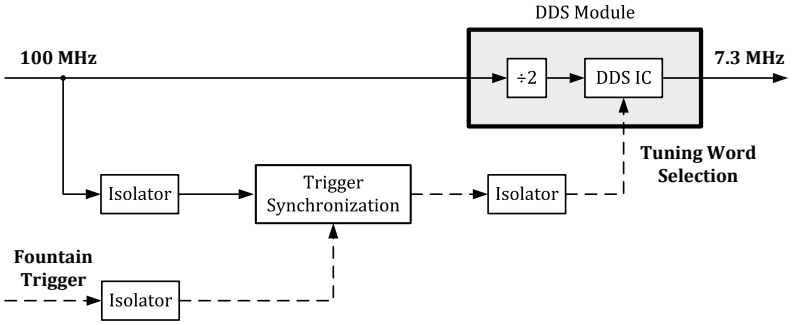

Figure 5.8: Phase-coherent frequency detuning - setup

t_d was kept at a fixed value of 500 ms. In the future, the synchronization will be realized with a field programmable gate array (FPGA), allowing full control of the detuning timing by the fountain control computer.

5.2.4 Detuning timing

Two frequency detunings were selected to evaluate the timing parameters, 400 Hz and 500 kHz. Detuning the Ramsey interrogation signal by 400 Hz will reduce the frequency shifting effect of microwave leakage by at least one order of magnitude [115]. A greater suppression of microwave leakage can be achieved at higher detunings [26]. The frequency detuning is limited by the DDS tuning range, making detunings much larger than 500 kHz impractical.

The method depends on the exact timing of the detuning pulse. The edges of the tuning word selection signal have to be aligned with the falling edge of f_{sysclk}. If the detuning time t_d is shortened by one period of the reference clock f_{Ref}, the phase accumulator would miss one addition of the tuning word, resulting in a phase slip $\Delta\varphi_{\mathrm{slip}}$:

$$\Delta\varphi_{\mathrm{slip}} = f_{\mathrm{Ref}} \cdot \frac{M_{\mathrm{Det}}}{2^{48}} \cdot 2\pi. \tag{5.6}$$

For frequency detunings of 400 Hz and 500 kHz, a missed clock cycle would result in phase slips of 200 µrad and 250 mrad, respectively.

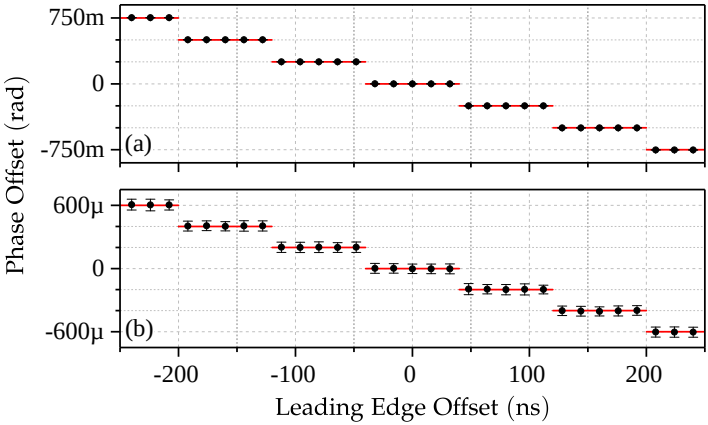

Figure 5.9: Ramsey interaction phase differences for different timings of the detuning pulse leading edge. a) Frequency detuning 500 kHz, b) Frequency detuning 400 Hz.

Using the phase transient analyzer, we evaluated the phase difference between the two Ramsey interactions in relation to the timing of the trigger pulse. The leading and trailing pulse edges were evaluated separately. These parameters were recorded for a range of pulse delays at detunings of 400 Hz and 500 kHz. All delays were set with respect to the synchronized trigger pulse. The measurement data for the leading edge of the detuning pulse are given in Figure 5.9. The data agree with the calculated values that are shown as red lines with steps of 250 mrad (Figure 5.9(a)) and 200 µrad (Figure 5.9(b)). The steps have a width of 80 ns, corresponding to the period of the system clock. Measurements of the trailing edge delay yielded comparable results.

The phase slip $\Delta\varphi_{\text{slip}}$ corresponds to a fountain frequency shift. Using equations 5.6 and 4.2, the frequency shift Δf_{slip} due to a missed clock cycle can be estimated:

$$\Delta f_{\text{slip}} = \frac{1}{f_0 \cdot T_{\text{R}}} \cdot \frac{f_{\text{Det}}}{f_{\text{sysclk}}}. \tag{5.7}$$

If the frequency is detuned by 500 kHz during a 550 ms Ramsey time, a missed clock cycle results in a frequency step of 73 mHz, equivalent to a relative frequency difference of 8×10^{-12}. Likewise, with a detuning of

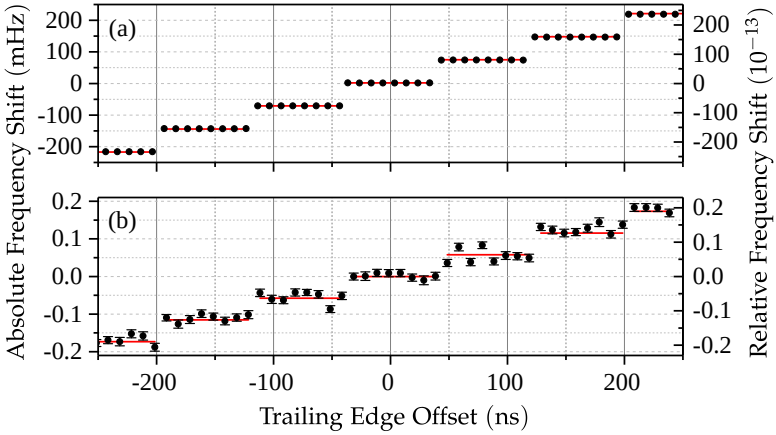

Figure 5.10: Fountain frequency offset for different timings of the detuning pulse trailing edge. a) Frequency detuning 500 kHz, b) Frequency detuning 400 Hz.

400 Hz, a missed clock cycle will cause a frequency step of 58 µHz and a relative difference of 6×10^{-15}.

The fountain was put into operation with the detuning-enabled synthesizer, recording the fountain frequency while shifting the edges of the detuning trigger pulse. The measurement data for the trailing edge delays are given in Figure 5.10. The top graph shows the results for a frequency detuning of 500 kHz, 20 frequency measurements were made for each point. The calculated values are shown as red lines, exhibiting distinctive plateaus with a width of 80 ns that agree very well with the measured data. The frequency values for a frequency detuning of 400 Hz are shown in Figure 5.10(b), the steps in frequency are smaller by 3 orders of magnitude, again agreeing very well with the calculations shown as red lines. For each point, over 1000 fountain cycles were averaged, requiring a measurement time of 30 minutes per point.

Measurements of the fountain frequency shift in relation to the leading edge delay yielded similar results. The fountain frequency data closely resemble the results of the phase measurements as presented in Figure 5.9. For determining the delay parameters, a fountain frequency measurement is therefore equivalent to a measurement with a phase transient analyzer. At a detuning of 500 kHz, a timing error will cause a frequency step that is

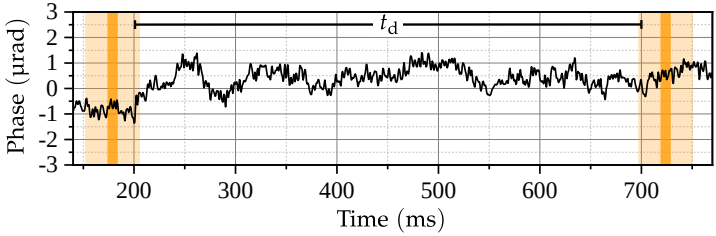

Figure 5.11: Ramsey interrogation signal phase with 0 Hz detuning. The two Ramsey interactions are symbolized by orange boxes. The time interval the atoms spend in the cut-off tubes is indicated by light orange boxes.

detectable instantaneous during regular fountain operation. This allows for an online monitoring of the detuning scheme.

5.2.5 Phase transients

The phase transient analyzer presented in Chapter 4 was used to evaluate detrimental effects on the phase of the Ramsey interrogation signal. Phase disturbances are most likely caused by the trigger signals, activated right before and after the Ramsey interrogations.

To assess the effect of the trigger signals, the detuning frequency was set to 0 Hz. The acquired phase values of the Ramsey interrogation signal for a bandwidth of 500 Hz are given in Figure 5.11. The two Ramsey interactions of 10 ms duration are symbolized by orange boxes, light orange boxes indicate the time interval the atoms spend in the cut-off tubes. The detuning interval of length t_d is centered between the two Ramsey interactions. No effects of the register switching at the micro-radian level can be identified at the beginning or the end of the detuning interval.

Additional phase measurements of the Ramsey interrogation signal were performed, this time setting a frequency detuning of 400 Hz. The results are given in Figure 5.12. No phase perturbations during the two Ramsey interactions are discernible. Taking into account the standard deviation of the measurement, the phase difference between the two interactions is well below 1 µrad, corresponding to an uncertainty contribution u_{phase} of 3×10^{-17}. Phase measurements at 500 kHz detuning also showed no evidence of phase distortions that could lead to a frequency shift above this level.

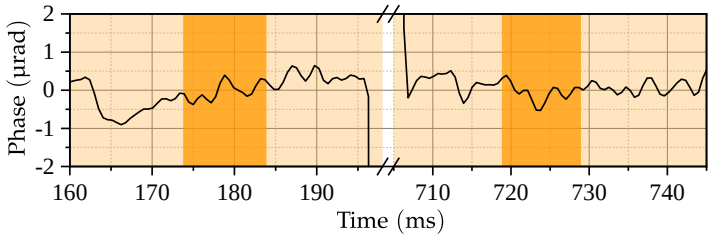

Figure 5.12: Phase of the CSF2 Ramsey interrogation signal with 400 Hz detuning. The two Ramsey interactions are symbolized by orange boxes. The time interval the atoms spend in the cut-off tubes is indicated by light orange boxes.

5.2.6 Assessment

To estimate an upper limit for remaining frequency shifts when using this method, a frequency measurement was performed with CSF2. The fountain was operated with the detuning-enabled synthesizer, using two modes of operation. In the detuning mode, the phase-coherent frequency detuning is triggered synchronously to the cycle. In the normal mode, the interrogation signal is not detuned. For the measurement, a detuning of 400 Hz was used. A relative frequency difference of $(-0.1 \pm 2.0) \times 10^{-16}$ was obtained.

In Section 5.2.2, the uncertainty contribution u_{quant} due to the quantization error was estimated to be 0.6×10^{-17}. The uncertainty contribution due to phase transients (u_{phase}) could be verified in the previous section to be below 3×10^{-17}. We need to take into account that in an unfavorable case a microwave leakage induced shift could be correlated with the shifts u_{quant} and u_{phase}. By adding linearly these detuning-caused shift estimates to the leakage shift estimate (2.1×10^{-16}) obtained from the frequency difference measurement, we get a worst case estimate of the leakage shift without detuning of 2.5×10^{-16}.

Taking into account a reduction by a factor of 10, the frequency detuning would result in a leakage shift (and a corresponding uncertainty u_{det}) of 2.5×10^{-17}. The uncertainty due to residual microwave leakage shifts is obtained from the quadratic addition of the uncertainties u_{phase}, u_{quant} and u_{det}. When the phase coherent frequency detuning method is used with a Ramsey time frequency detuning of 400 Hz, the systematic uncertainty contribution due to microwave leakage in CSF2 would thus be 4.0×10^{-17}.

5.3 Comparison of the methods

This thesis presented two methods to reduce the effect of microwave leakage in CSF1 and CSF2, currently associated with a systematic uncertainty contribution of 1×10^{-16} [82, 130]. The interferometric switch relies on a reduction of the Ramsey interrogation signal amplitude to diminish the effect of leakage fields. This method has been implemented in the caesium fountain CSF1, resulting in a systematic uncertainty contribution due to microwave leakage of 4.0×10^{-17}. We were also able to demonstrate that the effect of microwave leakage can be reduced by phase coherent frequency detuning to the 10^{-17} level. The demonstration was set up on CSF2 and the systematic uncertainty contribution of microwave leakage related effects was determined to be 4.0×10^{-17} at the most.

The interferometric switch has been introduced to several caesium fountains [21, 54, 96–98, 149–151]. Due to its analog nature, its implementation requires a careful selection of components, and ideally a phase transient analyzer. As the method relies on a variation of the amplitude, the thermal impact on the frequency synthesizer has to be considered and examined. The frequency range of the interferometric switch is limited, it is suitable for frequencies in the range of 50 MHz - 500 MHz. A temperature compensation of the switch can be necessary. The extinction ratio has to be checked regularly, as it can vary due to component aging and drift effects.

The phase-coherent frequency detuning method [28] relies on digital frequency synthesis and obviates the specific disadvantages of an analog design such as aging and drift. The most likely cause for phase transients in the Ramsey interrogation signal are disturbances from the trigger signals due to crosstalk. Other interfering effects are hardly conceivable. Crosstalk can be minimized with signal isolation and separated power supplies.

The approach requires a DDS-based synthesizer which is widely used in controlling the frequency of the Ramsey interrogation signal [71, 92, 93, 95, 96]. No temperature compensation of the frequency detuning setup itself is necessary and also the thermal impact on the synthesizer is negligible, as the amplitude of the Ramsey interrogation signal remains constant. The method presented is tolerant towards small fluctuations in the detuning timing; timing errors can be detected by monitoring the fountain frequency. This method has several advantages over the interferometric switch, especially fountain operation without the need for periodic evaluations.

The uncertainty contribution resulting from the quantization error, u_{quant}, can be eliminated. This error will be zero if the detuning frequency can be generated in a DDS without quantization. This is true for detuning frequencies f_{Det} that fulfill the equation $f_{\mathrm{Det}} = f_{\mathrm{clk}}/2^n$ (for integer n). It can be expected, that the systematic uncertainty of the method will then be limited only by statistical parameters of the fountain frequency measurement and the phase transient measurements. In this case, a systematic uncertainty due to microwave leakage of less then 1×10^{-17} is conceivable.

6 Assessment in a global context

This work demonstrated the potential of microwave signal generation for the reduction of uncertainties in atomic fountain clocks. In this section, the results will be reviewed and the current state of research will be discussed. For the discussion, caesium fountain clocks are taken into account that have been regularly contributing to the international atomic time scale in the period from July 2015 to June 2017. The following fountain clocks will be considered, their total systematic uncertainties reported for contributions to TAI is given in Table 6.1:

- FO2 from the Laboratoire national de métrologie et d'essais - Systèmes de Référence Temps Espace (LNE-SYRTE) in France [15]
- SU-CsFO2 from the All-Russian Scientific Research Institute of Physico-Technical Measurements (VNIIFTRI) [55]
- NIST-F1 from the National Institute of Standards and Technology (NIST) [56]
- ITCsF2 from the Italian Istituto Nazionale di Ricerca Metrologica (INRIM) [54]
- NPL-CsF2 from the National Physical Laboratory of England (NPL) [3]
- NIM5 from the National Institute of Metrology (NIM) of China [97]

Fountain Clock	Total systematic uncertainty
LNE-SYRTE-FO2	2.4×10^{-16} [152]
SU-CsFO2	2.4×10^{-16} [153]
NIST-F1	3.1×10^{-16} [154]
ITCsF2	1.7×10^{-16} [155]
NPL-CsF2	3.7×10^{-16} [156]
NIM5	1.4×10^{-15} [157]

Table 6.1: Total systematic uncertainties reported for TAI contributions

Phase transient analysis

A system that facilitates a detailed analysis of cycle-synchronous perturbations in the Ramsey interrogation signal has been presented. The developed phase analyzer system utilizes a FPGA and an analog-digital converter front-end [23]. Data acquisition and filtering is entirely carried out using the FPGA, enabling the implementation of variable filters and decimation techniques as well as digital demodulation and phase detection. The system proved indispensable for the evaluation of transient-free switching methods aimed at the reduction of microwave leakage effects in fountain clocks [27]. Cycle-synchronous phase transients below 1 µrad can be detected, allowing to evaluate the associated fountain uncertainties at the low 10^{-17} level. The phase analyzer was also used to investigate phase variations in optical frequency standards [23].

A detailed analysis of phase transients in fountain clocks was first described for the fountain LNE-SYRTE-FO2 [21]. Phase perturbations could be identified at the µrad level and frequency shifts caused by phase transients were verified to be below 3×10^{-17} [21].

A similar system has been used for the analysis of phase transients in NIM5, allowing to identify cycle-synchronous phase perturbations below 10 µrad [59, 150]. Associated frequency shifts were assessed at the low 10^{-16} level.

Up to now, no evaluation of frequency shifts caused by cycle-synchronous phase transients has been published for the fountains NPL-CsF2, SU-CsFO2, ITCsF2, and NIST-F1.

Synthesizer phase noise

Phase noise in the Ramsey interrogation signal can limit the frequency stability of the fountain (Dick effect) [9]. The phase noise of the Ramsey interrogation signal is constrained by the phase noise of the local oscillator used as a reference for the microwave synthesizer. In this work, a microwave synthesizer was presented that can be referenced to an optically stabilized microwave. During the design, great care was taken to minimize noise contributions from components and assemblies. The instability attributed to the Dick effect could be reduced to a level well below the instability resulting from quantum projection noise.

For CSF1, this instability limit has been reported to be $9.1 \times 10^{-14}(\tau/s)^{-1/2}$, while CSF2 can reach a level of $2.5 \times 10^{-14}(\tau/s)^{-1/2}$ [20]. The optically stabilized microwave offers a superior phase noise performance, but it is a rather complex system. An automatic fall-back system to a robust local quartz oscillator has been implemented to achieve a high availability.

The microwave synthesizer designed for LNE-SYRTE-FO2 is referenced to a cryogenic sapphire oscillator [87, 94]. This allows to operate the fountain at the quantum projection noise limit ($1.6 \times 10^{-14}(\tau/s)^{-1/2}$) [15, 71]. The application of an optically stabilized microwave as a local oscillator has been demonstrated [75].

The microwave synthesizer used for NPL-CsF2 is referenced to a local quartz oscillator. Hence, the attainable fountain instability is limited by the Dick effect to $1.7 \times 10^{-13}(\tau/s)^{-1/2}$ [96]. Operation of the fountain at the quantum projection noise limit has been demonstrated, using an optically stabilized microwave as a local oscillator. A fountain instability of $3.7 \times 10^{-14}(\tau/s)^{-1/2}$ was reported [3].

In the fountains NIM5, SU-CsFO2, ITCsF2, and NIST-F1, the interrogation signals are referenced to local quartz oscillators, resulting in fountain instabilities at the low 10^{-13} level [54, 55, 59, 92].

Spectral impurities

Frequency shifts due to spectral impurities in the Ramsey interrogation signal [8] had been taken into account with 1×10^{-17} in the uncertainty budget of PTB's caesium fountain CSF2 [158]. For CSF1, a contribution of 1×10^{-16} had been taken into account [159]. As a part of this work, the uncertainty contribution attributed to these frequency shifts was evaluated to be 2.3×10^{-18}.

In the uncertainty budgets of the caesium fountains NIM5 [97] and NPL-CsF2 [96], an uncertainty contribution of 1×10^{-17} is specified. An identical value has been given for SU-CsFO2 [153] and ITCsF2 [54]. For the fountain NIST-F1, the uncertainty contribution from spurious components were determined to be 3×10^{-18} [154].

Microwave leakage

Interactions between the caesium atoms and microwave fields are only intended for short periods of time during the fountain cycle. Uncontrolled interactions of the atoms with leakage fields outside these periods can lead to frequency shifts [24]. In the fountains CSF1 and CSF2, this effect had been taken into account so far with a systematic uncertainty contribution of 1×10^{-16} [82, 130]. By manipulating the parameters of the Ramsey interrogation signal synchronous to the fountain cycle, it is possible to suppress the frequency-shifting effect of leakage fields and thus reduce the uncertainty contribution associated with microwave leakage.

In CSF1, a method was implemented that relies on manipulation of the field amplitude [21], a systematic uncertainty contribution of 4×10^{-17} could be demonstrated. This corresponds to the results published for the application of this method in the caesium fountains LNE-SYRTE-FO2 [15] and NPL-CsF2 [96]. This method has also been applied to the caesium fountain NIM5, here a significantly larger uncertainty contribution of 1.2×10^{-15} has been reported [97].

The effect of leakage fields can also be suppressed by detuning the field frequency [28]. An uncertainty contribution of 2×10^{-16} was estimated for the application of this method at NIM5. As a part of this work, a phase-coherent frequency detuning scheme for CSF2 was developed [27] and the uncertainty contribution due to microwave leakage was reduced to 4×10^{-17}. A further reduction to below the 10^{-17} level appears feasible.

In the fountain ITCsF2, the effect of leakage fields is suppressed using a combination of passive methods and a frequency shift keying scheme [84]. The systematic uncertainty associated with microwave leakage has been reported to be 1.5×10^{-16} [54].

For the fountain NIST-F1, the effect of microwave leakage has been reported to be below 1.1×10^{-16} [25, 154]. No evaluation of frequency shifts due to microwave leakage fields has been published for SU-CsFO2.

Collisional shift

Inter-atomic collisions can lead to significant fountain frequency shifts [79]. The shift can be estimated and corrected during fountain operation [112]. For the shift estimation, the fountain is operated with different atom densities by varying the parameters of the state selection process. Depending

on the method of density control, the applied correction can be subject to a large relative uncertainty [11].

Prior to this work, the atom density in CSF2 had been varied by changing the field amplitude in the state selection cavity [112]. With this method, the relative uncertainty of the shift estimation is about 10%. For atom numbers of 3×10^4, the collisional shift is on the order of 1×10^{-15} [12], resulting in a systematic uncertainty contribution of 1×10^{-16}. In this work, the method of rapid adiabatic passage [18] was implemented in CSF2 and the relative uncertainty of the collisional shift estimation was reduced by one order of magnitude to below 1% [19]. For 10^6 probed atoms, the systematic uncertainty contribution attributed to the collisional shift was reported to be 4×10^{-17}, taking into account a relative uncertainty of 0.5% [82].

The method of rapid adiabatic passage was originally developed for the fountain LNE-SYRTE-FO2 [18, 94]. The relative uncertainty of the collisional shift correction is estimated to be 0.5% [152]. A systematic uncertainty contribution of 5×10^{-17} is taken into account for atom numbers on the order of 10^6.

The fountain clock NPL-CsF2 is operated at the zero collisional shift point by modifying the composition of atomic states [160]. With this method, a systematic collisional shift uncertainty of 4×10^{-17} [3] could be achieved for atom numbers on the order of 10^6.

In the fountains NIM5, SU-CsFO2, ITCsF2, and NIST-F1 no particular technique for collisional shift reduction is applied. The systematic uncertainty contribution associated with the collisional shift in NIM5 is on the order of 1×10^{-16} for 1.5×10^6 probed atoms [97]. In the evaluation of the fountains SU-CsFO2, ITCsF2, and NIST-F1 the collisional shift is not taken into account as a systematic contribution to the total fountain uncertainty.

Conclusion

One of the objectives of this work was to reduce the contribution of the microwave synthesis to the systematic uncertainty of the fountains to an insignificant level. This goal has been reached. Moreover, the potential of the microwave generating electronics for the further reduction of systematic and statistical uncertainties was successfully exploited.

For CSF1, systematic uncertainty contributions associated with microwave-generating electronics and microwave leakage effects were addressed. Uncertainty contributions associated with electronics could be reduced from 2×10^{-16} to 2.3×10^{-18} while uncertainty contributions associated with microwave leakage could be reduced from 1×10^{-16} to 4×10^{-17}. The combined contribution of the two effects was reduced to 0.4×10^{-16}. Considering the total systematic uncertainty for CSF1 of 3.6×10^{-16}, the contribution of the microwave-generating electronics is now negligible.

For CSF2, the systematic uncertainty contributions associated with the microwave-generating electronics were reduced from 2×10^{-16} to 2.3×10^{-18} and the uncertainty contributions associated with microwave leakage were reduced from 1×10^{-16} to 4×10^{-17}. The implementation of rapid adiabatic passage allowed to increase the number of probed atoms by about two orders of magnitude while at the same time led to a reduction of the systematic uncertainty associated with the collisional shift from 1×10^{-16} to 4×10^{-17}. The combined uncertainty contribution of the three effects was reduced from 2.4×10^{-16} to 0.6×10^{-16}. This was a necessary condition for CSF2 to achieve a exceptionally low systematic uncertainty of 1.8×10^{-16}.

7 Summary

This work focuses on the reduction of the frequency instability and the systematic uncertainty in fountain clocks. The important techniques were presented, addressing detrimental effects closely related to microwave signal generation. Technical limitations to the fountain frequency stability were eliminated and the systematic uncertainty attributed to several effects was significantly reduced. For PTB's caesium fountain clock CSF2, the application of the techniques described herein will result in a record systematic uncertainty of 1.8×10^{-16}.

The microwave synthesizer outlined in Chapter 3 features a modular architecture, aspects such as operational reliability and ease of maintenance were taken into account during the development. It can be referenced to two different local oscillators, a quartz oscillator and an optically stabilized microwave. Using this synthesizer, the fountains can be operated in the quantum projection noise limited regime, removing technical limitations to their frequency instability.

To enable operation of CSF2 with high atom numbers, the method of rapid adiabatic passage was implemented. Using this method, the relative uncertainty of the collisional shift estimation was reduced by one order of magnitude to below 1%. The number of probed atoms was increased to 10^6 while maintaining a collisional shift uncertainty of 0.4×10^{-16}. With this atom number, CSF2 can be operated a frequency instability of $2.5 \times 10^{-14}(\tau/s)^{-1/2}$.

In this work, the development of a phase-transient analyzer is presented, covering the technical requirements, the design process, and the evaluation (Chapter 4). The system allows for the detection of cycle-synchronous phase transients below 1 µrad, the associated fountain uncertainties can be evaluated at the low 10^{-17} level. Using the transient phase analyzer, the impact of cycle synchronous phase transients on PTB's fountain clocks CSF1 and CSF2 could be investigated for the first time. This system can also be used to investigate phase variations in optical frequency standards.

Microwave leakage had been associated with a systematic uncertainty contribution of 1×10^{-16} in the uncertainty budgets of CSF1 and CSF2. In Chapter 5, two methods to reduce this contribution were presented, the phase transient analyzer proving indispensable for their evaluation. In CSF1, an interferometric switch was implemented, resulting in a uncertainty contribution due to microwave leakage of 4×10^{-17}. For CSF2, a phase coherent frequency detuning scheme was developed. With this scheme, a reduction of the uncertainty attributed to microwave leakage to below the 10^{-17} level is feasible.

PTB's fountains are among the world's best primary fountain clocks regarding systematic and statistical uncertainty as well as reliability. In 2017, they have been regularly contributing to the calibration of TAI with weights of $60 - 80\%$. The microwave systems presented in this work are integral components for the caesium fountains CSF1 and CSF2. Their potential for the reduction of fountain uncertainties was successfully exploited. The developed systems are highly reliable and allow for continuous fountain operation and dependable contributions TAI, further strengthening the prominent position of PTB's fountain clocks.

Bibliography

[1] BIPM, *SI brochure: The international system of units (SI)*, 2014. [Online]. Available: http://www.bipm.org/utils/common/pdf/si_brochure_8.pdf.

[2] P. Gill, "When should we change the definition of the second?", *Philosophical Transactions of the Royal Society of London A: Mathematical, Physical and Engineering Sciences*, vol. 369, no. 1953, pp. 4109–4130, 2011, ISSN: 1364-503X. DOI: 10.1098/rsta.2011.0237.

[3] K. Szymaniec, S. N. Lea, K. Gibble, S. E. Park, K. Liu, and P. Głowacki, "NPL Cs fountain frequency standards and the quest for the ultimate accuracy", *J. Phys. Conf. Ser.*, vol. 723, no. 1, p. 012 003, 2016, ISSN: 1742-6596. DOI: 10.1088/1742-6596/723/1/012003.

[4] N. Huntemann, M. Okhapkin, B. Lipphardt, S. Weyers, C. Tamm, and E. Peik, "High-accuracy optical clock based on the octupole transition in $^{171}Yb^{+}$", *Phys. Rev. Lett.*, vol. 108, no. 9, p. 090 801, 2012, ISSN: 0031-9007. DOI: 10.1103/PhysRevLett.108.090801.

[5] F. Riehle, "Towards a redefinition of the second based on optical atomic clocks", *C. R. Phys.*, vol. 16, no. 5, pp. 506–515, 2015, ISSN: 1631-0705. DOI: 10.1016/j.crhy.2015.03.012.

[6] A. Bauch, S. Weyers, D. Piester, E. Staliuniene, and W. Yang, "Generation of UTC(PTB) as a fountain-clock based time scale", *Metrologia*, vol. 49, no. 3, p. 180, 2012. DOI: 10.1088/0026-1394/49/3/180.

[7] R. Wynands and S. Weyers, "Atomic fountain clocks", *Metrologia*, vol. 42, no. 3, Sp. Iss. SI, S64–S79, 2005, ISSN: 0026-1394. DOI: {10.1088/0026-1394/42/3/S08}.

[8] C. Audoin, M. Jardino, L. S. Cutler, and R. F. Lacey, "Frequency offset due to spectral impurities in cesium-beam frequency standards", *IEEE Trans. Instrum. Meas.*, vol. 27, no. 4, 325–329, 1978, ISSN: 0018-9456. DOI: 10.1109/TIM.1978.4314705.

[9] G. J. Dick, "Local oscillator induced instabilities in trapped ion frequency standards", *Proceedings of the Nineteenth Annual Precise Time and Time Interval (PTTI) Applications and Planning Meeting*, pp. 133–147, 1987.

[10] G. Rovera, G. Santarelli, and A. Clairon, "Frequency synthesis chain for the atomic fountain primary frequency standard", *IEEE Transactions on Ultrasonics, Ferroelectrics and Frequency Control*, vol. 43, no. 3, pp. 354–358, 1996. DOI: 10.1109/58.489391.

[11] S. Weyers, U. Hübner, R. Schröder, C. Tamm, and A. Bauch, "Uncertainty evaluation of the atomic caesium fountain CSF1 of the PTB", *Metrologia*, vol. 38, no. 4, pp. 343–352, 2001, ISSN: 0026-1394.

[12] V. Gerginov, N. Nemitz, S. Weyers, R. Schröder, D. Griebsch, and R. Wynands, "Uncertainty evaluation of the caesium fountain clock PTB-CSF2", *Metrologia*, vol. 47, no. 1, pp. 65–79, 2010. [Online]. Available: http://stacks.iop.org/0026-1394/47/i=1/a=008.

[13] W. M. Itano, J. C. Bergquist, J. J. Bollinger, J. M. Gilligan, D. J. Heinzen, F. L. Moore, M. G. Raizen, and D. J. Wineland, "Quantum projection noise: Population fluctuations in two-level systems", *Phys. Rev. A*, vol. 47, no. 5, pp. 3554–3570, 1993. DOI: 10.1103/PhysRevA.47.3554.

[14] G. Santarelli, P. Laurent, P. Lemonde, A. Clairon, A. G. Mann, S. Chang, A. N. Luiten, and C. Salomon, "Quantum projection noise in an atomic fountain: A high stability cesium frequency standard", *Phys. Rev. Lett.*, vol. 82, no. 23, pp. 4619–4622, 1999. DOI: 10.1103/PhysRevLett.82.4619.

[15] J. Guena, M. Abgrall, D. Rovera, P. Laurent, B. Chupin, M. Lours, G. Santarelli, P. Rosenbusch, M. E. Tobar, R. Li, K. Gibble, A. Clairon, and S. Bize, "Progress in atomic fountains at LNE-SYRTE", *IEEE Trans. Ultrason. Ferroelectr. Freq. Control*, vol. 59, no. 3, pp. 391–409, 2012, ISSN: 0885-3010. DOI: 10.1109/TUFFC.2012.2208.

[16] P. J. Leo, P. S. Julienne, F. H. Mies, and C. J. Williams, "Collisional frequency shifts in ^{133}Cs fountain clocks", *Phys. Rev. Lett.*, vol. 86, pp. 3743–3746, 2001. DOI: 10.1103/PhysRevLett.86.3743.

[17] K. Gibble and S. Chu, "Laser-cooled Cs frequency standard and a measurement of the frequency-shiftdue to ultracold collisions", *Phys. Rev. Lett.*, vol. 70, no. 12, 1771–1774, 1993, ISSN: 0031-9007. DOI: {10.1103/PhysRevLett.70.1771}.

[18] F. Pereira Dos Santos, H. Marion, S. Bize, Y. Sortais, A. Clairon, and C. Salomon, "Controlling the cold collision shift in high precision atomic interferometry", *Phys. Rev. Lett.*, vol. 89, no. 23, p. 233 004, 2002, ISSN: 0031-9007. DOI: {10.1103/PhysRevLett.89.233004}.

[19] M. Kazda, V. Gerginov, N. Nemitz, and S. Weyers, "Investigation of rapid adiabatic passage for controlling collisional frequency shifts in a caesium fountain clock", *IEEE Trans. Instrum. Meas.*, vol. 62, no. 10, pp. 2812–2819, 2013, ISSN: 0018-9456. DOI: 10.1109/TIM.2013.2248303.

[20] B. Lipphardt, V. Gerginov, and S. Weyers, "Optical stabilization of a microwave oscillator for fountain clock interrogation", *IEEE Trans. Ultrason. Ferroelectr. Freq. Control*, vol. 64, no. 4, pp. 761–766, 2017, ISSN: 0885-3010. DOI: 10.1109/TUFFC.2017.2649044.

[21] G. Santarelli, G. Governatori, D. Chambon, M. Lours, P. Rosenbusch, J. Guena, F. Chapelet, S. Bize, M. E. Tobar, P. Laurent, T. Potier, and A. Clairon, "Switching atomic fountain clock microwave interrogation signal and high-resolution phase measurements", *IEEE Trans. Ultrason. Ferroelectr. Freq. Control*, vol. 56, no. 7, pp. 1319–1326, 2009, ISSN: 0885-3010. DOI: {10.1109/TUFFC.2009.1188}.

[22] G. Santarelli, G. Governatori, M. Lours, D. Chambon, F. Chapelet, S. Bize, M. E. Tobar, T. Potier, and A. Clairon, "Phase transient measurement at the micro radian level for atomic fountain clocks", in *Proc. 20th European Frequency Time Forum*, 2006, pp. 166–172.

[23] M. Kazda, V. Gerginov, N. Huntemann, B. Lipphardt, and S. Weyers, "Phase analysis for frequency standards in the microwave and optical domains", *IEEE Trans. Ultrason. Ferroelectr. Freq. Control*, vol. 63, no. 7, pp. 970–974, 2016, ISSN: 0885-3010. DOI: 10.1109/TUFFC.2016.2515759.

[24] S. Weyers, R. Schröder, and R. Wynands, "Effects of microwave leakage in caesium clocks: Theoretical and experimental results", in *Proc. 20th European Frequency Time Forum*, 2006, pp. 173–180.

[25] J. H. Shirley, F. Levi, T. P. Heavner, D. Calonico, Y. D.-H., and S. R. Jefferts, "Microwave leakage-induced frequency shifts in the primary frequency standards NIST-F1 and IEN-CSF1", *IEEE Trans. Ultrason. Ferroelectr. Freq. Control*, vol. 53, no. 12, pp. 2376–2385, 2006, ISSN: 0885-3010. DOI: 10.1109/TUFFC.2006.186.

[26] J. Vanier and C. Audoin, *The quantum physics of atomic frequency standards*. Philadelphia: Adam Hilger, 1989, vol. 2, ISBN: 0852744331.

[27] M. Kazda and V. Gerginov, "Suppression of microwave leakage shifts in fountain clocks by frequency detuning", *IEEE Trans. Instrum. Meas.*, vol. 65, no. 10, pp. 2389–2393, 2016, ISSN: 0018-9456. DOI: 10.1109/TIM.2016.2581439.

[28] P. Lin, S. Liu, and N. Liu, "Microwave leakage shift suppression based on home made DDS", *Proceedings of the 2009 Joint IFCS and EFTF*, pp. 1026–1029, 2009, ISSN: 2327-1914. DOI: 10.1109/FREQ.2009.5168349.

[29] A. Sen Gupta, R. Schröder, S. Weyers, and R. Wynands, "A new 9-GHz synthesis chain for atomic fountain clocks", in *Proc. IEEE Int. Frequency Control Symp. joint with 20th European Frequency Time Forum*, 2007, pp. 234–237, ISBN: 978-1-4244-0646-3. DOI: 10.1109/FREQ.2007.4319071.

[30] D. A. Steck. (2010). Cesium D line data, [Online]. Available: http://steck.us/alkalidata.

[31] I. I. Rabi, J. R. Zacharias, S. Millman, and P. Kusch, "A new method of measuring nuclear magnetic moment", *Physical Review*, vol. 53, pp. 318–318, 1938. DOI: 10.1103/PhysRev.53.318.

[32] I. I. Rabi, S. Millman, P. Kusch, and J. R. Zacharias, "The molecular beam resonance method for measuring nuclear magnetic moments. the magnetic moments of $_3Li^6$, $_3Li^7$ and $_9F^{19}$", *Physical Review*, vol. 55, pp. 526–535, 1939. DOI: 10.1103/PhysRev.55.526.

[33] N. F. Ramsey, "A molecular beam resonance method with separated oscillating fields", *Phys. Rev.*, vol. 78, no. 6, pp. 695–699, 1950. DOI: 10.1103/PhysRev.78.695.

[34] N. F. Ramsey, "Experiments with separated oscillatory fields and hydrogen masers", *Rev. Mod. Phys.*, vol. 62, pp. 541–552, 1990. DOI: 10.1103/RevModPhys.62.541.

[35] D. W. Allan, "Statistics of atomic frequency standards", *Proceedings of the IEEE*, vol. 54, no. 2, pp. 221–230, 1966, ISSN: 0018-9219. DOI: 10.1109/PROC.1966.4634.

[36] L. S. Cutler and C. L. Searle, "Some aspects of the theory and measurement of frequency fluctuations in frequency standards", *Proceedings of the IEEE*, vol. 54, no. 2, pp. 136–154, 1966, ISSN: 0018-9219. DOI: 10.1109/PROC.1966.4627.

[37] W. Riley, *Handbook of frequency stability analysis*, Special Publication (NIST SP) - 1065, 2008. [Online]. Available: https://tf.nist.gov/general/pdf/2220.pdf.

[38] BIPM. (2008). Guide to the Expression of Uncertainty in Measurement, [Online]. Available: http://www.bipm.org/utils/common/documents/jcgm/JCGM_100_2008_E.pdf.

[39] M. A. Kasevich, E. Riis, S. Chu, and R. G. DeVoe, "RF spectroscopy in an atomic fountain", *Phys. Rev. Lett.*, vol. 63, no. 6, pp. 612–615, 1989. DOI: 10.1103/PhysRevLett.63.612.

[40] A. Clairon, C. Salomon, S. Guellati, and W. D. Phillips, "Ramsey resonance in a Zacharias fountain", *Europhys. Lett.*, vol. 16, no. 2, p. 165, 1991. [Online]. Available: http://stacks.iop.org/0295-5075/16/i=2/a=008.

[41] K. Gibble and S. Chu, "Future slow-atom frequency standards", *Metrologia*, vol. 29, no. 2, p. 201, 1992. [Online]. Available: http://stacks.iop.org/0026-1394/29/i=2/a=008.

[42] A. Clairon, P. Laurent, G. Santarelli, S. Ghezali, S. Lea, and M. Bahoura, "A cesium fountain frequency standard: Preliminary results", *IEEE Transactions on Instrumentation and Measurement,*, vol. 44, no. 2, pp. 128–131, 1995. DOI: 10.1109/19.377790.

[43] P. D. Lett, W. D. Phillips, S. L. Rolston, C. E. Tanner, R. N. Watts, and C. I. Westbrook, "Optical molasses", *J. Opt. Soc. Am. B*, vol. 6, no. 11, pp. 2084–2107, 1989. DOI: 10.1364/JOSAB.6.002084.

[44] S. Chu, "Nobel lecture: The manipulation of neutral particles", *Rev. Mod. Phys.*, vol. 70, pp. 685–706, 1998. DOI: 10.1103/RevModPhys.70.685.

[45] W. D. Phillips, "Nobel lecture: Laser cooling and trapping of neutral atoms", *Rev. Mod. Phys.*, vol. 70, pp. 721–741, 1998. DOI: 10.1103/RevModPhys.70.721.

[46] C. N. Cohen-Tannoudji, "Nobel lecture: Manipulating atoms with photons", *Rev. Mod. Phys.*, vol. 70, pp. 707–719, 1998. DOI: 10.1103/RevModPhys.70.707.

[47] G. D. Rovera, S. Bize, B. Chupin, J. Guéna, P. Laurent, P. Rosenbusch, P. Uhrich, and M. Abgrall, "UTC(OP) based on LNE-SYRTE atomic fountain primary frequency standards", *Metrologia*, vol. 53, no. 3, S81, 2016. [Online]. Available: http://stacks.iop.org/0026-1394/53/i=3/a=S81.

[48] F. Arias, G. Panfilo, and G. Petit, "Timescales at the BIPM", *Metrologia*, vol. 48, no. 4, S145, 2011. [Online]. Available: http://stacks.iop.org/0026-1394/48/i=4/a=S04.

[49] A. Bauch and S. Weyers, "New experimental limit on the validity of local position invariance", *Phys. Rev. D*, vol. 65, no. 8, p. 081 101, 2002. DOI: 10.1103/PhysRevD.65.081101.

[50] P. Wolf, F. Chapelet, S. Bize, and A. Clairon, "Cold atom clock test of Lorentz invariance in the matter sector", *Phys. Rev. Lett.*, vol. 96, p. 060 801, 2006. DOI: 10.1103/PhysRevLett.96.060801.

[51] H. Marion, F. Pereira Dos Santos, M. Abgrall, S. Zhang, Y. Sortais, S. Bize, I. Maksimovic, D. Calonico, J. Grünert, C. Mandache, P. Lemonde, G. Santarelli, P. Laurent, A. Clairon, and C. Salomon, "Search for variations of fundamental constants using atomic fountain clocks", *Phys. Rev. Lett.*, vol. 90, no. 15, p. 150 801, 2003. DOI: 10.1103/PhysRevLett.90.150801.

[52] M. Fischer, N. Kolachevsky, M. Zimmermann, R. Holzwarth, T. Udem, T. W. Hänsch, M. Abgrall, J. Grünert, I. Maksimovic, S. Bize, H. Marion, F. Pereira dos Santos, P. Lemonde, G. Santarelli, P. Laurent, A. Clairon, C. Salomon, M. Haas, U. D. Jentschura, and C. H. Keitel, "New limits on the drift of fundamental constants from laboratory measurements", *Phys. Rev. Lett.*, vol. 92, no. 23, p. 230 802, 2004. DOI: 10.1103/PhysRevLett.92.230802.

[53] S. N. Lea, "Limits to time variation of fundamental constants from comparisons of atomic frequency standards", *Rep. Prog. Phys.*, vol. 70, no. 9, p. 1473, 2007. [Online]. Available: http://stacks.iop.org/0034-4885/70/i=9/a=R01.

[54] F. Levi, D. Calonico, C. E. Calosso, A. Godone, S. Micalizio, and G. A. Costanzo, "Accuracy evaluation of ITCsF2: A nitrogen cooled caesium fountain", *Metrologia*, vol. 51, no. 3, pp. 270–284, 2014. [Online]. Available: http://stacks.iop.org/0026-1394/51/i=3/a=270.

[55] Y. S. Domnin, V. N. Baryshev, A. I. Boyko, G. A. Elkin, A. V. Novoselov, L. N. Kopylov, and D. S. Kupalov, "The MTsR-F2 fountain-type cesium frequency standard", *Meas. Tech.*, vol. 55, no. 10, pp. 1155–1162, ISSN: 0543-1972, 1573-8906. DOI: 10.1007/s11018-012-0102-0.

[56] S. R. Jefferts, J. Shirley, T. E. Parker, T. P. Heavner, D. M. Meekhof, C. Nelson, F. Levi, G. Costanzo, A. De Marchi, R. Drullinger, L. Hollberg, W. D. Lee, and F. L. Walls, "Accuracy evaluation of NIST-F1", *Metrologia*, vol. 39, no. 4, pp. 321–336, 2002, ISSN: 0026-1394. [Online]. Available: http://stacks.iop.org/0026-1394/39/i=4/a=1.

[57] T. P. Heavner, E. D. Donley, F. Levi, G. Costanzo, T. E. Parker, J. H. Shirley, N. Ashby, S. Barlow, and S. R. Jefferts, "First accuracy evaluation of NIST-F2", *Metrologia*, vol. 51, no. 3, pp. 174–182, 2014. [Online]. Available: http://stacks.iop.org/0026-1394/51/i=3/a=174.

[58] A. Acharya, V. Bharath, P. Arora, S. Yadav, A. Agarwal, and A. S. Gupta, "Systematic uncertainty evaluation of the cesium fountain primary frequency standard at NPL India", *MAPAN*, pp. 1–10, 2016. DOI: 10.1007/s12647-016-0190-4.

[59] F. Fang, N. Liu, K. Liu, W. Chen, R. Suo, and T. Li, "Operation of NIM5 fountain with 1.5×10^{-15} uncertainty and design of new NIM6 in NIM", *J. Phys. Conf. Ser.*, vol. 723, no. 1, p. 012 009, 2016, ISSN: 1742-6596. DOI: 10.1088/1742-6596/723/1/012009.

[60] S. Bize, P. Laurent, M. Abgrall, H. Marion, I. Maksimovic, L. Cacciapuoti, J. Grünert, C. Vian, F. Pereira dos Santos, P. Rosenbusch, P. Lemonde, G. Santarelli, P. Wolf, A. Clairon, A. Luiten, M. Tobar, and C. Salomon, "Advances in atomic fountains", *C. R. Phys.*, vol. 5, no. 8, pp. 829–843, 2004, ISSN: 1631-0705. DOI: DOI:10.1016/j.crhy.2004.09.003.

[61] S. Bize, P. Laurent, M. Abgrall, H. Marion, I. Maksimovic, L. Cacciapuoti, J. Grünert, C. Vian, F. Pereira dos Santos, P. Rosenbusch, P. Lemonde, G. Santarelli, P. Wolf, A. Clairon, A. Luiten, M. Tobar, and C. Salomon, "Cold atom clocks and applications", *J. Phys. B: At., Mol. Opt. Phys.*, vol. 38, no. 9, S449, 2005. [Online]. Available: http://stacks.iop.org/0953-4075/38/i=9/a=002.

[62] F. Riehle, *Basics of frequency standards*. Wiley, 2005, ISBN: 9783527605996. DOI: 10.1002/3527605991.ch2.

[63] K. Szymaniec, H.-R. Noh, S. E. Park, and A. Takamizawa, "Spin polarization in a freely evolving sample of cold atoms", *Appl. Phys. B*, vol. 111, no. 3, pp. 527–535, 2013, ISSN: 1432-0649. DOI: 10.1007/s00340-013-5368-7.

[64] Z. T. Lu, K. L. Corwin, M. J. Renn, M. H. Anderson, E. A. Cornell, and C. E. Wieman, "Low-velocity intense source of atoms from a magneto-optical trap", *Phys. Rev. Lett.*, vol. 77, no. 16, pp. 3331–3334, 1996. DOI: 10.1103/PhysRevLett.77.3331.

[65] E. Donley, T. Heavner, and S. Jefferts, "Optical molasses loaded from a low-velocity intense source of atoms: An atom source for improved atomic fountains", *IEEE Trans. Instrum. Meas.*, vol. 54, no. 5, pp. 1905–1910, 2005. DOI: 10.1109/TIM.2005.853218.

[66] G. Dobrev, V. Gerginov, and S. Weyers, "Loading a fountain clock with an enhanced low-velocity intense source of atoms", *Phys. Rev. A*, vol. 93, p. 043 423, 2016. DOI: 10.1103/PhysRevA.93.043423.

[67] L. L. Presti, D. Rovera, and A. D. Marchi, "A simple analysis of the Dick effect in terms of phase noise spectral densities", *IEEE Trans. Ultrason. Ferroelectr. Freq. Control*, vol. 45, no. 4, pp. 899–905, 1998, ISSN: 0885-3010. DOI: 10.1109/58.710552.

[68] C. Audoin, G. Santarelli, A. Makdissi, and A. Clairon, "Properties of an oscillator slaved to a periodically interrogated atomic resonator", *IEEE Transactions on Ultrasonics, Ferroelectrics and Frequency Control*, vol. 45, no. 4, pp. 877–886, 1998. DOI: 10.1109/58.710546.

[69] G. Santarelli, C. Audoin, A. Makdissi, P. Laurent, G. Dick, and A. Clairon, "Frequency stability degradation of an oscillator slaved to a periodically interrogated atomic resonator", *IEEE Trans. Ultrason. Ferroelectr. Freq. Control*, vol. 45, no. 4, pp. 887–894, 1998. DOI: 10.1109/58.710548.

[70] A. Luiten, A. Mann, and D. Blair, "Cryogenic sapphire microwave resonator-oscillator with exceptional stability", *Electron. Lett.*, vol. 30, no. 5, pp. 417–419, 1994. [Online]. Available: http://ieeexplore.ieee.org/document/273259/.

[71] D. Chambon, S. Bize, M. Lours, F. Narbonneau, H. Marion, A. Clairon, G. Santarelli, A. Luiten, and M. Tobar, "Design and realization of a flywheel oscillator for advanced time and frequency metrology", *Rev. Sci. Instrum.*, vol. 76, no. 9, 094704, 2005. DOI: 10.1063/1.2018567.

[72] J. G. Hartnett, N. R. Nand, and C. Lu, "Ultra-low-phase-noise cryocooled microwave dielectric-sapphire-resonator oscillators", *Appl. Phys. Lett.*, vol. 100, no. 18, 183501, 2012. DOI: 10.1063/1.4709479.

[73] B. Lipphardt, G. Grosche, U. Sterr, C. Tamm, S. Weyers, and H. Schnatz, "The stability of an optical clock laser transferred to the interrogation oscillator for a Cs fountain", *IEEE Trans. Instrum. Meas.*, vol. 58, no. 4, pp. 1258–1262, 2009, ISSN: 0018-9456. DOI: 10.1109/TIM.2008.2007051.

[74] S. Weyers, B. Lipphardt, and H. Schnatz, "Reaching the quantum limit in a fountain clock using a microwave oscillator phase locked to an ultrastable laser", *Phys. Rev. A*, vol. 79, no. 3, p. 031 803, 2009, ISSN: 1050-2947. DOI: {10.1103/PhysRevA.79.031803}.

[75] J. Millo, M. Abgrall, M. Lours, E. M. L. English, H. Jiang, J. Guena, A. Clairon, M. E. Tobar, S. Bize, Y. L. Coq, and G. Santarelli, "Ultralow noise microwave generation with fiber-based optical frequency comb and application to atomic fountain clock", *Applied Physics Letters*, vol. 94, no. 14, 141105, p. 141 105, 2009. DOI: 10.1063/1.3112574.

[76] C. Tamm, N. Huntemann, B. Lipphardt, V. Gerginov, N. Nemitz, M. Kazda, S. Weyers, and E. Peik, "Cs-based optical frequency measurement using cross-linked optical and microwave oscillators", *Phys. Rev. A*, vol. 89, p. 023 820, 2014. DOI: 10.1103/PhysRevA.89.023820.

[77] M. Natrella, *NIST/SEMATECH e-Handbook of Statistical Methods*, C. Croarkin, P. Tobias, J. J. Filliben, B. Hembree, W. Guthrie, L. Trutna, and J. Prins, Eds. NIST/SEMATECH, 2010. [Online]. Available: http://www.itl.nist.gov/div898/handbook/.

[78] B. Verhaar, K. Gibble, and S. Chu, "Cold-collision properties derived from frequency shifts in a cesium fountain", *Phys. Rev. A*, vol. 48, no. 5, pp. 3429–3432, 1993. DOI: 10.1103/PhysRevA.48.R3429.

[79] E. Tiesinga, B. J. Verhaar, H. T. C. Stoof, and D. van Bragt, "Spin-exchange frequency shift in a cesium atomic fountain", *Phys. Rev. A*, vol. 45, pp. 2671–2673, 1992, ISSN: 1050-2947. DOI: 10.1103/PhysRevA.45.R2671.

[80] S. Weyers, A. Bauch, R. Schröder, and C. Tamm, "The atomic caesium fountain CSF1 of PTB", in *Proceedings of the 6th Symposium on Frequency Standards and Metrology*, University of St Andrews, Fife, Scotland: World Scientific, 2001, pp. 64–71. DOI: 10.1142/9789812777713_0009.

[81] B. W. Shore, M. V. Gromovyy, L. P. Yatsenko, and V. I. Romanenko, "Simple mechanical analogs of rapid adiabatic passage in atomic physics", *American Journal of Physics*, vol. 77, no. 12, pp. 1183–1194, 2009. DOI: 10.1119/1.3231688.

[82] BIPM. (2017). Evaluation of PTB primary caesium fountain frequency standard CSF2 between MJD 57809 - MJD 57839, [Online]. Available: ftp://ftp2.bipm.org/pub/tai/data/PFS_reports/ptb-csf1_57809-57839.pdf.

[83] B. Boussert, G. Theobald, P. Cerez, and E. de Clercq, "Frequency shifts in cesium beam clocks induced by microwave leakages", *IEEE Trans. Ultrason. Ferroelectr. Freq. Control*, vol. 45, no. 3, pp. 728–738, 1998, ISSN: 0885-3010. DOI: 10.1109/58.677617.

[84] F. Levi, C. Calosso, D. Calonico, L. Lorini, E. K. Bertacco, A. Godone, G. A. Costanzo, B. Mongino, S. R. Jefferts, T. P. Heavner, and E. A. Donley, "Cryogenic fountain development at NIST and INRIM: Preliminary characterization", *IEEE Trans. Ultrason. Ferroelectr. Freq. Control*, vol. 57, no. 3, pp. 600–605, 2010, ISSN: 0885-3010. DOI: 10.1109/TUFFC.2010.1453.

[85] Oscilloquartz. (2013). OCXO 8607 data sheet, [Online]. Available: http://www.oscilloquartz.com/files/1363164953-Br_%200CXO%208607.pdf.

[86] C. R. Locke, E. N. Ivanov, J. G. Hartnett, P. L. Stanwix, and M. E. Tobar, "Design techniques and noise properties of ultrastable cryogenically cooled sapphire-dielectric resonator oscillators", *Rev. Sci. Instrum.*, vol. 79, no. 5, p. 051 301, 2008. DOI: 10.1063/1.2919944.

[87] M. Abgrall, J. Guéna, M. Lours, G. Santarelli, M. E. Tobar, S. Bize, S. Grop, B. Dubois, C. Fluhr, and V. Giordano, "High-stability comparison of atomic fountains using two different cryogenic oscillators", *IEEE Transactions on Ultrasonics, Ferroelectrics, and Frequency Control*, vol. 63, no. 8, pp. 1198–1203, 2016, ISSN: 0885-3010. DOI: 10.1109/TUFFC.2016.2570898.

[88] A. Takamizawa, S. Yanagimachi, T. Tanabe, K. Hagimoto, I. Hirano, K. i. Watabe, T. Ikegami, and J. G. Hartnett, "Atomic fountain clock with very high frequency stability employing a pulse-tube-cryocooled sapphire oscillator", *IEEE Trans. Ultrason. Ferroelectr. Freq. Control*, vol. 61, no. 9, pp. 1463–1469, 2014, ISSN: 0885-3010. DOI: 10.1109/TUFFC.2014.3060.

[89] J. J. McFerran, E. N. Ivanov, A. Bartels, G. Wilpers, C. W. Oates, S. A. Diddams, and L. Hollberg, "Low-noise synthesis of microwave signals from an optical source", *Electron. Lett.*, vol. 41, no. 11, pp. 650–651, 2005, ISSN: 0013-5194. DOI: 10.1049/el:20050505.

[90] J. Kim, F. Ludwig, M. Felber, and F. X. Kärtner, "Long-term stable microwave signal extraction from mode-locked lasers", *Opt. Express*, vol. 15, no. 14, pp. 8951–8959, 2007. DOI: 10.1364/OE.15.008951.

[91] A. Bauch, "The PTB primary clocks CS1 and CS2", *Metrologia*, vol. 42, no. 3, S43, 2005. [Online]. Available: http://stacks.iop.org/0026-1394/42/i=3/a=S06.

[92] T. P. Heavner, S. R. Jefferts, E. A. Donley, T. E. Parker, and F. Levi, "A new microwave synthesis chain for the primary frequency standard NIST-F1", in *Proc. IEEE Int. Frequency Control Symp. Exposition*, 2005, pp. 308–311. DOI: 10.1109/FREQ.2005.1573950.

[93] A. Boyko, L. Kopylov, and A. Novoselov, "Microwave interrogation system for VNIIFTRI cesium fountain", in *Proc. 20th European Frequency and Time Forum (EFTF)*, 2006, pp. 213–215. [Online]. Available: http://ieeexplore.ieee.org/document/6230975/.

[94] D. Chambon, M. Lours, F. Chapelet, S. Bize, M. E. Tobar, A. Clairon, and G. Santarelli, "Design and metrological features of microwave synthesizers for atomic fountain frequency standard", *IEEE Trans. Ultrason. Ferroelectr. Freq. Control*, vol. 54, no. 4, pp. 729–735, 2007, ISSN: 0885-3010. DOI: 10.1109/TUFFC.2007.306.

[95] M. Kumagai, H. Ito, M. Kajita, and M. Hosokawa, "Evaluation of caesium atomic fountain NICT-CsF1", *Metrologia*, vol. 45, no. 2, pp. 139–148, 2008. DOI: 10.1088/0026-1394/45/2/00.

[96] K. Szymaniec, S. E. Park, G. Marra, and W. Chalupczak, "First accuracy evaluation of the NPL-CsF2 primary frequency standard", *Metrologia*, vol. 47, no. 4, p. 363, 2010, ISSN: 0026-1394. [Online]. Available: http://iopscience.iop.org/0026-1394/47/4/003.

[97] F. Fang, M. Li, P. Lin, W. Chen, N. Liu, Y. Lin, P. Wang, K. Liu, R. Suo, and T. Li, "NIM5 Cs fountain clock and its evaluation", *Metrologia*, vol. 52, no. 4, p. 454, 2015, ISSN: 0026-1394. DOI: 10.1088/0026-1394/52/4/454.

[98] M. S. Heo, S. E. Park, W. K. Lee, S. B. Lee, H. G. Hong, T. Y. Kwon, C. Y. Park, D. H. Yu, G. Santarelli, A. P. Hilton, A. N. Luiten, and J. G. Hartnett, "Drift-compensated low-noise frequency synthesis based on a cryoCSO for the KRISS-F1", *IEEE Trans. Instrum. Meas.*, vol. 66, no. 6, pp. 1343–1348, 2017, ISSN: 0018-9456. DOI: 10.1109/TIM.2016.2620187.

[99] A. Gupta, D. Popovic, and F. Walls, "Cs frequency synthesis: A new approach", *IEEE Trans. Ultrason. Ferroelectr. Freq. Control*, vol. 47, no. 2, pp. 475–479, 2000, ISSN: 0885-3010. DOI: 10.1109/58.827439.

[100] P. Arora, S. Purnapatra, A. Acharya, A. Agarwal, S. Yadav, K. Pant, and A. Gupta, "NPLI cesium atomic fountain frequency standard: Preliminary results", *IEEE Trans. Instrum. Meas.*, vol. 62, no. 7, pp. 2037–2042, 2013, ISSN: 0018-9456. DOI: 10.1109/TIM.2013.2255974.

[101] J. R. Vigg, "IEEE standard definitions of physical quantities for fundamental frequency and time metrolog - random instabilities", *IEEE Std 1139-2008*, pp. c1–35, 2008. DOI: 10.1109/IEEESTD.2008.4797525.

[102] E. Rubiola, *Phase noise and frequency stability in oscillators*. Cambridge, U.K.: Cambridge Univ. Press, 2010, ISBN: 052115328X.

[103] V. F. Kroupa. (2000). Principles of phase locked loops (PLL), [Online]. Available: http://www.itl.nist.gov/div898/handbook/.

[104] W. Egan, "Modeling phase noise in frequency dividers", *IEEE Trans. Ultrason. Ferroelectr. Freq. Control*, vol. 37, no. 4, pp. 307–315, ISSN: 0885-3010. DOI: 10.1109/58.56498.

[105] Poseidon Scientific Instruments. (2003). DRO data sheet.

[106] Zarlink Semiconductors. (1994). SP8401 data sheet, Zarlink Semiconductors.

[107] Zarlink Semiconductors. (1994). SP8402 data sheet, Zarlink Semiconductors.

[108] J. Tierney, C. M. Rader, and B. Gold, "A digital frequency synthesizer", *IEEE Trans. Audio Electroacoust.*, vol. 19, no. 1, pp. 48–57, 1971, ISSN: 0018-9278. DOI: 10.1109/TAU.1971.1162151.

[109] Intersil. (2010). ISL5314 data sheet, [Online]. Available: https://www.intersil.com/content/dam/Intersil/documents/isl5/isl5314.pdf.

[110] J. F. Honey and D. K. Weaver, "An introduction to single-sideband communications", in *Proceedings of the IRE*, vol. 44, pp. 1667–1675. DOI: 10.1109/JRPROC.1956.275032.

[111] E. W. Pappenfus, W. B. Bruene, and E. O. Schoenike, *Single sideband principles and circuits*. New York: McGraw-Hill, 1964, ISBN: 0070484554.

[112] R. Wynands and S. Weyers, "Atomic fountain clocks", *Metrologia*, vol. 42, no. 3, pp. 64–79, 2005. DOI: 10.1088/0026-1394/42/3/S08.

[113] F. J. Harris, "On the use of windows for harmonic analysis with the discrete fourier transform", *Proceedings of the IEEE*, vol. 66, no. 1, pp. 51–83, 1978, ISSN: 0018-9219. DOI: 10.1109/PROC.1978.10837.

[114] M. Kasevich and S. Chu, "Laser cooling below a photon recoil with three-level atoms", *Phys. Rev. Lett.*, vol. 69, pp. 1741–1744, 1992. DOI: 10.1103/PhysRevLett.69.1741.

[115] V. Gerginov, N. Nemitz, and S. Weyers, "Initial atomic coherences and Ramsey frequency pulling in fountain clocks", *Phys. Rev. A*, vol. 90, p. 033 829, 2014. DOI: 10.1103/PhysRevA.90.033829.

[116] N. F. Ramsey, "Resonance transitions induced by perturbations at two or more different frequencies", *Phys. Rev.*, vol. 100, pp. 1191–1194, 1955. DOI: 10.1103/PhysRev.100.1191.

[117] J. H. Shirley, "Some causes of resonant frequency shifts in atomic beam machines. I. shifts due to other frequencies of excitation", *J. Appl. Phys.*, vol. 34, no. 4, pp. 783–788, 1963. DOI: 10.1063/1.1729536.

[118] A. Hati, D. A. Howe, F. L. Walls, and D. K. Walker, "Merits of PM noise measurement over noise figure: A study at microwave frequencies", *IEEE Trans. Ultrason. Ferroelectr. Freq. Control*, vol. 53, no. 10, pp. 1889–1894, 2006, ISSN: 0885-3010. DOI: 10.1109/TUFFC.2006.121.

[119] R. Boudot and E. Rubiola, "Phase noise in RF and microwave amplifiers", *IEEE Trans. Ultrason. Ferroelectr. Freq. Control*, vol. 59, no. 12, pp. 2613–2624, ISSN: 0885-3010. DOI: 10.1109/TUFFC.2012.2502.

[120] E. M. Mattison and L. M. Coyle, "Phase noise in direct digital synthesizers [atomic clocks application]", in *Proceedings of the 42nd Annual Frequency Control Symposium, 1988.*, pp. 352–356. DOI: 10.1109/FREQ.1988.27624.

[121] C. E. Calosso, E. K. Bertacco, S. Micalizio, A. Godone, D. Calonico, and G. A. Costanzo, "OCXO ensemble as improved local oscillator for atomic fountains", in *2012 European Frequency and Time Forum*, 2012, pp. 271–274. DOI: 10.1109/EFTF.2012.6502381.

[122] F. Levi, J. H. Shirley, T. P. Heavner, D.-H. Yu, and S. R. Jefferts, "Power dependence of the frequency bias caused by spurious components in the microwave spectrum in atomic fountains", *IEEE Trans. Ultrason. Ferroelectr. Freq. Control*, vol. 53, no. 9, 1584–1589, 2006, ISSN: 0885-3010. DOI: 10.1109/TUFFC.2006.1678186.

[123] J. Shirley, T. Heavner, and S. Jefferts, "First-order sideband pulling in atomic frequency standards", *IEEE Trans. Instrum. Meas.*, vol. 58, no. 4, pp. 1241–1246, 2009, ISSN: 0018-9456, 1557-9662. DOI: 10.1109/TIM.2008.2008590.

[124] T. P. Heavner, J. H. Shirley, F. Levi, D. Yu, and S. R. Jefferts, "Frequency biases in pulsed atomic fountain frequency standards due to spurious components in the microwave spectrum", in *2006 IEEE International Frequency Control Symposium and Exposition*, 2006, pp. 273–276. DOI: 10.1109/FREQ.2006.275394.

[125] D. Liebl. (2013). Measuring with modern spectrum analyzers, [Online]. Available: https://cdn.rohde-schwarz.com/pws/dl_downloads/dl_application/application_notes/1ma201_1/1MA201_9e_spectrum_analyzers_meas.pdf.

[126] (2016). FSWP phase noise analyzer specifications, [Online]. Available: https://cdn.rohde-schwarz.com/pws/dl_downloads/dl_common_library/dl_brochures_and_datasheets/pdf_1/service_support_30/FSWP_dat-sw_en_3607-2090-22_v0500.pdf.

[127] J. Grove, J. Hein, J. Retta, P. Schweiger, W. Solbrig, and S. R. Stein, "Direct-digital phase-noise measurement", in *Proceedings of the 2004 IEEE International Frequency Control Symposium and Exposition, 2004.*, pp. 287–291. DOI: 10.1109/FREQ.2004.1418466.

[128] J. Miles. (2013). TimePod 5330A user manual, [Online]. Available: http://www.miles.io/TimePod_5330A_user_manual.pdf.

[129] Microsemi. (2016). 3120A data sheet, [Online]. Available: https://www.microsemi.com/document-portal/doc_view/133331-3120a.

[130] BIPM. (2017). Evaluation of PTB primary caesium fountain frequency standard CSF1 between MJD 57854 - MJD 57869, [Online]. Available: ftp://ftp2.bipm.org/pub/tai/data/PFS_reports/ptb-csf1_57854-57869.pdf.

[131] C. Azeredo-Leme, "Clock jitter effects on sampling: A tutorial", *IEEE Circuits Syst. Mag.*, vol. 11, no. 3, pp. 26–37, 2011, ISSN: 1531-636X. DOI: 10.1109/MCAS.2011.942067.

[132] R. G. Lyons, *Understanding digital signal processing*, 1st ed. Boston, MA, USA: Addison-Wesley Longman Publishing Co., Inc., 1996, ISBN: 0201634678.

[133] H. Nyquist, "Certain topics in telegraph transmission theory", *Trans. Am. Inst. Electr. Eng.*, vol. 47, no. 2, pp. 617–644, 1928, ISSN: 0096-3860. DOI: 10.1109/T-AIEE.1928.5055024.

[134] (2015). Virtex-5 family overview, [Online]. Available: https://www.xilinx.com/support/documentation/data_sheets/ds100.pdf.

[135] Analog Devices. (2009). AD9268 data sheet, Analog Devices, [Online]. Available: http://www.analog.com/media/en/technical-documentation/data-sheets/AD9268.pdf.

[136] National Instruments Corporation. (2011). NI 5734R user guide and specifications, National Instruments Corporation, [Online]. Available: http://www.ni.com/pdf/manuals/375653a.pdf.

[137] R. E. Crochiere and L. Rabiner, "Optimum FIR digital filter implementations for decimation, interpolation, and narrow-band filtering", *IEEE Trans. Instrum. Meas.*, vol. 23, no. 5, pp. 444–456, 1975, ISSN: 0096-3518. DOI: 10.1109/TASSP.1975.1162719.

[138] R. G. Lyons, *Understanding digital signal processing (2nd edition)*. Upper Saddle River, NJ, USA: Prentice Hall PTR, 2004, ISBN: 0131089897.

[139] J. E. Volder, "The birth of cordic", *Journal of VLSI signal processing systems for signal, image and video technology*, vol. 25, no. 2, pp. 101–105, 2000, ISSN: 0922-5773. DOI: 10.1023/A:1008110704586.

[140] W. Kester, "Understand SINAD, ENOB, SNR, THD, THD+N, and SFDR", *Tutorial MT-003, Analog Devices*, 2008. [Online]. Available: http://www.analog.com/media/en/training-seminars/tutorials/MT-003.pdf.

[141] M. Abgrall, "Evaluation des performances de la fontaine atomique pharao , participation à l'étude de l'horloge spatiale pharao", PhD thesis, University Paris VI, 2003. [Online]. Available: https://tel.archives-ouvertes.fr/tel-00003079/document.

[142] R. Schröder, U. Hübner, and D. Griebsch, "Design and realization of the microwave cavity in the PTB caesium atomic fountain clock CSF1", *IEEE Trans. Ultrason. Ferroelectr. Freq. Control*, vol. 49, no. 3, pp. 383–392, 2002. DOI: 10.1109/58.990959.

[143] C. Rauscher, "Fundamentals of spectrum analysis", Tech. Rep., 2001. [Online]. Available: http://wireless.ictp.it/school_2005/download/rohdeschwarz/SpectrumAnalysysis.pdf.

[144] J. Vankka, "Direct digital synthesizers: Theory, design and applications", PhD thesis, Helsinki University of Technology, 2000. [Online]. Available: http://lib.tkk.fi/Diss/2000/isbn9512253186/isbn9512253186.pdf.

[145] L. Cordesses, "Direct digital synthesis: A tool for periodic wave generation (part 1)", *IEEE Signal. Proc. Mag.*, vol. 21, no. 4, pp. 50–54, 2004, ISSN: 1053-5888. DOI: 10.1109/MSP.2004.1311140.

[146] L. Cordesses, "Direct digital synthesis: A tool for periodic wave generation (part 2)", *IEEE Signal. Proc. Mag.*, vol. 21, no. 5, pp. 110–112, 2004, ISSN: 1053-5888. DOI: 10.1109/MSP.2004.1328096.

[147] Analog Devices. (2004). AD9956 data sheet, Analog Devices, [Online]. Available: http://www.analog.com/media/en/technical-documentation/data-sheets/AD9956.pdf.

[148] B. Widrow and I. Kollár, *Quantization noise: Roundoff error in digital computation, signal processing, control, and communications*. Cambridge, UK: Cambridge University Press, 2008, ISBN: 9780521886710.

[149] Y. Ovchinnikov and G. Marra, "Accurate rubidium atomic fountain frequency standard", *Metrologia*, vol. 48, no. 3, p. 87, ISSN: 0026-1394. DOI: 10.1088/0026-1394/48/3/003.

[150] Y. Zhang, K. Liu, F. Fang, N. Liu, and T. Li, "Thermal effect of the microwave Mach-Zehnder interferometric switch", in *IEEE Int. Frequency Control Symp. Exposition*, 2014, pp. 1–3. DOI: 10.1109/FCS.2014.6859945.

[151] A. Takamizawa, S. Yanagimachi, T. Tanabe, K. Hagimoto, I. Hirano, K.-I. Watabe, T. Ikegami, and J. G. Hartnett, "Preliminary evaluation of the cesium fountain primary frequency standard NMIJ-F2", *IEEE Trans. Instrum. Meas.*, vol. 64, no. 9, pp. 2504–2512, 2015, ISSN: 0018-9456. DOI: 10.1109/TIM.2015.2415015.

[152] BIPM. (2017). Frequency comparison (H-MASER 140 0889) - (LNE-SYRTE-FO2) for the period MJD 57844 to MJD 57869, [Online]. Available: ftp://ftp2.bipm.org/pub/tai/data/PFS_reports/syrte-fo2_57844-57869.pdf.

[153] BIPM. (2017). Frequency comparison (H-MASER 40 3853) - (SU-CsFO2) for the period MJD 57869 to MJD 57904, [Online]. Available: ftp://ftp2.bipm.org/pub/tai/data/PFS_reports/su-csfo2_57869-57904.pdf.

[154] BIPM. (2016). February 2016 evaluation of NIST-F1, [Online]. Available: ftp://ftp2.bipm.org/pub/tai/data/PFS_reports/nist-f1_57419-57439.pdf.

[155] BIPM. (2017). ITCsF2 TAI evaluation MJD 57909-57934 (5/6/2017-30/6/2017), [Online]. Available: ftp://ftp2.bipm.org/pub/tai/data/PFS_reports/it-csf2_57909-57934.pdf.

[156] BIPM. (2015). Evaluation of the frequency of the H-maser 1401708 by the primary frequency standard NPL-CsF2, [Online]. Available: ftp://ftp2.bipm.org/pub/tai/data/PFS_reports/npl-csf2_57289-57314.pdf.

[157] BIPM. (2016). Nim5 57664-57684, [Online]. Available: ftp://ftp2.bipm.org/pub/tai/data/PFS_reports/nim5_57664-57684.pdf.

[158] BIPM. (2016). Evaluation of PTB primary caesium fountain frequency standard CSF2 between MJD 57659 - MJD 57689, [Online]. Available: ftp://ftp2.bipm.org/pub/tai/data/PFS_reports/ptb-csf1_57474-57504.pdf.

[159] BIPM. (2016). Evaluation of PTB primary caesium fountain frequency standard CSF1 between MJD 57474 - MJD 57504, [Online]. Available: ftp://ftp2.bipm.org/pub/tai/data/PFS_reports/ptb-csf1_57474-57504.pdf.

[160] K. Szymaniec, W. Chalupczak, E. Tiesinga, C. J. Williams, S. Weyers, and R. Wynands, "Cancellation of the collisional frequency shift in caesium fountain clocks", *Phys. Rev. Lett.*, vol. 98, no. 15, p. 153 002, 2007, ISSN: 0031-9007. DOI: 10.1103/PhysRevLett.98.153002.

Acknowledgements

It's been a long travel through time and frequency, all the more I would like to acknowledge the widespread encouragement I received. Not only during this work but throughout my career I have enjoyed the support and advice of countless colleagues, mentors and friends.

First of all I want to thank my supervisors Professor Meinhard Schilling and Professor Fritz Riehle for their support and their thoughtful guidance throughout the process of this thesis. I'd like to thank Ekkehard Peik and Stefan Weyers for their steady support and encouragement and the confidence they have shown in me.

I would like to express my great appreciation to Vladislav Gerginov for his many ideas, his enthusiastic encouragement and the intensive professional exchange. We had a great time making time! Moreover, I'd like to thank Burghardt Lipphard, who introduced me to my current position and shared his vast knowledge with me. I thank Robert Wynands for putting me in contact with Professor Schilling and the Braunschweig International Graduate School of Metrology. I highly appreciated his interest in my work and his admonishing comments concerning my timeline.

Furthermore, I would like to offer my special thanks to Roland Schröder, who had shaped the field of microwave electronics at our department for several decades. His ingenious handwritten notes and calculations provided a wealth of knowledge to me. A special thanks goes to Nils Huntemann for his expedient advice regarding the design of my experiments and the presentation of my results. I thank Mattias Misera for valuable technical discussions, due to his hands-on approach they often yielded unconventional solutions. I would also like to express my sincere thanks to Johannes Rahm for fruitful technical discussions and extensive proofreading.

I am particularly grateful for the assistance given by Christof Richter and Christof Hellmann; they have built countless prototypes and electronics equipment, commonly thinking out of the box. The experimental setups involved many mechanical components, usually provided by Thomas Leder and Martin Menzel. Their speedy manufacture of mechanical masterpieces

was greatly appreciated. Also, I would like to thank Martina Bäumler and Eva-Maria Berber for their administrative support and guidance through the SAP-jungle. Your delicious cookies kept the morale high during difficult times. My special thanks are extended to all the staff of the Time and Frequency department for the great atmosphere that made my work all the more an enjoyable experience.

I'd like to thank Giorgio Santarelli, Michel Abgrall and all the other great people I met at LNE-SYRTE, they inspired me and helped me become familiar with the time and frequency community. Also, the European Frequency and Time Forums and International Frequency Control Symposia I attended have always served as a source of inspiration and an opportunity to meet a host of great people. I'd especially like to thank Archita Hati, Craig Nelson, Maria Delgado, Franklin Ascarrunz and Claudio Calosso for valuable discussions on subjects ranging from noise floor to dance floor. I would also like to express my sincere thanks to Amitava Sen Gupta, whose coherent overall approach and broad perspective provided inspiration for me.

My special thanks are extended to my former colleagues at Dräger Safety. I had a great time at Kst5430 and learned a host of technical tidbits that proved to be useful later on. I am especially indebted to Matthias Martens und Andreas Sürig, who had been a great source of inspiration at the initial point of my engineering career.

This work has been partly supported by the Braunschweig International Graduate School of Metrology. I'd like to offer my special thanks to Dezhen Li und Judith Krakowski for organizing a fruitful and entertaining graduate school. Support and advice given by Christian Hummert und Marian Kazda during the preparation of the thesis was greatly appreciated.

Finally, I wish to thank my parents for their support and encouragement throughout my career.